# SOURCE-SINK CONNECTIVITY: A NOVEL INTERICTAL EEG MARKER OF THE EPILEPTIC BRAIN NETWORK

by
Kristin Maria Gunnarsdottir

A dissertation submitted to The Johns Hopkins University in conformity with the requirements for the degree of Doctor of Philosophy

Baltimore, Maryland
October, 2021

# Abstract

Epilepsy affects over 60 million people worldwide. Epilepsy diagnosis depends on abnormalities in scalp electroencephalography (EEG) signals but their presence varies from 29-55%, resulting in a delayed diagnosis. Additionally, artifacts mimicking abnormalities and conditions imitating epileptic seizures contribute to a misdiagnosis rate of 30%.

Antiepileptic drugs (AEDs) are the mainstay of epilepsy treatment, but around 30% of patients do not respond to AEDs. Surgical treatment is a hopeful alternative but outcomes depend on precise identification of the epileptogenic zone (EZ), the brain region(s) where seizures originate, and success rates range from 20-80%. Localization of the EZ requires visual inspection of intracranial EEG (iEEG) recordings during seizures which is costly and time-consuming and, in the end, clinicians ignore most of the data captured.

Diagnosis and management of epilepsy rely on detecting sporadic EEG signatures. Thus, there is a great need to more quickly and accurately identify the underlying cause and location of seizures in the brain. We developed and tested the source-sink index (SSI) as an interictal (between seizures) EEG marker of epileptogenic activity. We hypothesized that seizures are suppressed when the EZ is inhibited by neighboring regions. We developed an algorithm that identifies two groups of nodes from the EEG network: those inhibiting their neighboring nodes ("sources") and the inhibited nodes themselves ("sinks"). Specifically, dynamical network models were estimated from EEG data and their connectivity properties revealed top sources and sinks in

the network. We tested and validated a twofold application of SSI, as: i) an iEEG marker of the EZ, and ii) a scalp EEG marker of epilepsy. We found that SSI highly agreed with the annotated EZ in successful outcome patients but identified untreated regions in failure patients. Further, SSI outperformed high frequency oscillations, a frequently proposed interictal EZ marker, in predicting surgical outcomes. When used to predict diagnostic outcomes, SSI showed significant improvement over the gold standard's reported sensitivity and specificity. Our results suggest that SSI captures the characteristics of regions responsible for seizure initiation. As such, it is a promising marker of epileptogenicity that could significantly improve the speed and outcomes of epilepsy management and diagnosis.

## Thesis Readers

Dr. Sridevi V. Sarma (Primary Advisor)
Associate Professor
Department of Biomedical Engineering
Johns Hopkins University

Dr. René Vidal
Professor
Department of Biomedical Engineering
Johns Hopkins University

Dr. Anna Korzeniewska
Assistant Professor
Department of Neurology
Johns Hopkins University

Dr. Khalil Husari
Assistant Professor
Department of Neurology
Johns Hopkins University

*Dedicated to my parents*

*for being my biggest supporters and best cheerleaders.*

*Takk fyrir allt!*

# Acknowledgements

I could have never completed my PhD without all the mentors, colleagues, friends and family members who in one way or another supported me along my journey.

First and foremost, I would like to thank my amazing advisor, Dr. Sridevi Sarma, for all her guidance, support, help and patience over the past years. Sri is some of the most intelligent, hard working and inspiring people I know and I have learned so much from her. She is truly someone who doesn't see problems, only solutions, and without her constant encouragement and enthusiasm I could have never completed my degree. I could not have imagined having a better advisor, mentor and role model for my PhD and I feel so grateful and lucky to have been her student.

I would also like to thank my thesis committee members, Dr. René Vidal, Dr. Anna Korzeniewska and Dr. Khalil Husari, for all their valuable feedback, suggestions and discussions during our meetings. I am grateful for their interest and engagement and for all their input that helped make the study better.

This work would also not have been possible without our clinical collaborators who not only shared data with us but also played a very important role in interpreting the results. I would specifically like to thank Dr. Jorge Gonzalez-Martinez for all his help, patience, and extremely valuable input in forming the hypothesis and explaining the results. I realize how lucky I am to get the opportunity to work with some of the best neurologists, neurosurgeons and clinicians in the country and I have learned so much from interacting with every single one of them.

I would like to also thank my lab members and friends in the Neuromedical Control Systems Lab. In particular, I would like to thank Patrick Myers, who did most of the scalp EEG analysis, and Adam Li and Rachel Smith for their help with the intracranial study. I lucked out with both colleagues and friends in the NCSL lab. I am thankful for all our awesome lab lunches, lab meetings, our research related – and totally unrelated – discussions, all the conferences we have been to and all the places we traveled to together.

I would, of course, also like to thank all my friends, near and far, for their support every step of the way. My friends in Baltimore, who been like my US family, have both been there for me through the difficult times and celebrated all the good times with me. We have shared so many amazing memories over the years and I will cherish these times forever. It is thanks to them that Baltimore has felt like home. Meanwhile, my amazing friends in Iceland have been so patient throughout the years and have always made sure to reach out and keep in touch when I haven't been as good at it. Being so far away has made the time we get to spend together whenever I have been in Iceland even more precious. I appreciate every single one of them.

Finally, I would like to thank the most important people in my life, my family. Always being able to reach out to my two sisters, Dísa and Hildur, who I am so lucky to also call my best friends, and our almost daily chats about anything and everything has been so important to me. I cannot mention my sisters without also mentioning our furry little brother, Dúskur, who has brought so much joy to my life. My little niece, Emma Kristín, has also been the brightest ray of sunshine in all our lives and I love and miss her so incredibly much. Last but not least, I want to thank my parents, my two rocks and role models! I am so thankful for everything they have done for me and for their endless support, love and encouragement. I truly could not have done any of this if it wasn't for the two of them.

# Contents

**Abstract** . . . . . ii

**Dedication** . . . . . iv

**Acknowledgements** . . . . . v

**Contents** . . . . . vii

**List of Tables** . . . . . xiii

**List of Figures** . . . . . xiv

**Chapter 1 Introduction** . . . . . 1

1.1 Epilepsy . . . . . 1

1.2 Challenges in diagnosing epilepsy . . . . . 2

1.3 Management of epilepsy . . . . . 3

1.3.1 Anti-epileptic drugs . . . . . 3

1.3.2 Drug resistant epilepsy . . . . . 3

1.4 Treatment options for DRE patients . . . . . 4

1.4.1 Pre-surgical evaluation . . . . . 4

1.5 Limitations of current clinical practice . . . . . 6

1.6 Thesis aims . . . . . 7

**Chapter 2 Detecting sources and sinks from EEG recordings . . . 10**

2.1 Source-sink hypothesis: Sources and sinks in the epileptic brain network 10

2.1.1 Biological evidence supporting the source-sink hypothesis . . . 12

2.1.2 iEEG studies supporting the source-sink hypothesis . . . . . 13

2.2 Dynamical network models . . . . . 14

2.3 Sources and sinks in the EEG DNM . . . . . 15

2.4 Computing source-sink indices . . . . . 16

2.4.1 Identifying top sources and sinks in the interictal EEG network 16

2.4.2 Definition of source-sink indices . . . . . 17

**Chapter 3 Source-sink analysis for localization of the epileptogenic zone on interictal intracranial EEG data . . . . . 19**

3.1 Introduction . . . . . 19

3.1.1 Computational approaches to identify iEEG markers to assist in EZ localization . . . . . 19

3.2 Materials and methods . . . . . 21

3.2.1 Patient population . . . . . 21

3.2.2 Data collection . . . . . 22

3.2.2.1 sEEG recordings . . . . . 22

3.2.2.2 Clinical annotations of the EZ . . . . . 22

3.2.2.3 Clinical classification of surgical outcomes . . . . . 23

3.2.3 Data pre-processing . . . . . 23

3.2.4 Source-sink analysis to localize the EZ . . . . . 24

3.2.4.1 Computing dynamic and constant interictal SSIs . . 24

3.2.5 Quantifying temporal stability of source-sink metrics . . . . . 25

3.2.6 Predicting surgical outcomes using source-sink indices . . . . . 26
3.2.7 Predicting surgical outcomes using HFOs . . . . . 28
3.2.8 Clinical annotations of CA-EZ and SSI correspondence . . . . 29
3.2.9 Statistical analysis . . . . . 29
3.3 Results . . . . . 31
3.3.1 The source-sink index highlights CA-EZ regions in patients with successful outcomes . . . . . 31
3.3.2 Temporal stability of sources and sinks during interictal periods 34
3.3.3 Identifying channels with highest SSI . . . . . 34
3.3.4 Source-sink metrics outperform HFOs in predicting surgical outcomes . . . . . 36
3.3.5 The source-sink metrics are highly correlated with treatment outcomes . . . . . 38
3.3.6 Generalizability of the SSI . . . . . 39
3.3.7 Top SSI regions have high correspondence to CA-EZ in success patients but lower in failure patients . . . . . 41
3.3.8 CA-EZ regions are sinks at rest but become sources during seizures in success patients . . . . . 43
3.4 Discussion . . . . . 45
3.4.1 Challenges . . . . . 47
3.4.1.1 Validating iEEG markers of the EZ . . . . . 47
3.4.1.2 Why the source-sink algorithm may disagree with clinicians in success patients . . . . . 48
3.4.1.3 Why the source-sink algorithm may agree with clinicians in failure patients . . . . . 48

3.4.1.4 Other interictal iEEG markers of the EZ . . . . . 49
3.4.1.5 Translating an iEEG marker into the clinical workflow 51

**Chapter 4 Source-sink analysis for diagnosis of epilepsy on interictal scalp EEG data . . . . . 53**

4.1 Introduction . . . . . 53
4.1.1 Challenges with EEG interpretation . . . . . 53
4.1.2 SSI as a biomarker for diagnosing epilepsy . . . . . 55
4.2 Materials and methods . . . . . 55
4.2.1 Patient population . . . . . 55
4.2.2 Data collection . . . . . 56
4.2.3 Scalp EEG recordings . . . . . 56
4.2.4 Classification of abnormal versus normal EEGs . . . . . 57
4.2.5 Data pre-processing . . . . . 57
4.2.5.1 Artifact removal . . . . . 57
4.2.6 Source-sink analysis to diagnose epilepsy . . . . . 58
4.2.6.1 Computing stationary interictal SSIs . . . . . 59
4.2.7 Predicting diagnostic outcomes using the source-sink index . . 60
4.3 Results . . . . . 63
4.3.1 SSI is high in one or a few channels in epilepsy patients but lower in non-epilepsy patients . . . . . 63
4.3.2 SSI performs well in predicting epilepsy diagnosis . . . . . 63
4.4 Discussion . . . . . 65
4.4.1 Limitations of current computational approaches for diagnosing epilepsy . . . . . 66

4.4.2 Limitations of current clinical gold standard for diagnosing epilepsy 67

4.4.3 Advantages of the SSI as an EEG marker of epilepsy . . . . . 68

**Conclusions and future work** . . . . . **69**

4.4.4 Conclusions . . . . . 69

4.4.5 Future work . . . . . 70

4.4.5.1 Intracranial EEG study . . . . . 70

4.4.5.2 Scalp EEG study . . . . . 72

**References** . . . . . **75**

**Appendix I Additional results for predicting surgical outcomes using the random forest classifier** . . . . . **85**

A Statistical analysis of SSI distributions . . . . . 85

B Test set ROC curves . . . . . 86

C Probability of success stratified by clinical covariates . . . . . 87

**Appendix II Predicting surgical outcomes using logistic regression** . **89**

A Methods . . . . . 89

A.1 Modeling the probability of a successful outcome as a function of source-sink indices . . . . . 89

A.2 Statistical Analysis . . . . . 90

A.2.1 Predictive Power of SSIs . . . . . 90

B Results . . . . . 91

B.1 Source-sink metrics perform well in predicting surgical outcomes 91

B.2 The source-sink metrics are highly correlated with treatment outcomes . . . . . 93

B.3 Generalizability of source-sink indices . . . . . 94

**Appendix III Clinical correspondence stratified by clinical covariates 98**

# List of Tables

3-I Dataset demographics . . . . . 21

I-I Comparison of SSI distributions in EZ versus non-EZ channels . . . . 85

# List of Figures

**Figure 1-1** Clinical workflow of invasive monitoring . . . . . 5

**Figure 2-1** Source-sink hypothesis . . . . . 11

**Figure 2-2** An example of actual versus estimated iEEG signals . . . . . 15

**Figure 2-3** Diagram of the source-sink algorithm . . . . . 16

**Figure 3-1** Schematic of the experimental design for predicting surgical outcomes . . . . . 26

**Figure 3-2** Source-sink results for three patient examples . . . . . 33

**Figure 3-3** Temporal stability of source-sink indices . . . . . 35

**Figure 3-4** Results of predicting surgical outcomes . . . . . 37

**Figure 3-5** Predicted probability of success stratified by surgical outcomes 40

**Figure 3-6** Clinical correspondence between CA-EZ and top SSI regions 42

**Figure 3-7** Source-sink characteristics as the brain moves towards a seizure 44

**Figure 3-8** Temporal SSI modulation in CA-EZ versus CA-NEZ channels 46

**Figure 4-1** Simplified schematic of the scalp EEG approach . . . . . 58

**Figure 4-2** Source-sink hypothesis in scalp EEG . . . . . 60

**Figure 4-3** Schematic of the experimental design for predicting diagnostic outcomes . . . . . 61

**Figure 4-4** Source-sink results for two patient examples . . . . . 64

**Figure 4-5** Results of predicting diagnostic outcomes . . . . . 65

**Figure I-1** Test set ROC curves . . . . . 86

**Figure I-2** Predicted probability of success stratified by clinical covariates 87

**Figure I-3** Predicted probability of success stratified by clinical centers . 88

**Figure II-1** ROC curves and coefficients of the logistic regression model . 92

**Figure II-2** Training and test set performance of the logistic regression model . . . . . 93

**Figure II-3** Predicted probability of success using the logistic regression model . . . . . 94

**Figure II-4** Predicted probability of success stratified by clinical covariates 96

**Figure II-5** Predicted probability of success stratified by clinical centers . 97

**Figure III-1** Clinical correspondence stratified by clinical covariates . . . 99

**Figure III-2** Clinical correspondence stratified by clinical centers . . . . . 100

# Chapter 1

# Introduction

## 1.1 Epilepsy

Epilepsy is one of the most common neurological disorders and affects over 60 million people worldwide [1]. It is characterized by unprovoked, recurrent seizures, which are described as a sudden alteration of neurologic function caused by excessive, hypersynchronous electrical activity of neurons in the brain [2]. Epilepsy can take many forms which manifest in different types of seizures. Seizures are defined based on their initial manifestations as focal, generalized, unknown or unclassifiable [3, 4]. Focal seizures originate in one or a few regions of the brain before spreading to other brain regions and are limited to one hemisphere [3], whereas several regions in both hemispheres are activated simultaneously at the onset of generalized seizures. In seizures of unknown onset, the initial signs remain unknown, but other symptoms are known, and finally, unclassifiable seizures are seizures with unknown onset and manifestations [4]. Although seizures are the main characteristic of epilepsy, a single seizure event is not necessarily synonymous with epilepsy. In fact, approximately 8-10% of the population will experience a seizure during their lifetime, but about 2-3% of individuals go on to develop epilepsy [5].

## 1.2 Challenges in diagnosing epilepsy

When an individual first presents with a seizure, evaluation and management of the patient depend primarily on clinical analysis and scalp electroencephalography (EEG) findings as clinicians work through a comprehensive evaluation process to make a diagnosis and simultaneously exclude other possible causes for the seizure event. Namely, the diagnosis of epileptic seizures and epilepsy depends on various factors such as a thorough clinical history, recounting of events by the patient or family, neurological examination, MRI scan, and a 20-30 minute scalp EEG recording [5–8].

Scalp EEG plays a central role in confirming epilepsy as the correct diagnosis, but is only useful if abnormalities, such as interictal (i.e., between seizures) epileptiform discharges (IEDs) or focal slow activity, are present in the signals. Unfortunately, the presence of EEG abnormalities varies from 29-55% [9, 10], thus often requiring multiple repeated EEG recordings and resulting in delayed diagnosis for a significant number of epilepsy patients. After a single unprovoked seizure, the risk for another is 40-52% [11] and consequently, if the epilepsy syndrome is left untreated as correct diagnosis is being confirmed, patients experience an increased risk of seizure recurrence and status epilepticus.

Conversely, artifacts that obscure the EEG and diminish its readability are present in almost all EEG recordings. These artifacts commonly lead to misinterpretation of the EEG as being abnormal [12] and overinterpretation of EEG is a major contributor to misdiagnosis [13]. In addition, seizures are a symptom of an underlying disease process and they can occur with a variety of conditions involving the central nervous system (CNS) [14]. Before determining whether paroxymal events are the result of an epileptic syndrome, two alternatives must be considered. First, some non-neurological conditions may trigger an epileptic seizure. Febrile seizures are, for example, relatively common during early childhood and conditions such as sleep deprivation, hypoglycemia,

CNS infection or head traumas may all trigger a single seizure event [15]. The second alternative are non-epileptic events that mimic epileptic seizures, such as vasovagal syncope, parasomnias and movement disorders. These events most commonly involve psychogenic non-epileptic seizures (PNES), but as many as 25-35% of patients who undergo prolonged EEG monitoring have PNES [10, 16, 17]. Overall, many conditions can imitate epileptic seizures and misdiagnosis rates reach nearly 30% [10]. A false-positive diagnosis not only comes with mistreatment of the actual underlying disease and unnecessary exposure to side effects of anti-epileptic medications, but carries with it all the handicaps of an epilepsy diagnosis and may have severe psychological, social and economic consequences [16–19].

## 1.3 Management of epilepsy

### 1.3.1 Anti-epileptic drugs

Once an individual has been diagnosed with epilepsy, the first step involves identification of the epileptic syndrome and seizure types so that adequate treatment options can be provided to the patient [15]. Anti-epileptic drugs (AEDs) have the ability to protect against onset and spread of seizures while still allowing normal functioning of the nervous system and generally serve as the first treatment of choice for most patients with epilepsy. For around two thirds of epilepsy patients, the use of AEDs is sufficient to keep their seizures under control. However, the remaining 30% have drug resistant epilepsy and continue to experience seizures despite appropriate AED treatment [20–23].

### 1.3.2 Drug resistant epilepsy

Drug resistant epilepsy (DRE) is defined as a failure of adequate trials of two or more tolerated, appropriately chosen AEDs to achieve freedom from seizures [21] and is a significant determinant of low quality of life in epilepsy patients. Patients with

DRE commonly experience comorbid illnesses, an increased risk of mortality and are frequently hospitalized, accounting for 80% of the $16 billion spent annually treating epilepsy patients [24–27]. The burden of DRE, however, is much greater than direct financial costs. In combination with physical consequences of uncontrolled seizures, DRE is a debilitating illness where individuals lose their independence and is strongly associated with an increased risk of behavioral, psychological and cognitive issues. Patients often experience social stigma and exclusion and have restricted educational, employment and driving opportunities, all of which may have great emotional, social and even financial impact and ultimately contribute to a reduced quality of life in these individuals [24, 28–30].

## 1.4 Treatment options for DRE patients

When seizure control is not achieved with medication, other alternatives including surgery, neurostimulation or ketogenic diet, must be considered [31]. The most effective treatments for DRE are interventions that surgically remove or disconnect the epileptogenic zone (EZ), which is defined as the minimal area of brain tissue that is responsible for initiating seizures and whose removal (or disconnection) is necessary for complete seizure-freedom. [32]. A successful surgical outcome depends on the type of epilepsy and the ability to precisely identify and completely remove the EZ, but current surgical success rates vary significantly, rendering between 20-80% of patients seizure free, depending on a variety of clinical factors [33, 34].

### 1.4.1 Pre-surgical evaluation

The objective of resective surgery is the complete removal, inactivation or disconnection of the EZ, with preservation of eloquent cortex (i.e., brain areas that directly control language, motor or sensory functions). Before surgery, patients undergo a thorough evaluation process to determine the location and extent of the EZ. First, scalp EEG

recordings and an MRI scan are obtained, and a detailed assessment of seizure semiology is performed to hypothesize the location of the EZ and determine if the epilepsy is focal, multi-focal or generalized. Second, functional testing with functional MRI (fMRI), PET, SPECT, and in some cases MEG, may be performed to further define the EZ boundaries and provide additional evidence of epilepsy type. If seizures are focal and arising from an area in or near a visible lesion on the MRI scan, then patients may go directly to surgery. If seizures are focal but the non-invasive methods are discordant or inconclusive in localizing the EZ (e.g., imaging findings are not consistent with scalp EEG findings), invasive monitoring with intracranial EEG (iEEG) is often needed [35].

Fig. 1-1 provides an overview of the clinical workflow of invasive monitoring. First, intracranial electrodes are placed either directly onto the surface of the brain (electrocorticography - ECoG [36]), or inside the brain penetrating cortical and deep brain structures (stereoelectroencephalography - sEEG [37]). Following electrode implantation, the patient remains in the hospital for several days to weeks waiting

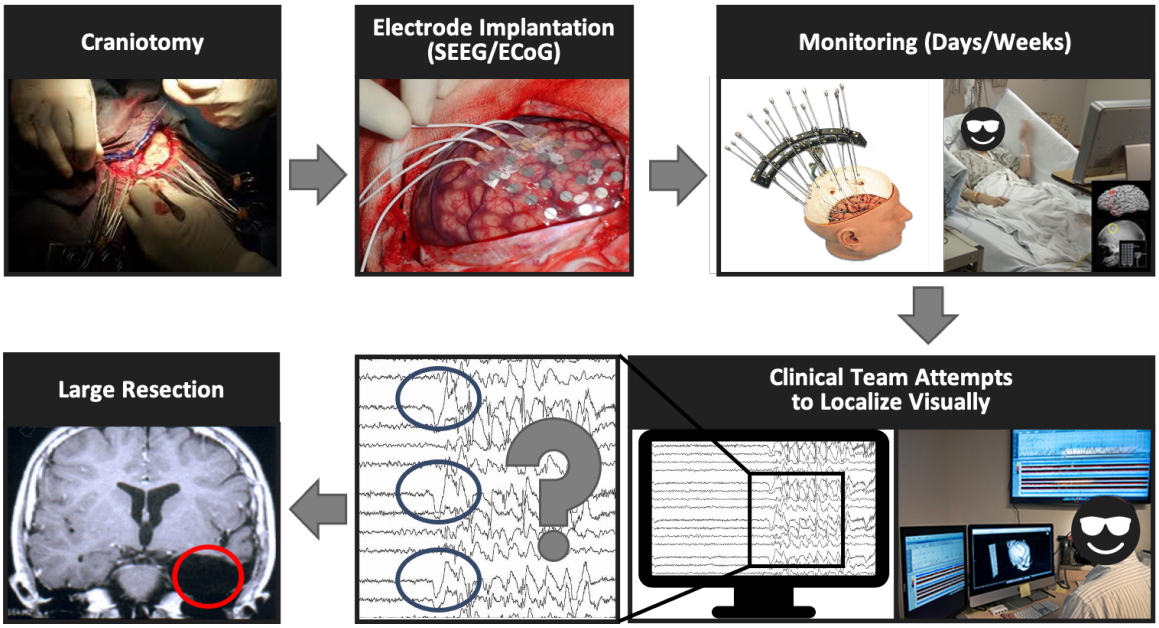


**Figure 1-1.** Clinical workflow of invasive monitoring during pre-surgical evaluation.

for a sufficient number of seizure (ictal) events because the current clinical standard primarily entails visually analyzing multiples of these events, looking for abnormal epileptic activities to localize the EZ [38]. Specifically, two types of iEEG analyses are performed by highly qualified epileptologists [39]. Ictal (seizure) recordings are inspected to identify various epileptic signatures such as repetitive spikes, rhythmic slow waves or rapid fast intracortical frequencies [38, 40, 41]. Based on these findings, a multidisciplinary team of clinicians then form a hypothesis on which electrodes are recording from the EZ. Ictal iEEG data are of higher value for localization purposes, but interictal (between seizure) iEEG data are also inspected to identify abnormal electrographic spikes. The area of cortex that generates interictal spikes is referred to as the irritative zone and channels on which such spikes are observed are denoted as possible EZ nodes [35]. However, it is often difficult to distinguish between propagated and locally generated discharges in iEEG recordings, making interictal spikes an unreliable iEEG marker for the EZ [38]. Thus, the gold standard predominantly relies on inspecting seizure events and as such, most of the iEEG recordings captured invasively from patients are not being utilized to localize the EZ.

## 1.5 Limitations of current clinical practice

Current diagnostic and management procedures in patients with epilepsy rely on detecting sporadic EEG signatures that may or may not be present when recordings are performed. In fact, to emphasize what was said above, the yield of abnormalities necessary to confirm epilepsy diagnosis on a patient's first scalp EEG recording is less than 50% on average and moreover, scalp EEG is prone to artifacts that can imitate epileptic EEG signatures. The result is a delayed diagnosis or misdiagnosis of the underlying condition, both of which may lead to serious consequences. Additionally, EZ localization primarily depends on seizure recordings, but waiting for seizures to occur results in prolonged monitoring times, which is both costly and risky to

DRE patients, and worse, in some patients no seizures are captured during invasive monitoring in which case the EZ cannot be localized from the iEEG data. Finally, current surgical success rates are only around 50% on average and many surgical candidates opt out of this potentially curative procedure [42].

## 1.6 Thesis aims

There is a great clinical need to more quickly and accurately identify the underlying cause and location of seizures in the brain. The fundamental limitation of the current gold standard is its dependence on the presence of epileptic signatures in the EEG signals (scalp and invasive) during visual inspection. We aim to address some of the limitations of current clinical practice by developing a computational tool that computes an EEG marker called the source-sink index (SSI) based on a novel hypothesis on how seizures are triggered and suppressed in the epileptic brain. As such, the SSI is designed to detect the internal properties of an epileptic brain (e.g., abnormal network connectivity) not visible during visual inspection, which, unlike epileptiform activity, are always present in EEG signals. We developed and tested the source-sink index as an EEG marker through the following aims:

### Aim 1: To develop and validate source-sink algorithm

*(Aim 1.1)* We hypothesize that seizures are suppressed when the EZ is effectively inhibited by neighboring nodes. To test the hypothesis, we will develop an algorithm that identifies two groups of nodes from an interictal EEG network: those that are continuously inhibiting a set of their neighboring nodes (denoted as "sources") and the inhibited nodes themselves (denoted as "sinks"). Specifically, the tool i) estimates patient-specific dynamical network models (DNMs) from minutes of interictal EEG data, ii) uses connectivity properties of the models to reveal top sources and sinks in the EEG network and iii) quantifies the connectivity characteristics of each node

by a source-sink index (SSI). A high SSI indicates that the node is a top sink highly influenced by top sources and top sinks in the network. *Hypothesis: Epilepsy patients will have a high SSI in one or more regions (i.e., the source-sink phenomena is present in the EEG network), but non-epileptic patients will have a lower index across all regions, indicating that the regions are neither top sources nor top sinks. Further, the regions with the highest SSI in epilepsy patients belong to the EZ.*

## Aim 2: To apply the source-sink algorithm to interictal intracranial EEG to localize the epileptogenic zone

*(Aim 2.1)* We will validate the SSI as an iEEG marker of the EZ in a retrospective analysis of 65 DRE patients who underwent sEEG implantation followed by surgical treatment, and whose outcome is known. For each patient, we will apply our methods from Aim 1 to construct an iEEG DNM and compute SSI for each network node (iEEG channel) to identify pathological nodes that correspond to the EZ. *(Aim 2.2)* We will evaluate performance by i) comparing the EZ channels identified by our algorithm to those identified by clinicians and ii) predicting surgical outcomes as a function of source-sink features by employing the random forest and logistic regression frameworks. *Hypothesis: iEEG channels that belong to the clinically annotated EZ will have a high SSI in patients with successful surgical outcomes, but lower in patients with failed outcomes.*

## Aim 3: To test further application of the source-sink algorithm to other modalities

*(Aim 3.1)* 57 patients (27 epilepsy patients and 30 non-epileptic patients with PNES) will be used to test the SSI as an interictal scalp EEG marker of epilepsy. All patients will have normal EEGs, i.e. with no epileptic abnormalities present in the scalp EEG recordings. As scalp EEG is prone to artifacts, we will first perfom artifact removal before applying our methods from Aim 1 to construct an interictal DNM for each

patient and compute SSI for each EEG channel. *(Aim 3.2)* We will then split the data into a training and a test set and use the training set to construct a logistic regression model that predicts whether a patient has epilepsy or not from the SSI distribution across all EEG channels. Finally, we will apply the model to the test patients and evaluate performance by comparing the predicted diagnostic outcome to the actual clinical diagnosis of each patient. *Hypothesis: Epilepsy patients will have a high SSI in one or more EEG channels but non-epileptic patients will have lower SSI across all channels.*

# Chapter 2

# Detecting sources and sinks from EEG recordings

## 2.1 Source-sink hypothesis: Sources and sinks in the epileptic brain network

The clinical gold standard for pre-surgical evaluation of epilepsy patients primarily involves visual inspection of seizure events to localize the EZ. In contrast, we performed our analysis exclusively on interictal, seizure-free data. This leads to a fundamental question: *how can one identify where seizures start in the brain without ever observing a seizure?* Our source-sink hypothesis states that pathologic epileptogenic regions (denoted as "sinks") are persistently being inhibited by neighboring regions (denoted as "sources") during interictal periods to suppress seizures.

The concepts of sources and sinks within a network is well established and has been applied to many analyses of network systems [43]. As schematically represented in Fig. 2-1, a source node in our application is a region in the brain network that is highly influential to other nodes but is not being influenced by other nodes. In contrast, a sink node is a region that is being highly influenced by the activity of other nodes but is not influential itself. During rest (i.e., when patients are not having a seizure, Fig. 2-1, top), our conjecture is that seizure onset is prevented by a strong inhibition exerted on the EZ by its neighboring brain regions (sources), which restricts

the discharge and propagation of the seizure activity. In other words, EZ regions are sinks that cannot influence the rest of the network. When an epilepsy patient has a seizure however (Fig. 2-1, bottom), the EZ is triggered and the EZ nodes transition into sources as they work together as a collective group to initiate and spread seizure activity.

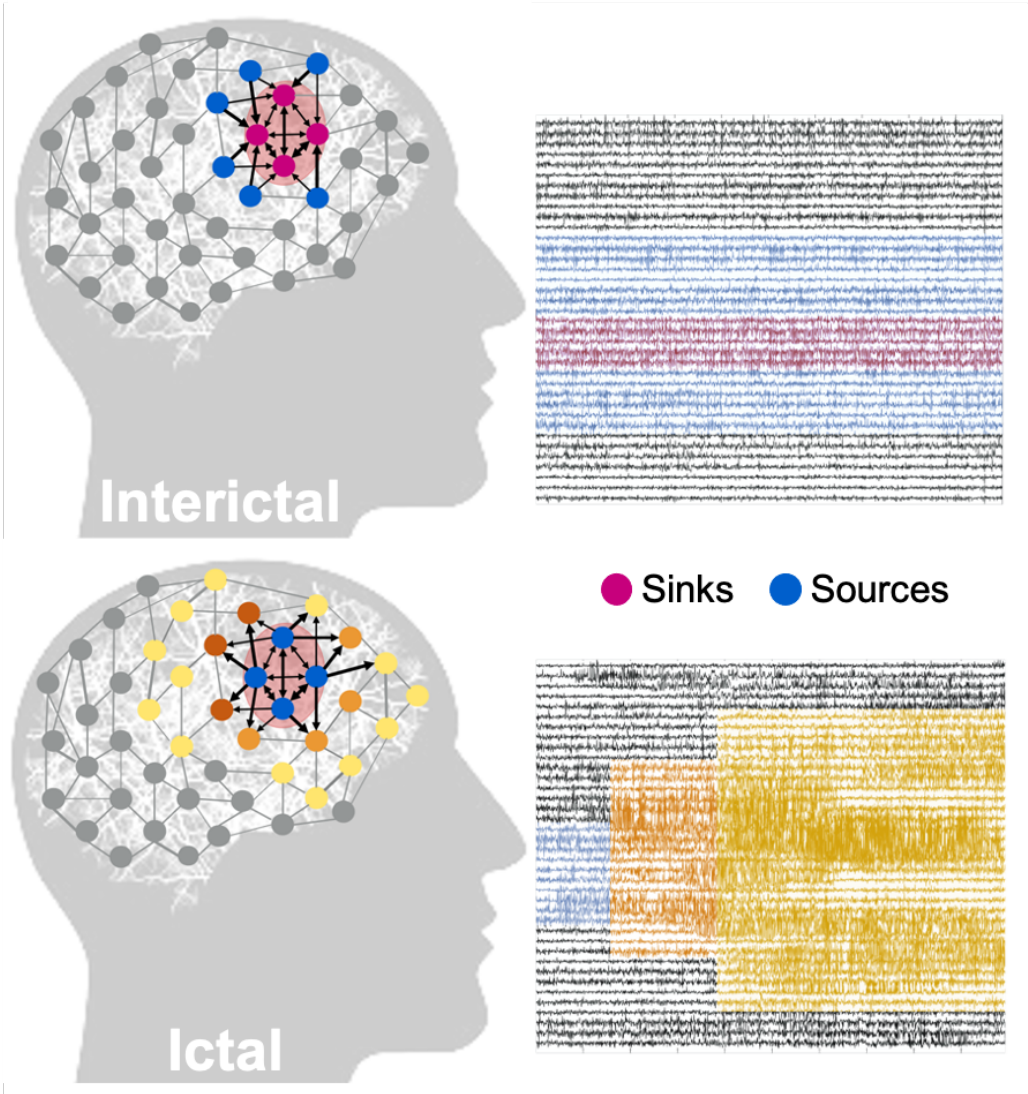


**Figure 2-1.** Source-sink hypothesis. Top: During interictal periods, epileptogenic nodes (shaded red region) are sinks that are strongly inhibited (influenced) by neighboring regions (sources) to prevent seizures. Bottom: During ictal (seizure) periods however, epileptogenic nodes become sources as they work together as a tightly coupled group to initiate and spread epileptogenic activity to other regions of the brain.

### 2.1.1 Biological evidence supporting the source-sink hypothesis

From a cytological perspective, the source-sink hypothesis is supported by evidence that seizures are prevented when the EZ is effectively inhibited by other brain regions. Glutamate, the primary excitatory neurotransmitter in the brain, has been implicated as a neurotoxic agent in epilepsy and studies have also suggested that a relative imbalance between glutamate and the inhibitory neurotransmitter GABA plays a central role in epilepsy [44]. Healthy brain function requires a balance between glutamate uptake and release to maintain the concentration of extracellular glutamate within a homeostatic range [45]. Several studies have demonstrated the existence of elevated levels of extracellular glutamate in animal models of epilepsy [46] and in human epilepsy patients [47]. In addition, the presence of sodium dependent glutamate transporters (GLTs) is thought to be crucial to prevent accumulation of neurotoxic levels of glutamate in the extracellular space by clearing unbound extracellular glutamate [47]. Findings suggest that fluctuations in the expression of GLTs may play a role in the expression of epileptogenicity [48]. In fact, previous studies have shown an increased number of GLTs in human dysplastic neurons and posit that this enables a "protective" inhibitory mechanism surrounding the epileptogenic cortex [49]. Taking this evidence together, the inhibitory (the sink phenomena) and the excitatory (the source phenomena) events within the potential EZ may have a biological substrate in the differential expression of glutamate transporters within the EZ. Finally, the inhibitory hypothesis is further supported by studies of microglia, a type of glial cells in the brain, which showed that microglia suppress (inhibit) neuronal activity and that the lack of these cells causes increased synchrony of neurons leading to seizure progression in the brain [50].

### 2.1.2 iEEG studies supporting the source-sink hypothesis

iEEG studies also provide evidence that support our source-sink hypothesis. Several studies have demonstrated a high inward directed influence to the EZ at rest [51–53]. In a recent study by Narasimhan et al. [51] the authors state that high inward connectivity may reflect inhibitory input from other regions to prevent the onset and spread of seizure activity, but the direction of these signals may flip when seizure activity begins. This conjecture is further supported by iEEG studies in neocortical epilepsy demonstrating functional isolation of epileptogenic areas at rest [54] and that increased synchronization in seizure-onset regions may be suggestive of an inhibitory surround [55, 56]. Specifically, Kini et al. showed that in patients with good (but not poor) post-surgical outcomes, removal of these regions causes an decreased network synchronizability at seizure onset, suggesting a greater resistance to the propagation of seizure activity throughout the network [55]. This was further demonstrated in a study by Schevon et al., where they demonstrated how hypersynchronous recruitment in seizure-onset regions leads to a seizure, but that desynchronized firing in the surrounding areas reflects a protective inhibitory restraint opposing epileptic spread [56]. It has also been hypothesized that widespread network inhibition seen in temporal lobe epilepsy may have evolved to prevent seizure propagation [55] and that a reduction of the inhibitory influence may lead to increased excitability and propagation of seizure activity [57].

In this work, we formalize the above evidence and build dynamical network models (DNMs) of the interictal EEG activity to identify sources and sinks of the network from DNM connectivity parameters. Source-sink indices are computed for each network node (see below) to i) identify pathological nodes most likely belonging to the EZ using invasive EEG data and ii) identify epileptogenic brain networks using scalp EEG data.

## 2.2 Dynamical network models

The DNMs are generative models that characterize how each EEG channel dynamically influences the rest of the network. The interictal DNM takes the form of a linear time-varying (LTV) model that mathematically describes how each observed brain region (i.e., EEG channel signal) interacts with the other regions. The LTV DNM is composed of a sequence of linear time invariant (LTI) DNMs derived from smaller windows of the data. Specifically, we split the EEG data into 500-msec windows and construct an LTI model in each window. Each LTI model takes the following form:

$$\boldsymbol{x}(t+1) = \boldsymbol{A}\boldsymbol{x}(t) \tag{2.1}$$

where $\boldsymbol{x}(t)\epsilon\mathbb{R}^{Nx1}$ is the state vector and represents the EEG channels, $\boldsymbol{A}\epsilon\mathbb{R}^{NxN}$ is the state transition matrix, which describes how the EEG channels interact and how their activity evolves over time and $N$ is the total number of EEG channels. The DNMs are generative and thus can simulate the EEG data given the initial state at $t = 0, x(0)$, and importantly, systems theory can be employed to uncover the dynamics and properties of the DNMs which we will use to ultimately assist in accurately localizing the EZ and identifying epileptogenic networks. In our previous work, we showed how LTV DNMs can be derived using least squares estimation and that they accurately reconstruct iEEG (ECoG and sEEG) time series [58]. See Fig. 2-2 for an example of actual versus reconstructed iEEG data using the DNMs.

In these models, element $\boldsymbol{A}_{ij}$ describes how the *present* activity of EEG channel $j$ influences the *future* activity of channel $i$. More generally, the $i$-th row of $\boldsymbol{A}$ dictates the EEG network's cumulative functional effect on node $i$, while the $j$-th column determines the functional effect that the activity of node $j$ exerts on the entire network.

Although the sensitivity of iEEG recordings is higher than that of traditional EEG and they provide a much more direct measure of local neuronal population activity, each iEEG channel records the activity of about half a million neurons [59].

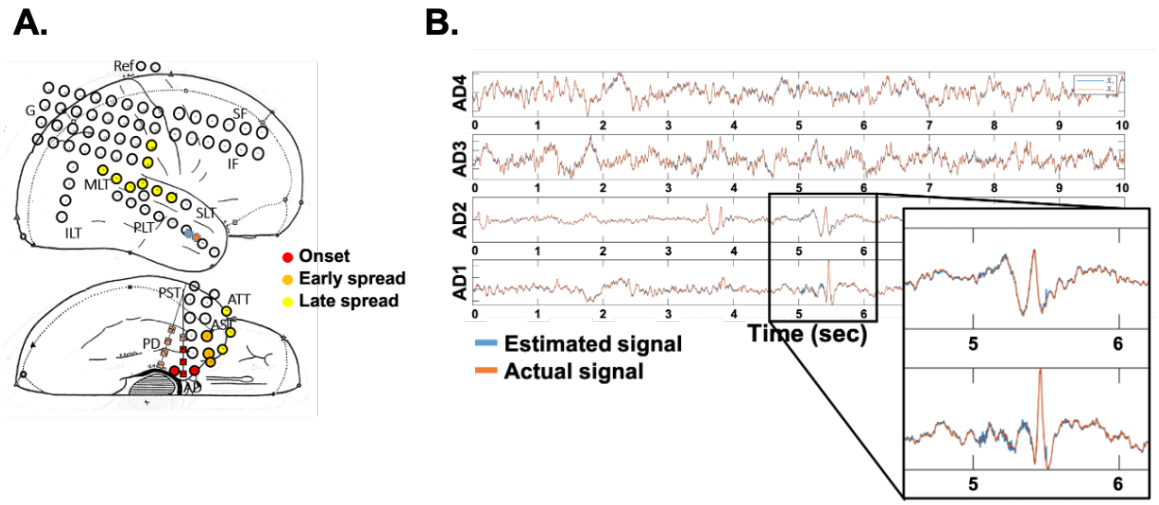


**Figure 2-2.** A. ECoG implantation of patient. B) 10 second snapshot of actual (orange) versus simulated (blue) signals of four iEEG channels from one depth electrode. All four channels belong to the clinically annotated EZ. Interictal spikes, present in two signals (AD1-2), are accurately captured by the network model.

Consequently, the DNMs (scalp EEG and iEEG) cannot distinguish between excitatory and inhibitory connections in the EEG network. Instead, we only quantify the strength of the connection between two nodes, hereafter referred to as the amount of "influence" one node has on another.

## 2.3 Sources and sinks in the EEG DNM

We define two special groups of nodes in the EEG network. A node is a *source* (blue nodes in Fig. 2-3A) if its activity has a high influence on the activity of other nodes in the network, but it is not highly influenced by other nodes. In contrast, a node is a sink (pink nodes in Fig. 2-3A) if it is being highly influenced by the activity of other nodes but does not have a high influence on others. This is reflected by the rows and columns, respectively, of the state transition matrix of the DNM ($\boldsymbol{A}$ in eq. 2.1 and Fig. 2-3C). Sources are channels that generally have high values (in magnitude) in their columns (high influence on others) but low values across their rows (low influence from others), whereas sinks exhibit the opposite pattern, high row values and low column

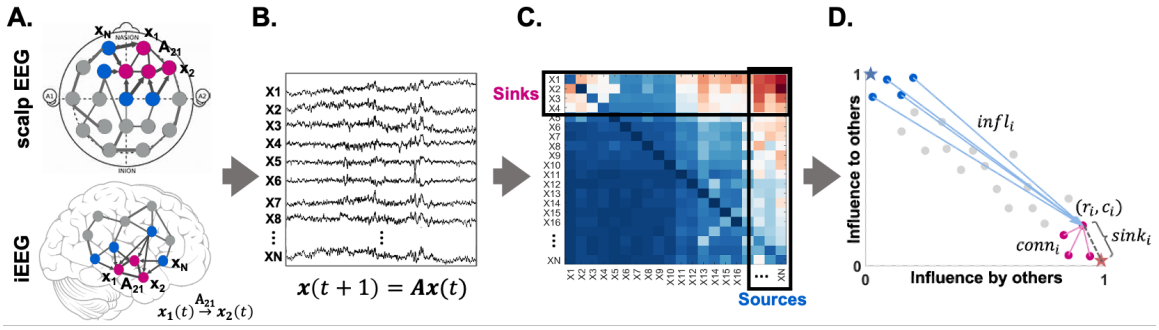


**Figure 2-3.** A. A N-channel scalp EEG (top) and iEEG (bottom) network example. B. Signals obtained from the EEG channels. C. Corresponding $\boldsymbol{A}$ matrix, estimated from the EEG signals. D. 2D source-sink representation of the EEG network with sink index ($sink_i$), source influence ($source_i$) and sink connectivity ($conn_i$) labeled.

values. In the context of the source-sink hypothesis stated above, our conjecture is that the EZ nodes are sources right before a seizure, as they unite and effectively influence other nodes in the network to start and spread the seizure activity, but become sinks at rest, when other regions are working diligently to prevent the seizures from spreading by exerting strong influence (inhibition) on the EZ.

## 2.4 Computing source-sink indices

### 2.4.1 Identifying top sources and sinks in the interictal EEG network

To identify the top sources and sinks in each DNM, we quantify the extent of each EEG channel's source or sink behavior by computing the amount of influence to and from the channel as follows. The total influence channel $i$ receives from the rest of the network in 500-msec window $w$ of the EEG data is defined as the sum of the absolute values across its row in $\boldsymbol{A}_w$ or in other words, it is equal to the 1-*norm* of its row. Similarly, we define the total influence from channel $i$ to the rest of the network as the 1-*norm* of its column in $\boldsymbol{A}_w$. Once we have the total influence to and from each channel, we place the EEG channels in the source-sink 2D space (Fig. 2-3D) by ranking the row and the column norms of all channels against each other (where rank

$1/N$ indicates the smallest 1-*norm* and rank 1 is the largest 1-*norm*) to obtain each channel's row rank ($rr$) and column rank ($cr$). When drawn in the source-sink space in Fig. 2-3D, sources are channels located at the top left (blue circles), whereas sinks (pink circles) are located at the bottom right.

### 2.4.2 Definition of source-sink indices

Once the top sources and sinks are identified, we compute a source-sink index (SSI) for each channel. The SSI is a product of three metrics subject to the source-sink hypothesis. For each channel $i$, we quantify the following metrics:

**Sink Index:** The first criterion from our source-sink hypothesis requires an EEG channel to be a top sink in the EEG network to be considered an EZ channel. The sink index captures how close channel $i$ is to the ideal sink, which is defined as a channel whose row rank ($rr$) is equal to 1 and column rank ($cr$) is equal to $1/N$ (see Fig. 2-3D, pink star). The sink index of channel $i$ is computed as:

$$sink_i^w = \sqrt{2} - ||(rr_i^w, cr_i^w) - (1, \frac{1}{N})|| \tag{2.2}$$

The larger the sink index, the more likely the channel is a sink.

**Source Index:** Similar to the sink index, the source index captures how close a channel is to the ideal source ($rr = 1/N$ and $cr = 1$, blue star in Fig. 2-3D). The source index is defined as:

$$source_i^w = \sqrt{2} - ||(rr_i^w, cr_i^w) - (\frac{1}{N}, 1)|| \tag{2.3}$$

The larger the source index, the more likely channel $i$ is a source.

**Source Influence:** The second criterion from our source-sink hypothesis for a channel to be considered an EZ channel is that it is highly influenced by the top sources of the EEG network. The source influence index quantifies how much the top sources

influence channel $i$ and is defined as:

$$infl_i^w = \sum_{j=1}^{N} abs(A_{ij}) * source_j \tag{2.4}$$

A high value of $infl_i^w$ suggests that channel $i$ receives strong influence from the top sources in the interictal DNM.

**Sink Connectivity:** The third and final criterion from our source-sink hypothesis for a node to be considered an EZ node is that it is highly connected to other sinks so that it can collaborate to generate a seizure. The sink connectivity index quantifies the strength of connections from the top sinks to channel $i$:

$$conn_i^w = \sum_{j=1}^{N} abs(A_{ij}) * sink_j \tag{2.5}$$

The higher the sink connectivity, the stronger influence channel $i$ receives from the top sinks in the network. All metrics are normalized by maximum value.

**Source-Sink Index (SSI):** Finally, a source-sink activation index is computed for each EEG channel in each window as:

$$ssi_i^w = sink_i^w * infl_i^w * conn_i^w \tag{2.6}$$

In line with the source-sink hypothesis, SSI is high if all three indices are high. Therefore, we expect EZ nodes to have a high source-sink index and non-EZ nodes to have a lower source-sink index during interictal periods.

# Chapter 3

# Source-sink analysis for localization of the epileptogenic zone on interictal intracranial EEG data

## 3.1 Introduction

### 3.1.1 Computational approaches to identify iEEG markers to assist in EZ localization

In recent years, epilepsy has been increasingly conceptualized as a network disorder rather than a single source of pathology in the human brain [60–63]. Intracranial EEG offers a unique opportunity to observe rich epileptic cortical network dynamics, which are most visible to the naked eye during seizures. However, the need for seizure occurrence makes localization of the EZ a costly and time-consuming process and the prolonged invasive monitoring poses an increased risk to DRE patients [36]. The process is also subjective, as no consensus objective iEEG markers are used in the clinical workflow to specifically assist in the identification of the EZ although many attempts have been made to automate the process.

In line with the standard of care visual analysis, most of the proposed localization methods depend on seizure data (e.g., [61, 64–73]). Nevertheless, using interictal data has been of high interest as well, as this could significantly speed up the invasive monitoring process. A large number of computational studies have applied network-

based measures to identify the EZ [61, 72–77]. However, such measures (e.g., degree distribution or nodal centrality) are not explicitly designed to capture the connectivity patterns of the EZ because they are not derived from the dynamics of the iEEG signals. Moreover, many different networks may result in identical metrics. Others have looked at spectral properties of individual iEEG channels, including detection of high frequency oscillations (HFOs) [74, 78–82] and/or interictal spikes [83–85]. However, the reliability of HFOs as an iEEG marker of the EZ is debatable [86] and by treating each channel independently, these methods fail to capture network properties of the brain. Additionally, a majority of the aforementioned methods depend on epileptiform signatures being observable in the signals rather than detecting the underlying dynamical properties of the epileptic network.

In this study, we aim to leverage interictal iEEG data to implement EZ localization. We hypothesize that when a patient is not having a seizure, it is because the EZ is being inhibited by neighboring regions. Based on this hypothesis, we tested the SSI (derived in chapter 2) as an interictal iEEG marker of the EZ by i) estimating patient-specific DNMs from interictal iEEG data and ii) using source-sink connectivity properties of the models to identify pathological nodes (iEEG channels) in the network that correspond to the EZ. We applied our algorithm to interictal iEEG snapshots from 65 patients treated across 6 clinical centers and evaluated performance by i) comparing the EZ channels identified by our algorithm to those identified by clinicians and ii) predicting surgical outcomes as a function of source-sink features by employing the random forest and logistic regression frameworks. Additionally, we compared the performance of the source-sink features to that of HFOs, a frequently proposed interictal iEEG marker of the EZ.

## 3.2 Materials and methods

### 3.2.1 Patient population

Sixty-five adults (mean age 33.5±13.0 (mean ± s.d.) years) with drug resistant epilepsy who underwent intracranial EEG monitoring with stereotacticly placed depth electrodes (sEEG) and received subsequent surgical treatment were selected retrospectively for the study. Post-sEEG surgical treatments included resective surgery (39 patients), laser ablation (17 patients) or responsive neurostimulation (RNS, 9 patients). Patients were treated at one of the following institutions: Cleveland Clinic (CC), Johns Hopkins Hospital (JHH), University of Kansas Medical Center (KUMC), University of Miami Hospital (UMH), National Institutes of Health (NIH) or University of Pittsburgh Medical Center (UPMC). All patients had a minimum of one year follow-up after their last treatment procedure to determine treatment outcomes. Patients who had a follow-up period of less than one year and patients who did not receive treatment following pre-surgical evaluation (e.g. due to non-localizable EZ or EZ located in eloquent cortex) were excluded from the study. Patient population statistics are summarized in Table 3-I. The study was approved by the Institutional Review Board (IRB) at each clinical institution; Cleveland Clinic's IRB, Johns Hopkins Medicine

**Table 3-I.** Dataset demographics

| | **Number of patients** | **Gender (M/F)[a]** | **Age (years)** | **Surgical outcome (S/F)[b]** | **MRI findings (NL/ABN)[c]** |
|---|---|---|---|---|---|
| **CC** | 29 | 15/14 | $30.5 \pm 12.3$ | 13/16 | 26/3 |
| **KUMC** | 9 | 4/5 | $39.7 \pm 16.9$ | 4/5 | 6/3 |
| **JHU** | 5 | 2/3 | $35.3 \pm 18.3$ | 3/2 | 0/5 |
| **UMH** | 8 | 6/2 | $35.3 \pm 12.7$ | 1/7 | 5/3 |
| **NIH** | 9 | 7/2 | $33.1 \pm 9.3$ | 4/5 | 5/4 |
| **UPMC** | 5 | 3/2 | $36.6 \pm 12.0$ | 3/2 | 4/1 |
| **Total** | **65** | **37/28** | $\mathbf{33.5 \pm 13.0}$ | **28/37** | **46/19** |

[a] M=males, F=females,
[b] S=successful outcome, F=failed outcome,
[c] NL=MRI normal, ABN=Abnormal findings on MRI

IRB, University of Kansas Medical Center IRB, University of Miami Human Subject Research Office, National Institutes of Health IRB, and the University of Pittsburgh IRB. All clinical decisions were made independently of this study.

### 3.2.2 Data collection

#### 3.2.2.1 sEEG recordings

The sEEG data were recorded using either Nihon Kohden (Nihon Kohden America, Foothill Ranch, CA, USA) or Natus (Natus Medical Inc., Pleasanton, CA, USA) monitoring and diagnostic systems at a typical sampling frequency of 1 or 2 kHz. A small subset of recordings was recorded at a sampling frequency of 500/512 Hz. The placement of each electrode was determined by the clinical team at each center based on patient history and available non-invasive data. For each patient, a minimum of 20 seconds and a maximum of 16 minutes of interictal snapshots (average duration $5.3 \pm 4.2$ minutes) were randomly selected for analysis. Interictal periods were sampled at least one hour away from seizures without application of specific selection criteria (such as the presence or absence of epileptiform activity).

#### 3.2.2.2 Clinical annotations of the EZ

At each epilepsy center, an EZ hypothesis was formulated independently of this study by the clinical team based on the comprehensive patient data (non-invasive and invasive) gathered throughout the presurgical evaluation process. Epileptologists describe the anatomical location and extent of the EZ by means of visual analysis of the invasive data by identifying regions involved at seizure onset. The clinically annotated EZ (CA-EZ) is defined as the anatomical area(s) to be treated (resected, ablated or stimulated) and includes sEEG channels demonstrating the earliest electrophysiological changes (generally characterized by low voltage fast activity) at the beginning of an ictal event (referred to as the seizure onset zone), as well as channels involved in early

propagation of the seizure activity.

#### 3.2.2.3 Clinical classification of surgical outcomes

Post-surgical clinical outcomes were classified by the clinical experts at each center according to the Engel Surgical Outcome Scale [87] and the International League Against Epilepsy (ILAE) classification system [88]. Successful surgical outcomes were defined as free of disabling seizures (Engel class I and ILAE scores 1-2) and failure outcomes as not free of disabling seizures (Engel classes II-IV and ILAE scores 3-6) at 12+ month post operation. Out of the 65 patients in the dataset, 28 patients had a successful surgical outcome whereas 37 patients experienced seizures after receiving treatment (failed outcome).

Previous outcome studies have shown that patients with visible lesions on MRI have higher success rates as seizures likely originate from the lesion or its vicinity thus making the EZ more easily localizable [89]. In contrast, non-lesional patients, and patients with extra-temporal or multi-focal epilepsy have higher rates of non-seizure free outcomes [40, 90–92]. To better define the clinical complexity of each patient, the clinical team assigned patients to three additional categories as follows: 1) lesional (visible lesions on MRI) or non-lesional, 2) mesial temporal or extra-temporal, and 3) focal or multi-focal.

### 3.2.3 Data pre-processing

The data were bandpass filtered between 0.5 and 300 Hz with a fourth order Butterworth filter, and notch filtered at 60 Hz with a stopband of 2 Hz. A common average reference was applied to remove common noise from the signals. Finally, sEEG channels not recording from grey matter or otherwise deemed "bad" (e.g., broken or excessively noisy or artifactual) by the clinical team's visual inspection were discarded from each patient's dataset. The continuous sEEG recordings were divided into

non-overlapping 500-msec windows for modeling and feature extraction (see details below). All data processing and analysis were performed using MATLAB R2020b (MathWorks, Natick, MA). Models for predicting surgical outcomes were built using Python3.6+ (Python Software Foundation, Wilmington, DE).

### 3.2.4 Source-sink analysis to localize the EZ

For each patient, the interictal sEEG recording was split into 500-msec non-overlapping windows and DNMs were estimated in every window $w$ of the data to obtain a sequence of $\boldsymbol{A}$ matrices over time, $\boldsymbol{A}_w, w\epsilon[1, 2, \ldots, T]$, where $T$ is the number of windows. In $\boldsymbol{A}_w$ (Fig. 2-3C), row $i$ represents the amount of influence sEEG channel $i$ receives from the rest of the network in window $w$, and column $j$ represents how the activity of channel $j$ influences the activity of all other channels in the network.

#### 3.2.4.1 Computing dynamic and constant interictal SSIs

Next, we computed SSI for every channel in each window $w$ using eqs. 2.2-2.6 resulting in a series of SSIs across windows. Unlike seizure activity, interictal activity is relatively stationary, with little deviation from a baseline value over time. As a result, there is little variation in the sequence of $\boldsymbol{A}_w$ matrices and consequently in the source-sink behavior of individual channels across windows during interictal periods. Thus, we also defined a single, constant, $\boldsymbol{A}$ matrix to represent each patient's interictal DNM as:

$$\boldsymbol{A} = \frac{1}{T}\sum_{w=1}^{T} abs(\boldsymbol{A}_w) \tag{3.1}$$

Finally, in addition to computing the dynamic source-sink metrics across windows using $\boldsymbol{A}_w$ we also computed a set of constant SSIs for each patient using $\boldsymbol{A}$ in eq. 3.1.

### 3.2.5 Quantifying temporal stability of source-sink metrics

Because of the stationarity of the interictal activity over time, we expect SSIs to be consistent and independent of the timing or duration of the interictal snapshot used for each patient. To verify that the channels reported to clinicians with the largest SSIs were consistent over time, we quantified the temporal stability of the source-sink indices (eq. 2.2-2.6) for each patient as follows. Let $A_m$ be the set of iEEG channels with the highest 10% of SSI values for each constant metric $m = \{sink, infl, conn, ssi\}$, computed from $\boldsymbol{A}$ averaged across the entire interictal recording (eq. 3.1), and let $B_m^{ws}$ be the set of the top 10% of channels with highest values for each metric $m$ computed from the average $\boldsymbol{A}$ of a smaller window $w\epsilon[1, \ldots, W]$ of length $ws$, where $W$ is the number of non-overlapping windows of length $ws$ across the patient's interictal recording. Finally, let $C_m^{ws}$ be a set of randomly selected channels of the same size as $A_m$ and $B_m^{ws}$. Then, in each window $w$, we computed the percentage of channels in $B_m^{ws}$ that were also $A_m$, i.e.

$$AB_m^{ws} = \frac{|A_m \cap B_m^{ws}|}{|A_m|} * 100 \tag{3.2}$$

Similarly, we computed $AC_m^{ws}$ as the percentage of channels in $A_m$ that were also in $C_m^{ws}$. Finally, we computed the average percentage of channels captured across all windows for each metric to obtain a distribution of values across patients, and compared to the average expected percentage of channels captured for randomly selected channels as described in Statistical Analysis below. We chose this analysis as a means to quantify whether the results presented back to clinicians, i.e., the channels with the largest SSIs, remained consistent across time.

### 3.2.6 Predicting surgical outcomes using source-sink indices

To evaluate the source-sink indices as interictal iEEG markers of the EZ, we tested their efficacy in predicting surgical outcomes by i) using them as features in a random forest (RF) classifier following the same procedure as Li et al. [64] (see Fig. 3-1 for a schematic of the experimental design), and ii) building a simple logistic regression (LR) model. We compared performance against that of clinicians as well as HFOs, the most commonly proposed interictal iEEG marker of the EZ.

In recent years, the RF prediction algorithm [93] has risen considerably in popularity. The models can however become rather complex and are more focused on prediction rather than explanation [94]. LR models on the other hand, are simple statistical models that use a logistic function to model a binary variable. In the context of

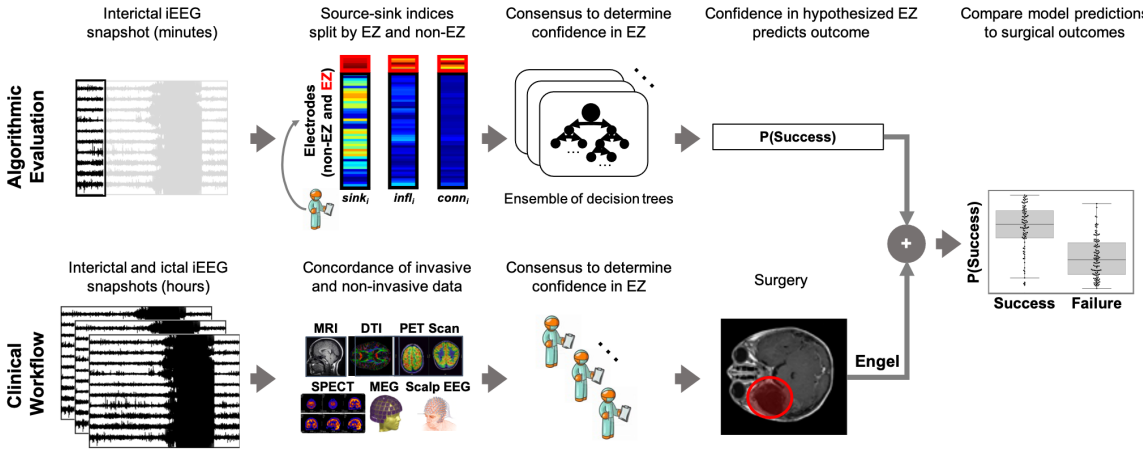


**Figure 3-1.** Schematic of the experimental design for predicting surgical outcomes. Top: From just minutes of each patient's iEEG data, we compute a set of constant source-sink indices for each iEEG channel. We summarize the indices by computing the mean and standard deviation of each index across i) EZ channels and ii) non-EZ channels and use as features in the RF classifier to compute a probability of success ($p_s$) for the patient. Finally, we apply a threshold to $p_s$ to predict surgical outcome and compare to the actual outcome of the patient. Bottom: A simplified diagram of the clinical workflow from pre-surgical evaluation to surgical treatment of DRE patients. The clinical team visually inspects hours of interictal and ictal iEEG data, in addition to various non-invasive data to come to a consensus on which electrodes are recording from the EZ. Lastly, surgery is planned to remove the EZ. Post-operatively, patients are followed for 12+ months and categorized as either success or failure based on their surgical outcome.

low-dimensional data, LR models are frequently used, particularly in scientific fields (e.g., medicine), where the focus is on both prediction and explanation [94] as they are simple and easily interpretable. In order to further explore the predictive value of the source-sink metrics, we chose to also build a LR model in comparison to the RF. Below, we briefly describe the modeling procedure using the RF classifier (see [64] for more details). Details of methodology and results for the logistic regression model are provided in Appendix II.

We modeled the probability of a successful surgical outcome $p_s$, as a function of the three source-sink index metrics (eq. 2.2-2.6) using a sparse oblique RF classifier, known as SPORF [95, 96]. Specifically, we computed the distribution of constant feature values in two sets of channels: i) the CA-EZ and ii) all other channels not labeled as CA-EZ (CA-NEZ). Feature distributions of each set of channels were summarized with the mean and standard deviation, resulting in 12 possible features presented to the RF classifier. Next, we performed a tenfold nested cross-validation (CV), considering a set of hyperparameters, and performed statistical analysis (described below) on the final classification performance to determine the most robust feature representation. Finally, we compared the predicted surgical outcome to the actual outcome of each patient.

The probability of success, $p_s$, can be conceptualized as a confidence score of the CA-EZ. In success patients, we assume that the CA-EZ was accurately identified and removed. Thus, if the source-sink indices are accurate markers of the EZ, we expect their values to be high in the iEEG channels corresponding to the CA-EZ, and consequently $p_s$ will be high. In contrast, if seizures continue (failed outcome), the CA-EZ was most likely not sufficient and $p_s$ should have a low value. In general, the prediction of surgical outcomes using any feature conditioned on the CA-EZ enables us to evaluate the overall value of the feature as a potential EZ marker.

### 3.2.7 Predicting surgical outcomes using HFOs

We compared the predictive value of the source-sink indices to that of HFOs, which have been actively explored as interictal biomarkers of the EZ. HFOs are defined as spontaneous events occurring on individual iEEG channels that clearly stand out from the background activity and are divided into three subgroups based on their frequency: ripples (80-250 Hz), fast ripples (250-500 Hz) and very-fast ripples (>500 Hz) [97, 98]. High rates of HFO events detected in the ripple and fast ripple frequency bands have been associated with seizure onset regions [99], and removal of tissue with high rates of HFOs has been associated with good surgical outcome [82, 100, 101]. We detected HFOs in the interictal data segments using the root-mean-square detector developed by Staba et al. [102] as described next.

First, the raw iEEG signals were re-referenced to a bipolar montage and artifactual segments were removed using an automated extreme value detector [103, 104]. Neural data in each channel were then bandpass filtered between 100-450 Hz (for data sampled at 1000 Hz or above) or between 100-200 Hz (for data sampled at 500 or 512 Hz) with a finite impulse response filter (passband frequency range of 100-450 Hz or 100-200 Hz with a stopband of 10 Hz). Signals were filtered both forwards and backwards in time to avoid phase distortion. The root-mean-square (RMS) of each point was computed, and segments of data in which the RMS value exceeded 5 standard deviations above the mean for at least 6 msec were recorded. After this initial detection, segments were defined as HFO events if the amplitude of at least 6 rectified peaks (three full oscillations) exceeded a threshold of 3 standard deviations above the mean of the rectified signal. HFO events were computed for each channel independently. We note that we did not perform parameter optimization when implementing this detector though optimization has been shown to impact performance [105, 106].

HFO rate (number of HFOs per minute per channel) is some of the most commonly

used metrics to test the value of HFOs as a biomarker of the EZ (e.g., [53, 78, 82, 85, 99–102, 107], to name a few). Thus, we chose to compare the performance of the source-sink indices to that of HFO rate. We computed each channel's HFO rate (HFOs/minute) by counting the total number of detected HFOs and dividing by the length of the patient's interictal iEEG snapshot in minutes. Finally, we modeled the probability of a successful surgical outcome, $p_s$, as a function of the HFO rate following the exact same paradigm as for the source-sink indices described in section 3.2.6 above.

### 3.2.8 Clinical annotations of CA-EZ and SSI correspondence

To further evaluate the SSI as an iEEG marker of the EZ, the clinical team at each center reviewed the source-sink results for each patient and ranked the correspondence between the CA-EZ and the nodes that had high SSIs. Specifically, for each patient, clinicians at the corresponding center were presented with a 2D map of the source-sink space (Fig. 2-3D) which shows the location of each implanted iEEG channel in the source-sink space, as well as the strongest connections from the top sources and sinks and where they point to. The clinical team then compared the source-sink results to the clinically annotated EZ regions and rated the clinical correspondence between the two sets as either: 1) *agreement*, defined as a) *strong agreement* if there was as a significant overlap with the clinically annotated EZ or b) *some agreement* if there was some overlap with the CA-EZ regions or the channels with the highest SSI were within the same functional network as the CA-EZ, or 2) *no agreement*, defined as no overlap with CA-EZ regions.

### 3.2.9 Statistical analysis

**Temporal stability of SSIs**: To determine the temporal stability of the interictal snapshots we first obtained distributions of $AB_m^{ws}$ and $AC_m^{ws}$ across patients by com-

puting the average percentage of captured channels over all windows for each patient. We repeated the analysis for five different window sizes, $ws = \{1, 2, 3, 5, 10\}$ minutes. Randomly selected channels (in $C_m^w s$) were resampled in each window of each window size. Then, we compared $AB_m^{ws}$ and $CB_m^{ws}$ for each $m$ and each $ws$ using a paired two-sample t-test with the null hypothesis that the two distributions have equal means and the alternate hypothesis that the means are different.

**Predictive power of SSIs**: Each RF model (source-sink and HFO) was validated using a stratified shuffle tenfold CV as done in [64], by creating ten random splits of the entire dataset into training and test sets. In each such split, the hyperparameters were tuned using the training data (70% of the dataset), and performance was then evaluated on the test set by applying a varying threshold to the model's output and computing a receiver operating characteristic (ROC) curve. The ROC curve plots true positive rates against false positive rates for various threshold values and the area under the curve (AUC) is a measure of discriminative power of the indices. The AUC ranges from 0.5 to 1, with 0.5 indicating that the model has no discrimination capacity to distinguish between the successes and failures and an AUC of 1 indicating that the model is able to perfectly distinguish between the two outcome classes. Thus, the larger the AUC, the more predictive the model is. We then selected the threshold that maximized prediction accuracy in each split and evaluated performance by comparing each patient's predicted outcome to the actual outcome.

In addition to the AUC, we used four metrics to measure model performance: a) prediction accuracy, which is the fraction of patients whose outcome the model predicted correctly, b) precision, which is the proportion of predicted successful outcomes that were actually successful, c) sensitivity, which measures the proportion of actual successful surgeries that were identified correctly and d) specificity, which refers to the proportion of failed surgeries that the models predicted correctly. We

report results of the ten CV folds (mean ± standard deviation) below.

Finally, we compared the performance metrics of the source-sink indices to those of HFO rates using a paired two-sample t-test. In all t-tests performed, the null hypothesis was that the two metrics being compared came from distributions with equal means and equal but unknown variances. The alternative hypothesis was that the metrics came from distributions with unequal means. Lastly, outcome predictions ($p_s$) of the two models were compared using a McNemar's test for paired nominal data. For all tests, a p-value $< 0.05$ was considered to be statistically significant.

## 3.3 Results

### 3.3.1 The source-sink index highlights CA-EZ regions in patients with successful outcomes

From each patient's interictal DNM (eq. 2.1), we quantified each implanted iEEG channel's source-sink characteristics by computing its SSI (eq. 2.6) and associated source-sink metrics (eq. 2.2-2.5) in every 500-msec sliding-window of the interictal recording (see Fig. 3-2A for examples of 1-minute snapshots of iEEG data and the corresponding spatiotemporal source-sink index heatmaps for three patients with different surgical outcomes). A high SSI (red/orange values) indicates that the channel is a top sink that is both highly connected to other sinks and strongly influenced by the top sources of the network. In Fig. 3-2A the channels are arranged from the highest to lowest constant interictal SSI on the y-axis and the red labels correspond to the CA-EZ regions. Fig. 3-2B shows the constant interictal SSI of each iEEG contact, overlaid on each patient's implantation map. In patient 1, the iEEG channels with the highest SSI matched the channels identified as the EZ by clinicians (three out of three). In this patient, all three CA-EZ channels were included in the surgical treatment (laser ablation) which led to a complete seizure freedom. In patient 2 however, only two out of thirteen CA-EZ regions had high SSI values whereas the other iEEG

channels with high values were not a part of the CA-EZ and thus were not treated during surgery. This patient did not become seizure free post-treatment. Finally, patient 3 demonstrates an interesting case. This patient had two surgeries; first a laser ablation of superior frontal and cingulate gyri (contacts on L' and G' electrodes) which resulted in seizure recurrence, and later a resection of pre- and post-central as well as supplementary motor areas (M' electrode) which led to a complete seizure freedom. Interestingly, when the iEEG channels first identified as CA-EZ (CA-$EZ_1$, red labels in Fig. 3-2A, bottom panel) are considered, none of these channels were amongst the channels with the top 10% highest interictal SSIs. However, the majority of the channels with highest SSI corresponded to the second identified CA-EZ (CA-$EZ_2$, M' electrode and orange labels in Fig. 3-2A, bottom panel) that ultimately led to a successful outcome in this patient.

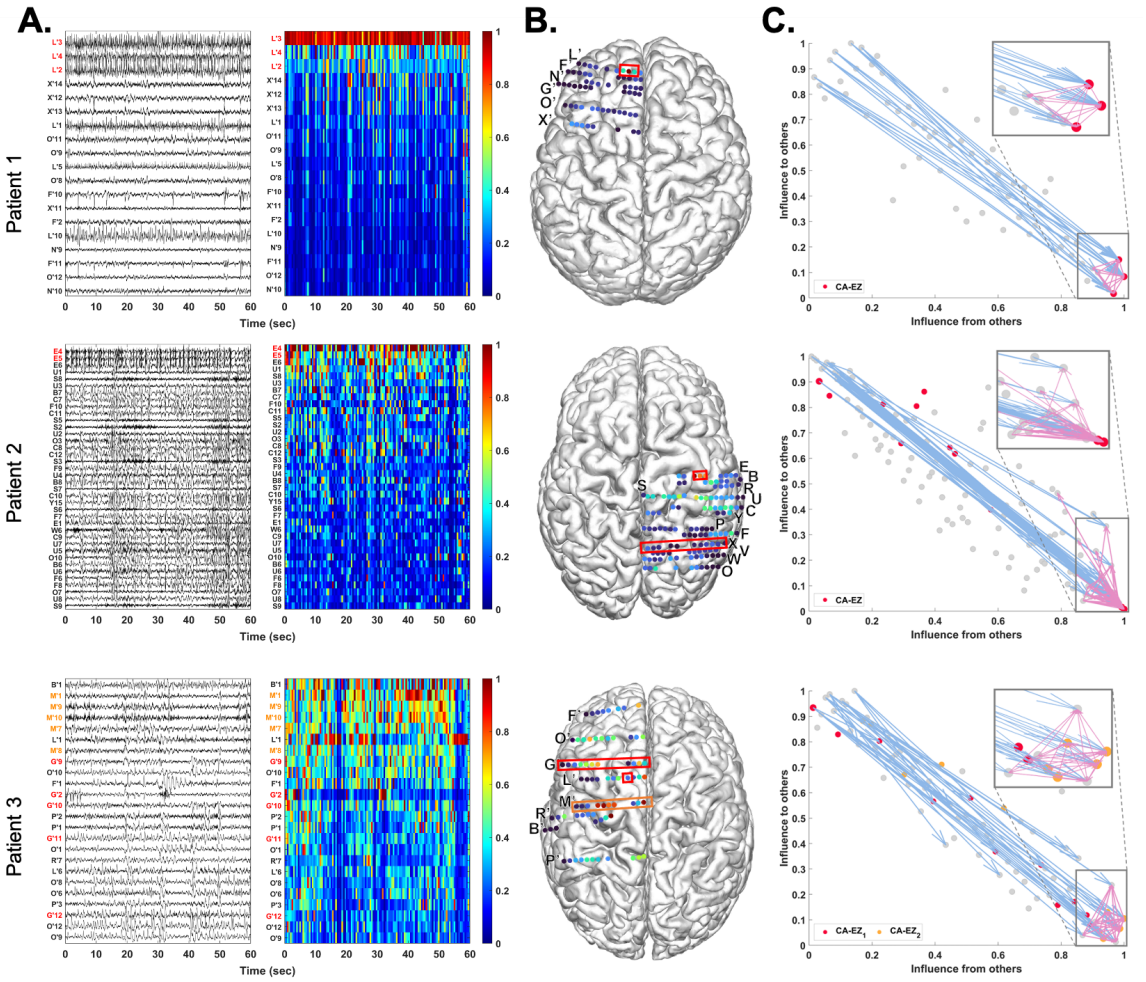


**Figure 3-2.** Three patient examples. Patient 1 (top) had a successful surgical outcome. Patient 2 (middle) had a failed surgical outcome. Patient 3 (bottom) had two surgeries. After the first surgery, the patient continued to have seizures (failed outcome) but became seizure free (successful outcome) after the second surgery. A. A 1-minute interictal iEEG snapshot (left) and the resulting SSI of every channel in that same window (right). Channels are arranged from highest to lowest constant interictal SSI. CA-EZ channels are colored red. For patient 3, the CA-EZ$_2$ channels, treated in the second surgery, are colored orange. Only the top 30% of channels are shown for better visualization purposes, and all channels not shown have low SSI values. In the success patient (top), CA-EZ channels have the highest SSIs, whereas only 2 out of 13 CA-EZ channels have a high SSI in the failure patient (middle). In patient 3 (bottom), the CA-EZ that rendered the patient seizure free corresponds to the highest SSIs. B. Stationary SSI of each channel overlaid on the patients' implantation maps. Red/orange boxes outline the CA-EZ channels. C. 2D source-sink space. Top sources are located in the top left and top sinks in the bottom right. CA-EZ channels are colored red. CA-EZ$_2$ in patient 3 is colored orange in the bottom panel. The most influential connections from sources (blue arrows) point to the sinks and the strongest connections from sinks (pink arrows) point to other sinks in patient 1 (top), whereas the top sources point to nodes other than top sinks in the failure patient (middle). Top sinks also point to these other nodes.

### 3.3.2 Temporal stability of sources and sinks during interictal periods

To test the sensitivity of the source-sink analysis to duration and timing of the interictal snapshot, we quantified the interictal stationarity of each source-sink metric and the SSI (eqs. 2.2-2.6) for five different window sizes, $ws = \{1, 2, 3, 5, 10\}$ minutes. For each $ws$, we split each patient's recording into non-overlapping windows of length $ws$ and computed the average percentage of channels with 10% highest values of the constant metric captured across all windows ($AB_m^{ws}$), as well as $AC_m^{ws}$, the average percentage of top channels that were captured by chance (Fig. 3-3). $AC_m^{ws}$ was computed for ten different sequences of randomly sampled channels in each window. As Fig. 3-3 shows, over 90% of the top channels were captured on average for all source-sink metrics—independent of the timing or duration of the interictal snapshot—compared to a much fewer channels (around 10%) captured by chance ($p \ll 0.05$ for all metrics). This suggests that given any snapshot of interictal data, even as short as 1 minute, the results would be highly comparable to those obtained from the entire interictal snapshot for each patient.

### 3.3.3 Identifying channels with highest SSI

Because of the strong stationarity of the source-sink metrics across the interictal recordings, we computed a constant, overall $\mathbf{A}$ matrix using eq. 3.1 to represent each patient's interictal DNM. From this $\mathbf{A}$ matrix, we identified the top sources and sinks in the iEEG network by computing the total influence to and from each channel and placing the channels in the 2D source-sink space (see Fig. 3-2C for three patient examples) based on their influence row and column ranks. In this space, sources are channels located at the top left, whereas sinks are located at the bottom right. In patients with successful surgical outcomes, the CA-EZ channels are expected to be a subset of top sinks (Fig. 3-2C, top). The blue and pink arrows represent the

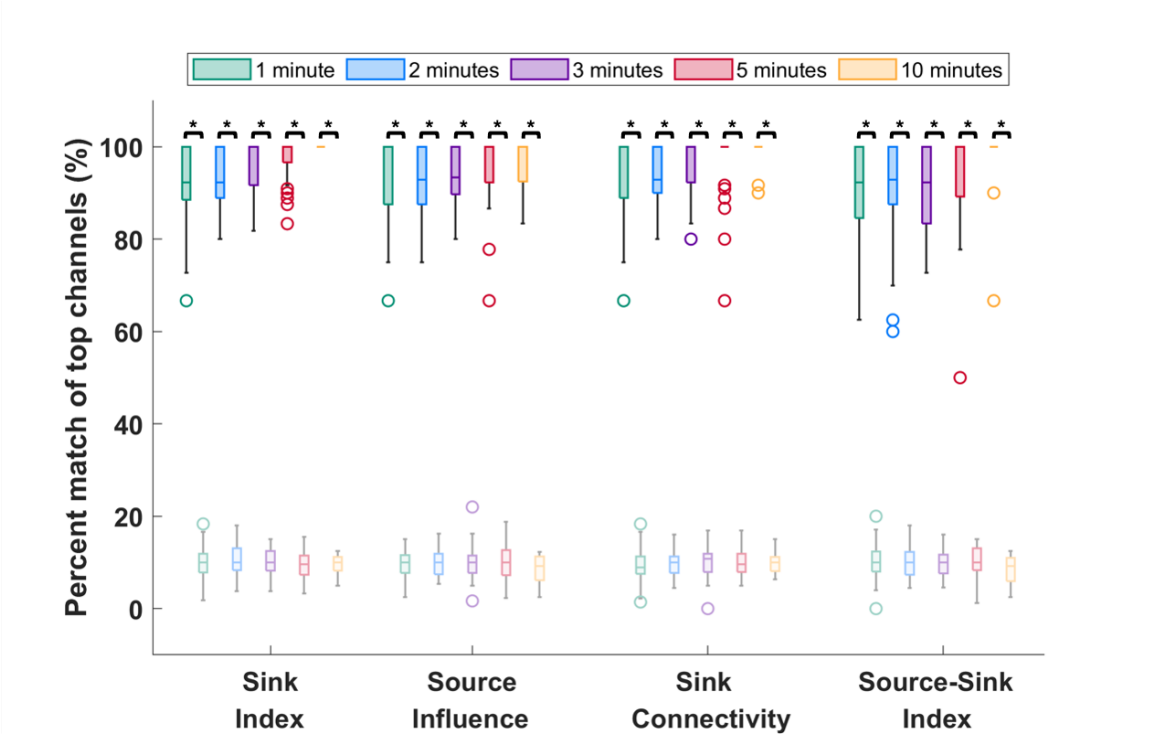


**Figure 3-3.** Temporal stability of source-sink indices. Darker colors represent distributions of source-sink indices whereas lighter colors represent channels captured by chance. On average, over 90% of channels are captured for all indices, independent of timing or duration of the interictal snapshot selected. Increasing the window size does not change the percentage of captured top channels significantly. In comparison, only around 10% of top channels are captured by chance. The asterisks indicate a statistically significant difference.

strongest connections (top 5%) from the top sources and sinks, respectively, and the channels they point to. The most likely candidates of the true EZ, based on the source-sink hypothesis, are the subset of top sinks that are highly connected to other sinks and strongly influenced by the top sources. In general, the top sources and sinks point to the CA-EZ channels in success patients (Fig. 3-2C, top), whereas they may also connect to other channels in patients with failed surgical outcomes (Fig. 3-2C, middle). In patient 3 (Fig. 3-2C, bottom), who continued to have seizures after the first surgery (failed outcome), the first set of treated channels (CA-$EZ_1$) are not amongst the top sinks in the iEEG network, whereas the majority of CA-$EZ_2$, the set of clinically annotated EZ channels that led to seizure-freedom post-surgery, are top

sinks. In addition, the latter set of channels are highly influenced by the top sources and sinks in the network and thus are considered likely candidates of the true EZ by the source-sink algorithm.

### 3.3.4 Source-sink metrics outperform HFOs in predicting surgical outcomes

As stated above, the SSI, and consequently the three metrics (sink index, source influence and sink connectivity) used to compute the SSI, are significantly higher in CA-EZ channels compared to the rest of the iEEG network in patients with successful surgical outcomes but not necessarily in failure patients ($p_{SSI}^{success} = 8.26 \times 10^{-7}$ and $p_{SSI}^{failure} = 0.151$, see other p-values in Appendix I, Table I-I). Taking advantage of this assumption, we built a RF model to predict the probability of a successful surgical outcome for each patient using i) the source-sink metrics and ii) HFO rate for comparison. The resulting test-set ROC curves are shown in Appendix I, Fig. I-1. In addition to the RF models, we also built a simple LR model using the source-sink metrics for comparison, and found that it performed very similarly. We report results of the RF model below. Results of the LR model are shown in Appendix IIB.

Figs. 3-4A and B show the predicted probabilities of success across all CV-folds, using the source-sink and the HFO model, respectively. The results are categorized by the clinical centers and the dots are color-coded based on each patient's surgical outcome. A decision threshold of $\alpha = 0.5$ (blue line) was applied to the estimated probabilities to predict each patient's outcome. Using the source-sink indices (Fig. 3-4A), the majority of success patients (red dots) are above the blue line, with $p_s > 0.5$ whereas most failure patients (black dots) are below the blue line, with a lower $p_s$ value. In contrast, there was not a clear separation between success and failure patients using HFO rate (Fig. 3-4B).

Fig. 3-4C compares the performance of the source-sink metrics and HFOs in

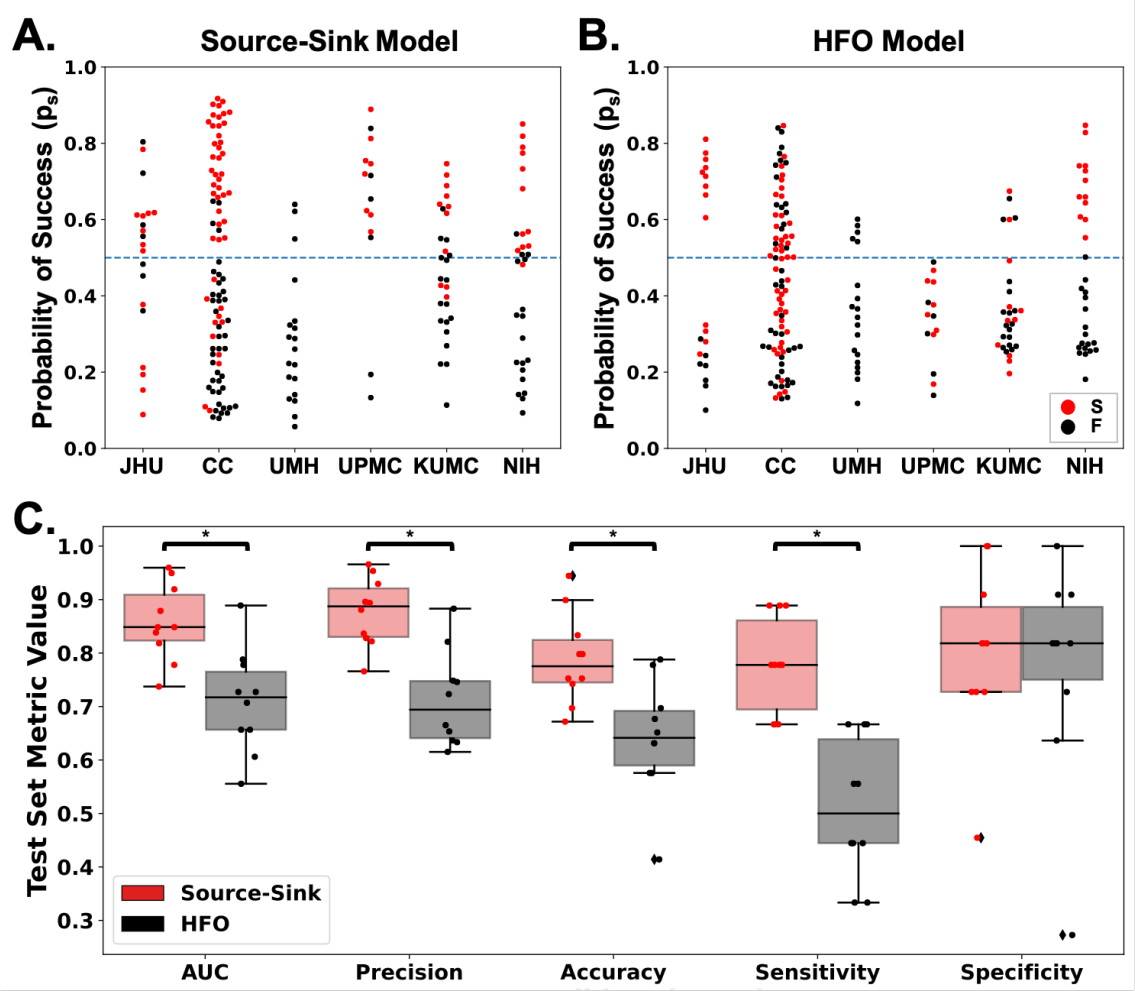


**Figure 3-4.** A. Predicted probability of success ($p_s$) by the source-sink model across all CV folds. Each dot represents one patient and dots are color-coded by surgical outcome. The dashed blue line represents the decision threshold applied to $p_s$ to predict outcomes. For the source-sink model, the majority of success patients (red dots) have $p_s$ values above the threshold whereas failure patients (black dots) generally have $p_s$ values below the threshold. B. Predicted probability of success ($p_s$) by the HFO model across all CV folds. S=success, F=failure. For the HFO model, there is not as clear separation between the success and failure patients, with both groups having $p_s$ above and below the decision threshold, thus resulting in a lower prediction accuracy. C. Performance comparison of the source-sink metrics (red) to HFO rate (black). Boxes show distributions of each metric across the ten CV folds. The source-sink model outperformed HFOs in terms of all performance metrics. The asterisks indicate a statistically significant difference.

predicting surgical outcomes.The source-sink metrics outperformed HFO rate in terms of AUC, precision and sensitivity ($p_{AUC} = 0.0096$, $p_{precision} = 0.0023$ and $p_{sensitivity} = 2.03 \times 10^{-4}$) whereas both models had a comparable specificity ($p_{specificity} = 0.7846$),

although it was slightly higher on average for the source-sink model. The source-sink metrics obtained a test-set AUC of $0.86 \pm 0.07$ compared to an AUC of $0.71 \pm 0.10$ using HFO rate. The source-sink model also outperformed HFOs in terms of average precision, which weighs the predictive power in terms of the total number of patients, with an average precision of $0.88 \pm 0.06$ compared to $0.71 \pm 0.09$ for the HFO rate. Using the source-sink indices, a threshold of $\alpha = 0.5$ applied to the estimated probability of a successful outcome for each subject ($p_s$) rendered a test-set accuracy of $79.0 \pm 9.1\%$, compared to a considerably lower accuracy of $65.5 \pm 11.4\%$ using HFOs and an even lower surgical success rate of 43% in this dataset. The biggest performance difference between the two models was in terms of sensitivity (true positive rate) where the source-sink model outperformed HFO rate by more than 50% with a sensitivity of $0.78 \pm 0.09$. However, both models performed similarly in predicting failed outcomes correctly, where the source-sink model had a slightly higher specificity of $0.80 \pm 0.16$ on average, compared to $0.77 \pm 0.20$ for the HFO model.

Note that HFO rate was computed across the entire interictal snapshot provided for each patient. The longer the snapshot, the more likely it is to capture HFOs. In contrast, although the source-sink metrics were also computed by averaging across the same recordings for each patient, we showed above that the results remain consistent independent of both timing and length of the recording.

### 3.3.5 The source-sink metrics are highly correlated with treatment outcomes

The source-sink metrics are also highly correlated with treatment outcomes. The separation between the $p_s$ distributions of success versus failure patients is greater for the source-sink model compared to the model using HFO rate, and consequently so is the model's ability to discriminate between the two outcome possibilities. In fact, we compared the performance of the two models with a contingency table (confusion

matrix) and observed that the source-sink model was statistically better with a p-value of $p = 0.007$. Fig. 3-5A compares the predicted probability of success ($p_s$) on the test set in success versus failure patients of the source-sink metrics (red) and HFOs (black). Each box represents the distribution of $p_s$ values across all CV folds. When further broken down by Engel class (Fig. 3-5B) or ILAE score (Fig. 3-5C), we observed a decreasing trend of $p_s$ as the outcome score (and thus also the severity of post-operative seizure outcome) increased using the source-sink metrics. Note that we define successful outcomes as Engel class I but as ILAE score of 1 or 2 (and failed outcome as Engel II-IV or ILAE 3-5). In contrast we did not see this clear separation of $p_s$ values using the HFO model, which had a much greater overlap between classes.

Finally, in comparison to the RF classifier, we also built a simple LR model to predict surgical outcomes using the source-sink metrics. Results of the LR model are shown in Appendix IIB. Despite being a simpler model (and as such not necessarily expected to perform as well), we found that the performance of the LR model was comparable, and only slightly worse than the performance of the RF model.

### 3.3.6 Generalizability of the SSI

We compared $p_s$ for three categories that describe the clinical complexity of each patient. Although lesional patients frequently have better localizable EZ and thus tend to have higher chances of successful outcomes, we saw no correlation to the predicted probability of success in our models (see distributions of $p_s$ color-coded by lesional versus non-lesional patients in Appendix I, Fig. I-2A). Similarly, patients with extra-temporal epilepsy (ETLE) generally have lower success rates compared to patients with mesial-temporal epilepsy (MTLE), but our tool was not sensitive to whether patients had ETLE or MTLE (Fig. I-2B). Patients with multi-focal epilepsy are often more difficult to treat because the seizures can originate from more than one brain area. This was reflected in our data where only one multi-focal patient had

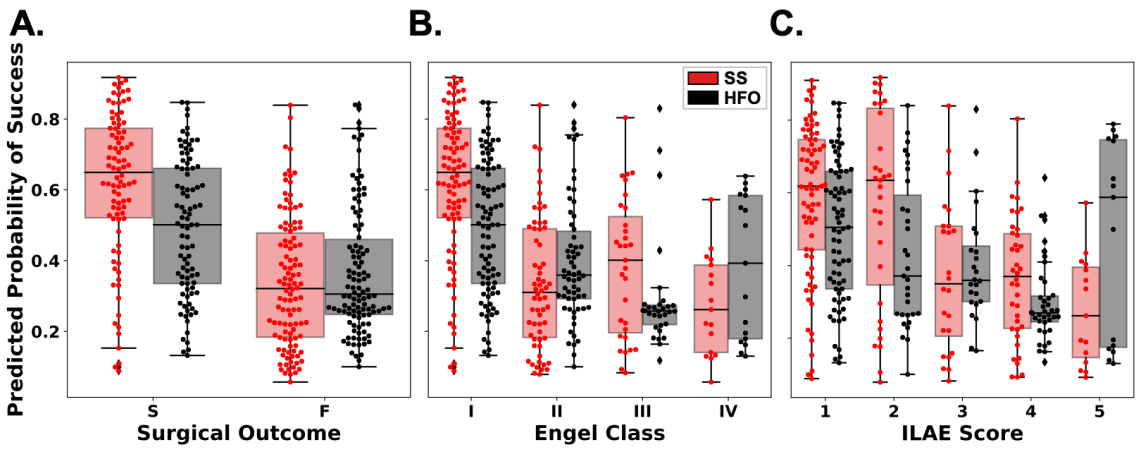


**Figure 3-5.** A. Distributions of $p_s$ as predicted by the source-sink model (red) and HFO model (black). There is a clear separation between the distributions for successful cases versus failed cases for the source-sink model whereas the distributions obtained using HFO rate significantly overlap and consequently the predictive value of HFO rates is lower. B. Distributions of $p_s$ stratified by Engel Class (Engel 1 = successful outcome, Engel 2-4 = failed outcome). For the source-sink metrics, there is a general trend of decreasing $p_s$ values as the Engel class (and thus also severity of surgical outcome) increases. In contrast, this does not hold for the HFO rate. C. Distributions of $p_s$ stratified by ILAE scores follow a similar trend to those observed for the Engel class in B. Note that for ILAE scores, we define ILAE 1-2 as successful surgical outcomes but failed outcomes as ILAE 3-5.

a successful surgical outcome and in turn, the predicted success probability of the source-sink model (Fig. I-2C) was commonly lower for these patients. Although we expect the tool to generalize across epilepsy types (focal or multi-focal), more data will be needed so that all groups are represented equally (i.e., multi-focal patients with successful and failed surgical outcomes) before conclusions can be made.

Next, we analyzed the success probability with respect to treatment method (Fig. I-2D). Patients who are surgical candidates (i.e., the seizure focus can be localized and treated) generally undergo either resective surgery or laser ablation. In patients with poorly localizable or multiple seizure foci, or when the EZ is located in eloquent cortex, surgical resection may not be an option. In these cases, many patients opt for RNS treatment instead. Because of the higher clinical case complexity, patients who receive RNS treatment are not expected to achieve complete seizure freedom, but

rather a reduction in seizure frequency [108–110]. This was reflected in the predicted probability of success by the source-sink model, which was overall lower for RNS patients compared to patients that received surgical treatment. In contrast, there was no observable correlation between $p_s$ and surgical resection or laser ablation.

Finally, we compared the distribution of $p_s$ across clinical centers. As Fig. I-3 shows, the range of $p_s$ values was similar across centers and consequently, the $p_s$ distributions were not skewed by values from any particular center (e.g., outlier patients in each surgical outcome distribution are from various centers). This robustness of performance across different clinical centers suggests that the model generalizes well to different datasets.

### 3.3.7 Top SSI regions have high correspondence to CA-EZ in success patients but lower in failure patients

The treating neurologist at each center was given the 2D source-sink maps for each patient from the corresponding center and asked to rate the correspondence between the CA-EZ and regions with top SSIs. Fig. 3-6 shows the clinical correspondence scores between the two sets of EZ regions for success versus failure patients across all centers. Correspondence scores of "some" or "strong" agreement were lumped into "agreement" for visualization purposes. In general, there was more agreement between the CA-EZ and regions with high SSIs in patients with successful outcomes compared to patients with failed surgical outcomes, which means that the source-sink analysis often highlighted other, non-treated potential onset regions, in failure patients. In fact, clinicians agreed with the algorithm in 26 out of 28 (93%) success patients, whereas only 54% of patients with failed outcomes were considered in agreement. When categorized by Engel scores (where Engel 1 is considered success and Engel 2-4 failure), the rate of agreement decreased as the Engel class increased, which likely also reflects the increased difficulty of treatment in these patients. A similar trend was observed

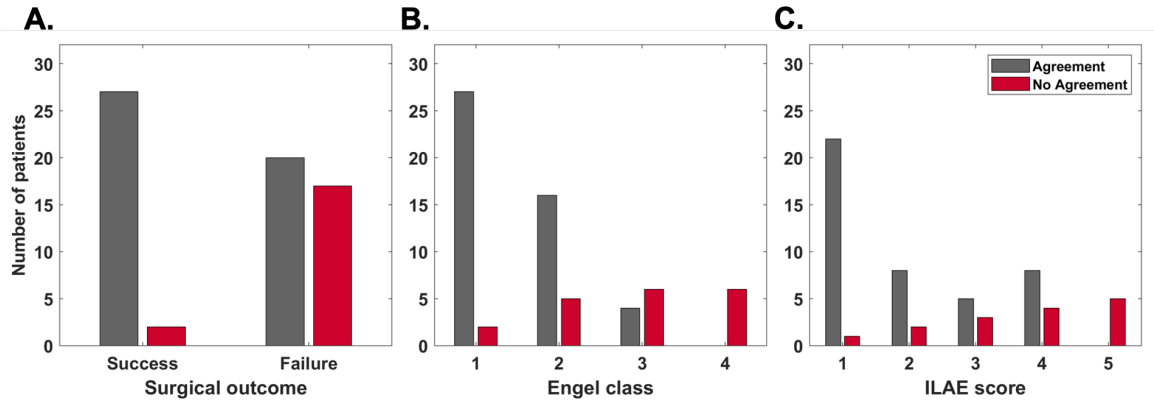


**Figure 3-6.** Clinical correspondence between CA-EZ and top SSI regions. A. Clinical correspondence stratified by surgical outcome. For almost all success patients, clinicians agree with the channels with highest SSI scores. The agreement is much lower in failure patients. Note that in some failure patients, clinicians may not be able to treat all or a proportion of the CA-EZ (e.g., if it is located in eloquent cortex). In those cases, the source-sink algorithm may agree with clinicians even though the patient had a failed surgical outcome. B. Clinical correspondence stratified by Engel class. The rate of agreement is highest for Engel 1 (complete seizure-freedom) but decreases as the Engel class increases. No-agreement scores follow the opposite trend. C. Clinical correspondence stratified by ILAE scores follow an overall similar trend with increasing disagreement (and decreasing agreement) as ILAE score increases.

for the ILAE scores, a different classification of post-surgical outcomes, with a higher rate of disagreement corresponding to a higher ILAE score. Further, we also looked at the distribution of clinical correspondence scores stratified by clinical complexity (e.g., whether patients were lesional or non-lesional, epilepsy type, treatment method, and more) and also categorized the scores by each clinical center. For all clinical complexity categories considered, the proportion of each group was similar across all correspondence scores, indicating that the tool is not sensitive to those factors. The distribution of correspondence scores was also similar across all centers, indicating that i) the tool generalized well across different datasets and ii) the overall scores were not biased by any particular center. Clinical correspondence scores grouped by clinical complexity and different centers are shown in Appendix III (Figs. III-1 and III-2, respectively).

### 3.3.8 CA-EZ regions are sinks at rest but become sources during seizures in success patients

In addition to computing the source-sink metrics across interictal recordings, we also investigated source-sink properties of the iEEG network during ictal periods. We did not receive ictal snapshots from all centers, so only a subset of the patient population ($n = 29$) was included in this part of the analysis. Fig. 3-7 demonstrates the source-sink characteristics of the iEEG network as the brain moves from interictal state towards a seizure in one success (left) and one failure (right) patient. For each patient, we computed spatiotemporal heatmaps of each iEEG channel's source-sink index (eq. 2.6) in 500-msec windows of one interictal and one ictal recording (Fig. 3-7A and B). Note that the two snapshots are not consecutive in time as the interictal snapshot is typically recorded hours before the seizure event. As Fig. 3-7A shows, the CA-EZ channels have high SSI values in the success patient during rest, suggesting they are tightly connected top sinks strongly influenced by top sources. However, during and right after seizure, the same channels have a low source-sink index, that is, they are exhibiting a strong source-like behavior, which further supports the source-sink hypothesis. In contrast, only a small subset of CA-EZ channels (2 out of 13) are amongst the top sinks in the patient with a failed surgical outcome (Fig. 3-7B) and there is little modulation of the source-sink index of these channels.

The temporal SSI modulation is summarized in Fig. 3-7C and D. We computed the average source-sink index for two groups of interest: i) CA-EZ channels, and ii) all other channels not labeled as CA-EZ (CA-NEZ). Each curve was obtained by computing the average SSI of each channel group, in each window. The curves were smoothed by computing the index across 10-second windows instead of 500 msec. As Fig. 3-7C shows, the CA-EZ channels have a much higher source-sink index compared to the rest of the network during the interictal period in the success patient. However, this does not hold true for the failure patient (Fig. 3-7D), where the mean SSI of the

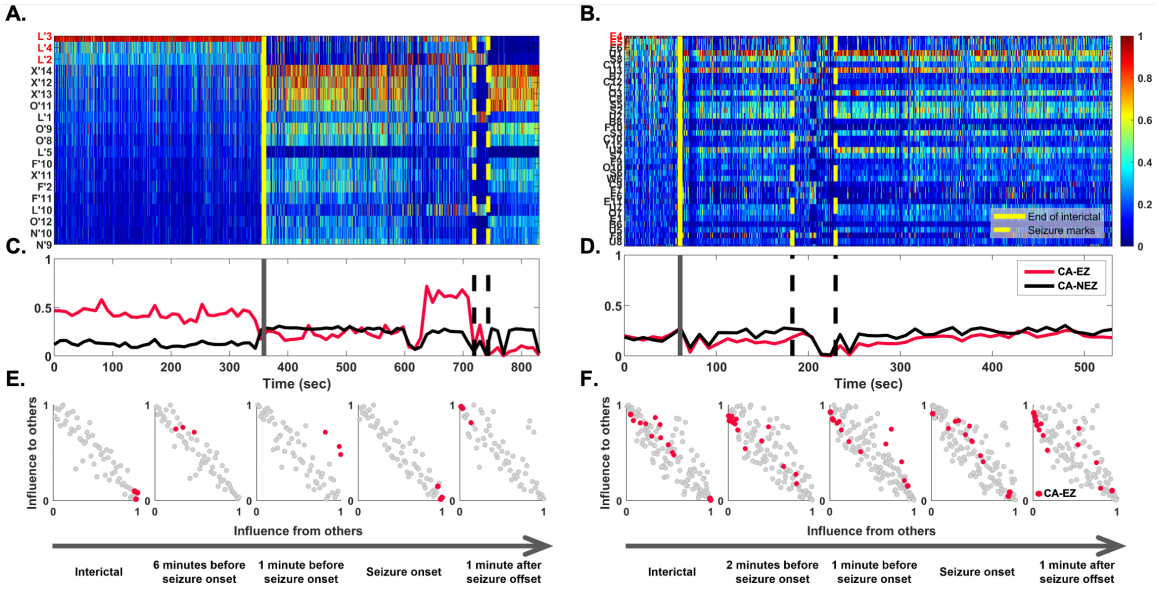


**Figure 3-7.** Source-sink characteristics as the brain moves from resting state towards a seizure. Two patient examples. A. Source-sink index of every channel during interictal (left) and ictal (right) periods, separated by the solid yellow line. Channels are arranged from highest to lowest constant interictal SSI. CA-EZ channels are colored red. Only the top 30% of channels are shown for better visualization purposes, and all channels not shown have low SSI values. B. Average source-sink index of CA-EZ versus CA-NEZ channels. In this success patient the CA-EZ channels have a much higher SSI compared to CA-NEZ channels during the interictal period. The SSI of CA-EZ channels drops significantly during seizure, as these channels become sources to initiate and spread seizure activity. D. Source-sink index of every channel over time. Only 2 out of 13 CA-EZ channels have a high SSI in this failure patient. E. Average SSI of the two groups. In this failure patient CA-EZ cannot be distinguished from CA-NEZ. E. Movement of CA-EZ channels in the 2D source-sink space over time. CA-EZ channels are top sinks during the interictal period (left), but move towards sources as the brain progresses towards a seizure. F. In this failure patient, there is little movement of CA-EZ channels as the brain moves from interictal to ictal state.

CA-EZ is not separable, or even slightly lower than the mean SSI of the CA-NEZ channels.

Fig. 3-7E and F show an example of the 2D source-sink space for the success and failure patient, respectively, computed in 10-second windows at different points in time relative to seizure onset. Despite the temporal stability of the source-sink metrics across interictal recordings, the source-sink properties of the iEEG network modulate around seizure events. In success patients (Fig. 3-7E) we frequently observed

a movement of CA-EZ towards top sources as the brain progresses towards a seizure. Right before and at the onset of seizure however, the CA-EZ channels become sinks for a short period, perhaps as the rest of the network makes one last attempt to prevent the seizure from starting. During and right after seizure, the CA-EZ channels are again exhibiting a strong source-like behavior. The same cannot be said about the CA-EZ channels in failure patients (Fig. 3-7F), where there was little movement of these channels in the source-sink space over time.

Finally, Fig. 3-8 compares the temporal SSI modulation in success versus failure patients. For each patient, SSI was computed in four predefined windows: a) a 30-second window of the interictal recording, b) 60-30 seconds before the seizure event, c) during the seizure event, and d) 60-90 seconds after the end of seizure. For each set of channels (CA-EZ and CA-NEZ), values were normalized to the average SSI of the entire network at rest (window a). At each time point, we then computed the mean $\pm$ standard error of SSI across all success patients ($n = 14$) and all failure patients ($n = 15$). In success patients (Fig. 3-8, top), the CA-EZ had a statistically significantly higher source-sink index compared to the rest of the channels in the network in all windows except after the end of seizure ($p_a = 0.0132$, $p_b = 0.0029$, $p_c = 0.0015$, $p_d = 0.4240$). The same cannot be said about failure patients, as the CA-EZ channels were not separable from the CA-NEZ channels at any time point ($p_{a,b,c,d} \gg 0.05$).

## 3.4 Discussion

We proposed a novel source-sink index (SSI) as a dynamical-network-based interictal iEEG marker to assist in the localization of the EZ. The index was developed based on the hypothesis that seizures are suppressed when the epileptogenic regions are effectively being inhibited by neighboring regions. We tested the source-sink index as a marker of the EZ by computing SSI for all implanted iEEG channels and examining

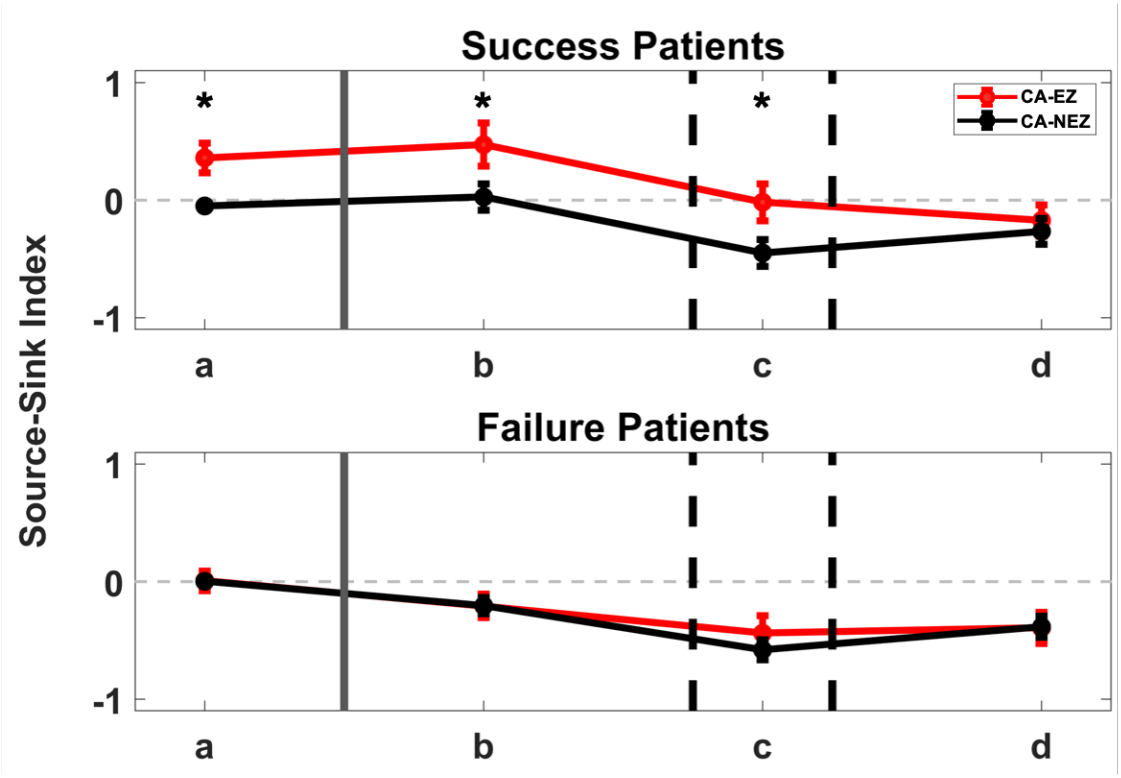


**Figure 3-8.** Temporal SSI modulation in CA-EZ versus CA-NEZ channels. Indices were averaged over all CA-EZ and all CA-NEZ channels for each patient. Each curve shows the mean ± standard deviation across 14 success patients (top) and 15 failure patients (bottom). CA-EZ channels have a higher SSI compared to CA-NEZ channels in success patients, but not in failure patients. The asterisks indicate a statistically significant difference between CA-EZ and CA-NEZ channels. a = 30 second window of the interictal recording, b = 60-30 seconds before the seizure event, c = during the seizure event, and d = 60-90 seconds after the end of seizure

its properties at rest and during seizures.

We evaluated the predictive value of the SSI by i) rating the correspondence between the hypothesized CA-EZ and regions with high SSIs and ii) building a random forest to model the probability of a successful surgery as a function of the source-sink metrics and compared the performance to that of HFOs, a commonly used interictal iEEG feature. The analysis was performed on data from 65 patients treated across 6 clinical centers. Out of 28 success patients in our dataset, the source-sink algorithm agreed (rated as "strong" or "some" agreement) with clinicians in 26 (93%) of patients. In contrast, only 54% of patients with failed outcomes were considered in

agreement with clinicians, suggesting that in failure patients, the source-sink algorithm highlighted other areas than the ones identified and treated by clinicians as potentially epileptogenic. Further, in terms of predicting surgical outcomes, the source-sink metrics outperformed HFO rate, with higher AUC, accuracy, precision and specificity on average, predicting 79% outcomes correctly with a precision of 88%, compared to a 65% accuracy and 71% precision of the HFO model.

### 3.4.1 Challenges

#### 3.4.1.1 Validating iEEG markers of the EZ

At present, identification of the EZ is a complicated and subjective process that is often unsuccessful, thus resulting in post-treatment recurrence of seizure activity in a large proportion of patients. To increase the likelihood of a successful treatment outcome, there is a great need to identify and validate reliable biomarkers that can determine the extent and location of the EZ with high precision and accuracy. However, validation of such markers remains challenging because the EZ is a theoretical concept that cannot be directly measured [35] and thus no ground truth of its exact location exists. Instead, the best estimate one can obtain is retrospectively, by assuming the EZ was included in the resected cortex if surgical treatment renders the patient seizure free. To complicate matters even further, a complete removal of the EZ is not the only basis of a successful surgery (e.g., a disconnection of the EZ from the early spread regions may also produce good outcomes) and although removing the EZ is typically necessary to achieve lasting seizure freedom, it may not always be sufficient. Post-operative outcome measures (e.g., Engel scores) are also based on subjective judgement and may be interpreted differently from center to center. Consequently, results from different centers cannot be compared easily [88]. Further, insufficient sampling of electrodes may also lead to inaccurate results as there is no way for the iEEG marker to capture the EZ if it is not covered, but this is a limitation of all computational approaches.

In the case of the source-sink algorithm, the results may also be less accurate if the sources, i.e., the regions inhibiting the EZ, are not covered.

#### 3.4.1.2 Why the source-sink algorithm may disagree with clinicians in success patients

For a majority of success patients, the source-sink algorithm was in agreement with the clinicians regarding the location of the EZ (Fig. 3-6), and only 2 out of 28 success patients were deemed in disagreement. In addition to completely removing the EZ, a disconnection of the EZ from the rest of the epileptogenic network or removal of the regions responsible for early spread of the seizure activity may also lead to a successful surgical outcome. Thus, it is possible that in those patients, the treated areas may have included the early spread regions instead of the onset zone and therefore are not overlapping with the areas highlighted by the source-sink algorithm.

#### 3.4.1.3 Why the source-sink algorithm may agree with clinicians in failure patients

Surgical treatment may also fail for various reasons and in more complex cases, removing the EZ may not be sufficient to achieve seizure freedom (e.g., a removal of the primary focus in multi-focal patients may lead to post-surgical emergence of seizures from a location that was previously not clinically evident). Consequently, the source-sink algorithm may be in full or some agreement with the treated areas, even in patients with failed outcomes. Additionally, incorrect or inaccurate localization of the EZ and incomplete treatment of these regions most likely leads to seizure recurrence after surgery. This can occur in cases where the implanted electrodes are not covering the true EZ, in which case it is impossible (for clinicians and algorithms) to detect the true EZ, or if the EZ is widely spread. Finally, in some patients, a complete resection of the EZ cannot be performed without causing a new, unacceptable deficit to the patient (e.g., if the EZ is located in eloquent cortex). Instead, palliative treatments,

including RNS or deep brain stimulation, have been increasingly used in patients who are not candidates for resective surgery. These treatments can be effective in reducing seizure frequency, but only a minority of patients experience complete seizure control [108–110].

#### 3.4.1.4 Other interictal iEEG markers of the EZ

The current gold standard visual analysis of hundreds of iEEG recordings to localize the EZ is time consuming and subject to individual expert biases. Although many interictal iEEG markers of the EZ have been proposed, no computational tools are used in the clinical workflow today to specifically assist in localizing the EZ. With epilepsy increasingly understood as a network disorder, a profound knowledge of the underlying network dynamics and interactions between brain regions is essential to understand how the internal properties of the brain network can generate or prevent seizures. An important limitation of the majority of proposed algorithms lies in the fact that they fail to capture these internal properties of the iEEG network. Instead, most existing methods either compute single-channel-based iEEG features (e.g., [74, 78, 80, 81, 83–85, 111–113]), thus not capturing dependencies between channels, or they apply network-based measures ([61, 62, 72–77, 114–116] to name a few) to capture pairwise dependencies (correlation or coherence) between the iEEG channels, but fail to characterize the underlying dynamics of the network. Channel-based iEEG features include various frequency-based features such as spectral power in frequency bands, phase amplitude coupling, or power spectral entropy, to name a few, in addition to features based on pattern recognition, such as spike counts or HFO rates. Network-based measures (e.g., node centrality, degree distributions or distance measures) are summary statistics computed from an adjacency matrix that is used to represent the pairwise dependencies between any two channels in the iEEG network. The main downside of networks-based metrics however, is that each network can be mapped to

multiple adjacency matrices (because connectivity between two nodes can be defined in numerous ways), and many different networks (adjacency matrices) can have identical summary statistics. Thus, such metrics are not based on well formulated hypotheses of the role of the EZ in the network and as such, they are not easily interpretable either.

HFOs are some of the most studied iEEG features as a potential interictal marker of the EZ (e.g., [78, 81, 82, 85, 97, 101, 117–129]). In the context of epilepsy, there is evidence that regions that belong to the EZ have higher HFO rates compared to non-epileptogenic regions [117] and studies have suggested that removal of regions that generate high rates of HFOs correlates with good post-surgical outcome [82, 101, 118, 120–122, 128, 129]. However, there still remains considerable controversy surrounding HFOs as a valid marker of the EZ. Other studies have not found a predictive value in the removal of these regions [118, 122] and two meta-analyses of existing studies concluded that the evidence of HFOs as a predictor of surgical outcome is weak [119, 130]. Höller et al. conducted a systematic review of 11 studies that related the resection of HFO-generating areas to post-surgical outcome [119]. Although their meta-analysis confirmed a higher resection rate of ripples or fast ripples in success versus failure patients, the effect sizes were small.

Furthermore, several studies have also questioned the reproducibility and reliability of HFOs as a marker [86, 121, 122, 131, 132]. First, no consensus has been reached on the exact features used to describe HFOs, because the exact underlying cellular mechanism by which they are generated remains unknown [121]. Instead, researchers rely on an empirical definition derived from visual observation [132], which gives rise to variability in the features chosen to define HFOs among current studies. Second, HFOs can also occur in non-epileptogenic regions and even in patients without epilepsy [86]. These physiologic, non-epileptic HFOs have features that overlap with those of pathological HFOs [133–135] and thus differentiation between the two types remains

an unresolved issue in iEEG studies [136–139]. Similar inconclusive results hold in completed prospective studies of HFOs in ictal recordings. A Cochrane review assessed the ability of ictal HFOs to improve surgical outcomes [130]. They identified only two small, prospective studies at the time and concluded that there is not enough evidence so far to draw reliable conclusions regarding the efficacy of using HFOs in epilepsy surgery decision making.

Finally, HFO rates are not stable over time. Gliske et al. tested the consistency of channels exhibiting the highest number of HFOs across different 10-minute segments of data [86]. They showed that the location of the highest HFO-rate channels varied greatly when different segments were used, thus questioning the reliability of such marker. In contrast, we showed above that the source-sink analysis returns consistent results independent of recording length and is in fact, robust to any random selection of interictal activity (Fig. 3-3). Further, we repeated the analysis with and without the removal of large artifacts from the sEEG snapshots and found that the results held regardless.

#### 3.4.1.5 Translating an iEEG marker into the clinical workflow

In order to translate an iEEG marker of the EZ into clinical workflow, it is critical to perform rigorous testing and validation to ensure the marker meets the stringent criteria needed for it to serve as a reliable source of information for clinical decision making. We sought to evaluate the performance of the SSI on a diverse group of patients, reflecting different epilepsy etiologies, treatment methods and post-treatment outcomes. We collected our iEEG data from six different clinical centers. As such, our dataset is comprised of a heterogeneous patient population, spanning varying case complexities (such as lesional or non-lesional, and temporal or extra-temporal epilepsy), epilepsy types (focal and multi-focal) and clinical practices, while at the same time reflecting the standard of care success rates of approximately 50% on

average.

In order to properly validate any biomarker, it is important to determine the range of conditions under which it will give reproducible and accurate results. Similarly, a profound understanding of when the tool performs well and when and why it fails is critical. For example, some patients present with a lower clinical case complexity (such as a visible lesion on MRI or some types of temporal epilepsy) and have as such higher chances of good surgical outcomes. A tool that performs well on these patients is not guaranteed to translate well to more complex cases. Importantly, we showed that the SSI is agnostic to the clinical complexity of each patient defined by our clinical team as: 1) lesional (visible lesions on MRI) or non-lesional (see Figs. II-4A and III-1A), 2) mesial temporal or extra-temporal (Figs. II-4B and III-1B), and 3) focal or multi-focal (Figs. II-4C and III-1C).

# Chapter 4

# Source-sink analysis for diagnosis of epilepsy on interictal scalp EEG data

## 4.1 Introduction

### 4.1.1 Challenges with EEG interpretation

Scalp EEG remains an important tool in the diagnosis and treatment of epilepsy and today millions of EEGs are performed each year in epilepsy centers, neurology clinics, emergency rooms and ICUs for this purpose [8]. Despite nearly 100 years of using this technique, visual analysis is still the gold standard in clinical EEG. Clinicians look for abnormalities including spikes and sharp waves, formally called interictal epileptiform discharges (IEDs), in addition to focal slowing of activity in the EEG waveforms, all of which are known indicators of epilepsy [5, 6].

Although interobserver reliability is high in trained individuals, it is less so in clinical units that do not specify in epilepsy (e.g., emergency rooms) and overall interobserver reliability in interpretation of EEG recordings has been found to be only moderate [140]. In fact, errors in EEG interpretation are not uncommon, particularly in mistakenly identifying normal variants as epileptiform discharges [141]. Additionally, scalp EEG recordings are subject to several other limitations that may prevent detection of these

abnormalities [9, 142–144]. First, routine EEGs are typically captured for a limited amount of time (generally 20-30 minutes) while the patient is not seizing or is "at rest" [6, 145]. Thus, such abnormalities may not occur in a short time window. In fact, 12-50% of patients with epilepsy have normal EEGs during their first visit, limiting traditional visual interpretation focused on IED or focal slowing detection [6, 145] and resulting in a need for one or more repeated EEGs and consequently a delayed diagnosis (*false negative*) for a significant number of epilepsy patients. Second, artifacts, such as those due to eye movement, eye blinks or muscle activity are often prevalent, which may mask true IEDs, or be mistaken as false IEDs, leading to a misdiagnosis (*false positive*) of the patient [144]. Third, scalp electrodes sample only about one-third of the cortex. Discharges arising within sulci, in basal regions (e.g., orbitofrontal cortex), and in interhemispheric regions (e.g., interhemispheric supplementary motor cortex) are not detected [9]. Furthermore, epileptiform activity generated by deep nuclei such as the amygdala and hippocampus may not be captured on scalp recordings [142]. Additionally, dipoles that are parallel to the scalp cannot be detected by electrodes. Orientation of an epileptiform spike dipole must be orthogonal or nearly orthogonal to the surface, decreasing the likelihood of it being captured on the EEG. The EEG signals are also attenuated by bone, dura and scalp tissue, which further hampers the ability to capture epileptiform activity from scalp recordings [143].

Interpretation of EEG recordings is mainly based on pattern recognition and diagnosis of epilepsy is often complicated due to the variety of events which may resemble a seizure. As a result, both false positive and false negative diagnoses commonly occur and overall misdiagnosis rates of epilepsy are nearly 30% [10]. Thus, there is a great clinical need to more quickly and more accurately diagnose whether a patient who experienced a seizure has epilepsy or not from their *first* EEG recording. Such a diagnostic tool can significantly reduce costs of misdiagnosis and enable both non-epilepsy and epilepsy patients to receive effective treatment immediately.

### 4.1.2 SSI as a biomarker for diagnosing epilepsy

To address several of the limitations of routine EEG in the management of epilepsy, we aim to develop a tool that diagnoses epilepsy from resting-state scalp EEG by testing the source-sink index (SSI) as a new biomarker of epilepsy. In this preliminary study, we developed and tested a computational tool that i) estimates patient-specific dynamical network models from a patient's first scalp EEG recording and ii) uses source-sink properties of the network to detect whether pathological connections are present in the network. Due to the frequent occurrence of artifacts in scalp EEG, our tool also automatically removes artifacts before performing the analysis and provides an easy-to-interpret output.

Importantly, unlike the current clinical standard and other existing computational approaches, which aim to detect abnormalities on individual EEG channels (e.g., [146–150]), the SSI is not detectable by visual inspection. Instead, our tool characterizes the internal properties of the brain necessary to reveal the abnormal epileptic network connections and the underlying dynamics of seizure generation.

## 4.2 Materials and methods

### 4.2.1 Patient population

We selected 57 patients who underwent routine scalp EEG monitoring following a seizure or seizure-like episode, and have already been diagnosed as having epilepsy (focal or generalized) or not, for this study. The diagnosis of each patient was based on an epilepsy monitoring unit (EMU) admission which recorded the patient's habitual clinical events. Patients who met the following criteria were included in the study: (i) Men or women aged 12 years and older. (ii) Patients who underwent scalp EEG monitoring as deemed appropriate by the ordering physician. (iii) Patients who are on one AED or no medication. (iv) Patients who presented with a transient neurological

symptom concerning for seizures and have been diagnosed with either epilepsy or PNES (v) Patients with no abnormal findings on first scalp EEG. Patients were excluded from the study if (i) their medical records were incomplete, (ii) clinical follow-up was deemed inadequate, or (iii) first scalp EEG demonstrated abnormal findings.

In our dataset, 27 patients were diagnosed with epilepsy and 30 patients did not have epilepsy. All non-epileptic patients were diagnosed with PNES. Out of the 27 epilepsy patients, 20 patients had focal epilepsy and 2 patients had generalized epilepsy. Information on epilepsy type was not available for the remaining 5 epilepsy patients. Patients were treated at the Johns Hopkins Hospital or Johns Hopkins Bayview Medical Center. The study was approved by the Johns Hopkins Medicine Institutional Review Board (IRB). The use of de-identified data in conjunction with relevant data from each patient's medical record was approved by the IRB for research purposes. All clinical decisions were made independently of this study.

### 4.2.2 Data collection

### 4.2.3 Scalp EEG recordings

The scalp EEG data were recorded using a standard 10-20 EEG montage at a sampling frequency of 200 Hz. For each patient, the clinical team extracted a 15-30 minute long resting-state (i.e., interictal, no seizures) EEG snapshot from the patient's first admission to the clinical center after experiencing a seizure or a seizure-like episode. All continuous EEG recordings were reviewed at the time of their selection for the study by a board-certified epileptologist and only EEGs with no findings of epileptiform abnormalities were selected for the study.

### 4.2.4 Classification of abnormal versus normal EEGs

Based on medical records and a review of EEG recordings, the clinical team classified epilepsy patients into two groups; i) patients with abnormalities present in the first EEG (abnormal EEG) and ii) patients with no abnormal findings (normal EEG). Since patients with abnormal findings on EEG generally represent the most straightforward cases to diagnose, epilepsy patients with abnormal EEGs were excluded and only epilepsy patients with normal EEGs were included in the study. All non-epilepsy patients had normal EEGs. Thus, in the final group of 57 patients, all patients had a normal EEG, i.e., IEDs or focal slowing were not present in the signals.

### 4.2.5 Data pre-processing

The scalp EEG recordings were notch filtered around the power line frequency (60 Hz) with a stopband of 2 Hz and bandpass filtered between 0.5 and 30 Hz with a fourth order Butterworth filter. Electrodes placed on the midline sagittal plane of the skull (Fz, Cz and Pz), along with the C3 and C4 electrodes, which were utilized as common reference points during the EEG recording, were removed from the data set. The continuous EEG recordings were divided into non-overlapping 500-msec windows for modeling and feature extraction (see details below). All data processing and analysis were performed using MATLAB R2020b (MathWorks, Natick, MA) and Python3.6+ (Python Software Foundation, Wilmington, DE).

#### 4.2.5.1 Artifact removal

Before any analysis was performed, we applied artifact removal to remove both major artifacts such as those caused by movement and muscle activity that obscured majority of the EEG channels, as well as smaller artifacts not generated by brain activity (e.g. artifacts caused by eye movements, eye blinks, cardiac activity, other equipment and more). To remove artifacts, the filtered data was input into EEGLab,

an interactive Matlab toolbox for processing EEG data [151]. Using EEGLab, we performed independent component analysis (ICA) for artifact removal using the Infomax algorithm presented in [152]. The output of the Infomax algorithm is a predefined number of independent components computed from the EEG data. Each component is labeled, with probability, as a brain signal or an artifact coming from muscle, eye, heart, line noise, channel noise, or other. These labels are generated by matching against an expertly labelled dataset of components using a pre-trained artificial neural network. Any component labelled as artifact with a probability greater than a predefined threshold of $\alpha > 70\%$ was automatically removed from the data. The resultant EEG data used for the remainder of the analysis had artifacts removed with minimal to no decline in brain signal fidelity.

### 4.2.6 Source-sink analysis to diagnose epilepsy

Fig. 4-1 provides a simplified overview of the approach we took on scalp EEG to diagnose patients with epilepsy. Analogous to the iEEG study in chapter 3, the interictal EEG recording from each patient was split into 500-msec non-overlapping windows and DNMs were estimated in every window $w$ of the data to obtain a sequence of $\boldsymbol{A}$ matrices over time, $\boldsymbol{A}_w, w\epsilon[1, 2, \ldots, T]$, where $T$ is the number of windows.

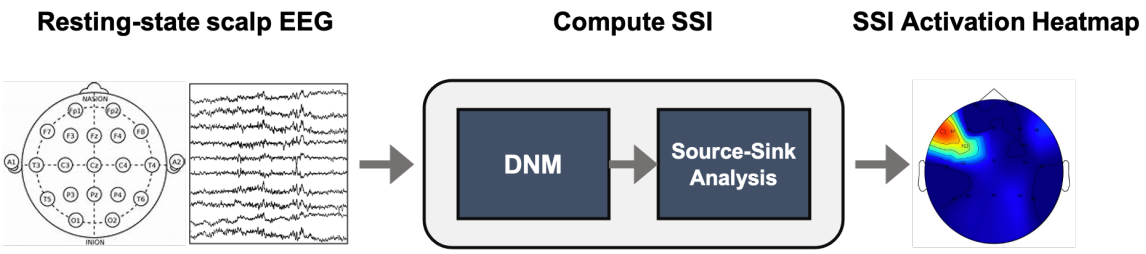


**Figure 4-1.** A simplified schematic of the scalp EEG approach. Scalp EEG recordings from each patient are put through the source-sink algorithm to build DNMs and compute source-sink indices of all EEG channels. The output is a SSI activation heatmap that can be used to determine whether a patient is likely to have epilepsy or not.

#### 4.2.6.1 Computing stationary interictal SSIs

We then computed one constant **A** matrix using eq. 3.1 to represent each patient's interictal EEG DNM. In $\boldsymbol{A}$ (Fig. 2-3C), row $i$ represents the amount of influence EEG channel $i$ receives from the rest of the network in window $w$, and column $j$ represents how the activity of channel $j$ influences the activity of all other channels in the network. Next, we placed the EEG channels in the 2-D source-sink space shown in Fig. 2-3D and computed SSI for each EEG channel as follows. First, we computed the sink index (eq. 2.2) of every channel, which captures how close the channel is to the ideal sink (2-3D, pink star). Then, we computed the source index (eq. 2.3) to capture how close each channel is to the ideal source (2-3D, blue star). Note that the ideal sink has a sink index of 1 and a source index of 0, whereas the ideal source has a sink index of 0 and a source index of 1. Thus, the larger the sink index (and consequently, the smaller the source index), the more likely the channel is a sink. Conversely, the larger the source index (and thus, the smaller the sink index), the more likely the channel is a source. Next, we computed the source influence and sink connectivity (eq. 2.4-2.5) of each channel, which quantify how much the channel is influenced by the top sources and sinks, respectively. Finally, the SSI was computed for each channel using eq. 2.6 and displayed in heatmap form as shown in Fig. 4-1.

The source-sink index (SSI) is high if the sink index, source influence and sink connectivity metrics are high, which is in line with the source-sink hypothesis describing how the epileptogenic zone is being "inhibited" by neighboring nodes when a patient is not seizing. Therefore, as demonstrated in Fig. 4-2, we expect a high SSI in one or more EEG channels in all epilepsy patients but a lower SSI across all EEG channels in non-epileptic patients. It is important to note that scalp EEG does not carry information about whether a channel covers an inhibitory or excitatory population of neurons. However, we can determine the level of influence one channel has on another, which is what the SSI captures.

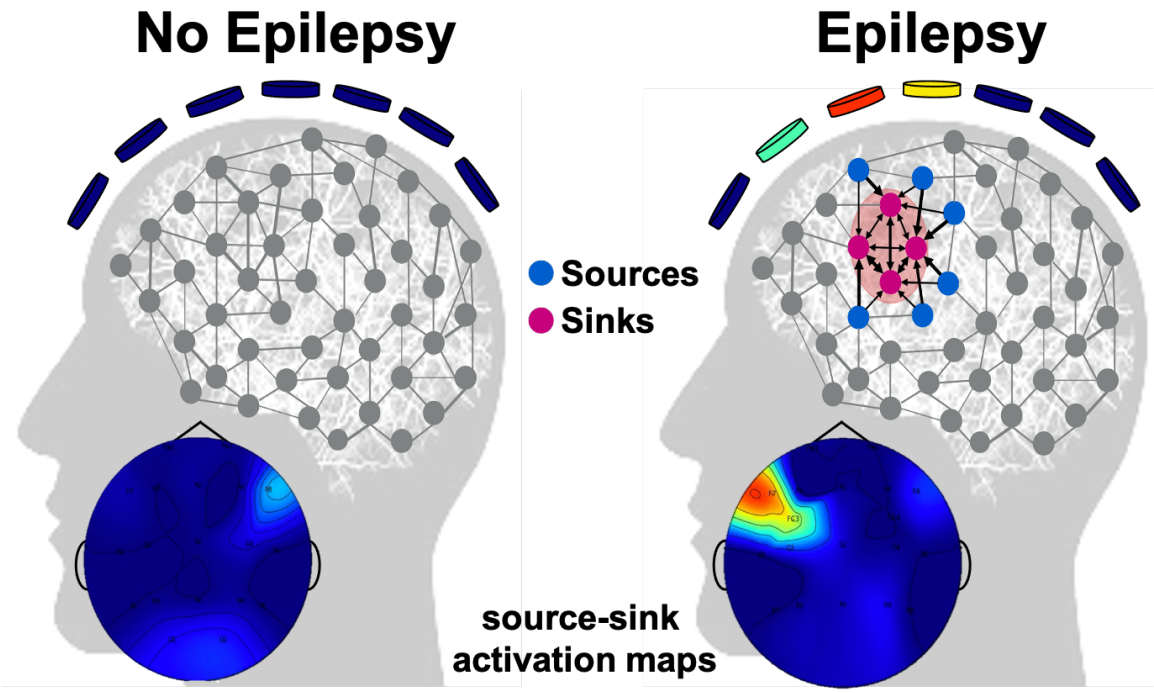


**Figure 4-2.** Source-sink hypothesis in scalp EEG. Left: Non-epilepsy patients have a uniform distribution of low SSI values across all channels as no strong sources or sinks exist in the network. Right: In epilepsy patients, the EZ nodes are sinks strongly inhibited by neighboring sources during rest. Thus, one or a few EEG channels will have a higher SSI in these patients.

### 4.2.7 Predicting diagnostic outcomes using the source-sink index

To evaluate the SSI as an interictal EEG marker of epilepsy we tested its value in predicting whether a patient has epilepsy or not (see Fig. 4-3 for a schematic of the validation process). Specifically, we modeled the probability of having epilepsy, $p_e$, as a function of the SSI using a logistic regression model as follows.

From each patient's SSI activation heatmap (SSI-map) we defined an SSI activation distribution over the EEG channels as the SSI per channel, normalized by the total SSI across all channels (see examples of SSI distributions in Fig. 4-3). We then computed the Kullback-Leibler (KL) divergence [153] between the patient's SSI distribution and a baseline distribution. The KL divergence is a measure of how one probability

distribution is different from a second, baseline or reference distribution. In our case, we assumed the baseline distribution to be a non-epileptic SSI distribution, which is *uniform* across all EEG channels. A uniform distribution represents equal, low, activation everywhere, that is, no pathological sinks (a blue SSI-map) in the network. The KL divergence was computed as:

$$KL(SS||B) = \sum_{x \epsilon X} SS(x) \log \left( \frac{SS(x)}{B(x)} \right) \tag{4.1}$$

where $x$ represents the scalp EEG channels, $SS(x)$ is the SSI activation distribution and $B(x)$ represents the baseline distribution $SS(x)$ is compared against. A higher KL value thus indicates that the patient's SSI distribution is different from the non-epilepsy baseline distribution, whereas a lower KL value means that the patient's SSI distribution resembles the distribution of a non-epilepsy patient.

Next, we partitioned the data into a training and a test set by assigning 70% of

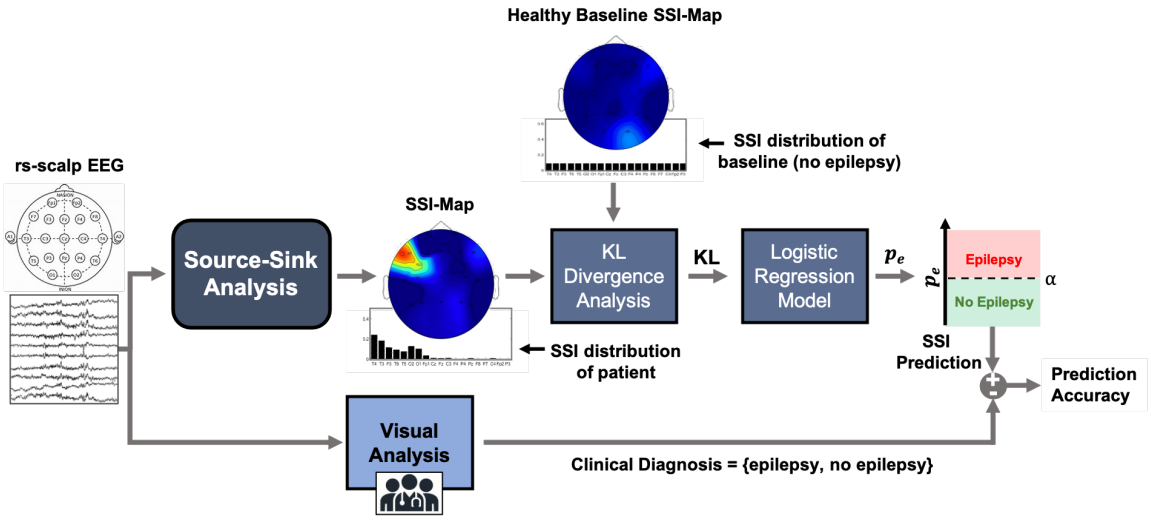


**Figure 4-3.** Validation steps of the SSI as an EEG marker of epilepsy. From each patient's first EEG recording, we compute a set of stationary source-sink indices for each EEG channel to generate a SSI activation map (SSI-map). The SSI-map defines an activation distribution over the EEG channels that is then compared to a baseline distribution of a healthy individual using KL divergence. Next, the probability of the patient having epilepsy $p_e$ is computed as a function of the KL divergence. Finally, we apply a threshold to $p_s$ to predict diagnostic outcome and compare to the actual diagnosis of the patient.

the patients ($n = 40$) to the training set while also ensuring a balanced number of epilepsy and non-epilepsy patients, and the remaining 30% ($n = 17$) were used for testing. Then we constructed the following logistic regression model to compute the probability of a patient having epilepsy, $p_e$, as a function of the KL divergence:

$$log\left(\frac{p_e}{1-p_e}\right) = \beta_0 + \beta_1 * KL \tag{4.2}$$

where $KL$ is the KL divergence of the patient's SSI distribution, computed from eq. 4.1.

The model was fit to the training data and validated on the test set by applying a varying threshold to the model's output and computing a ROC curve. We then selected the threshold ($\alpha$) that maximized prediction accuracy on the training data. If $p_e > \alpha$, we predicted that the patient had epilepsy, else that the patient was non-epileptic. Finally, we applied the model to the test dataset and evaluated performance by comparing each patient's predicted diagnostic outcome to the actual diagnosis of the patient.

We used four metrics to measure model performance: a) AUC, which measures the discriminative power of the SSI, b) prediction accuracy, which is the fraction of patients whose diagnosis the model predicted correctly, c) sensitivity, which measures the proportion of epilepsy patients that the model predicted correctly as having epilepsy and d) specificity which refers to the proportion of non-epilepsy patients that the model predicted correctly as not having epilepsy. Model performance results are reported below.

## 4.3 Results

### 4.3.1 SSI is high in one or a few channels in epilepsy patients but lower in non-epilepsy patients

From each patient's interictal EEG DNM (eq. 3.1) we computed SSI for all channels to generate a SSI-map and obtain a SSI distribution. See Fig. 4-4A and B for an EEG snapshot and the corresponding SSI-map and distribution for one non-epilepsy and one epilepsy patient, respectively. In the non-epilepsy patient (diagnosed with PNES), all channels had low, similar, SSI values, resulting in a fairly uniform SSI distribution and a blue SSI-map. In contrast, four channels (O1-2 and T5-6) had a higher SSI compared to the rest of the channels (warmer colors on the SSI-map) in the epilepsy patient. Note however, that both patients' scalp EEG recordings had no visible epileptic abnormalities and were as such not useful to clinicians in discriminating between the two conditions (epilepsy versus non-epilepsy).

### 4.3.2 SSI performs well in predicting epilepsy diagnosis

Based on the hypothesis that epilepsy patients have a high SSI in one or a few channels whereas the SSI distribution of non-epileptic patients is uniform across all channels, we built a logistic regression model to predict the probability of having epilepsy as a function of KL divergence between each patient's SSI distribution and that of a uniform, non-epilepsy, baseline distribution. Fig. 4-5A shows the ROC curve obtained by varying the threshold on the training set $p_e$ values. The area under the curve (AUC) of the ROC ranges from 0.5 to 1, and the larger the AUC, the more valid the SSI is as an EEG marker of epilepsy. The SSI model achieved an AUC of 0.92 on the training set.

As Fig 4-5B shows, there was a significant separation between the distributions of the estimated probability of epilepsy ($p_e$) in non-epilepsy patients (left) and epilepsy

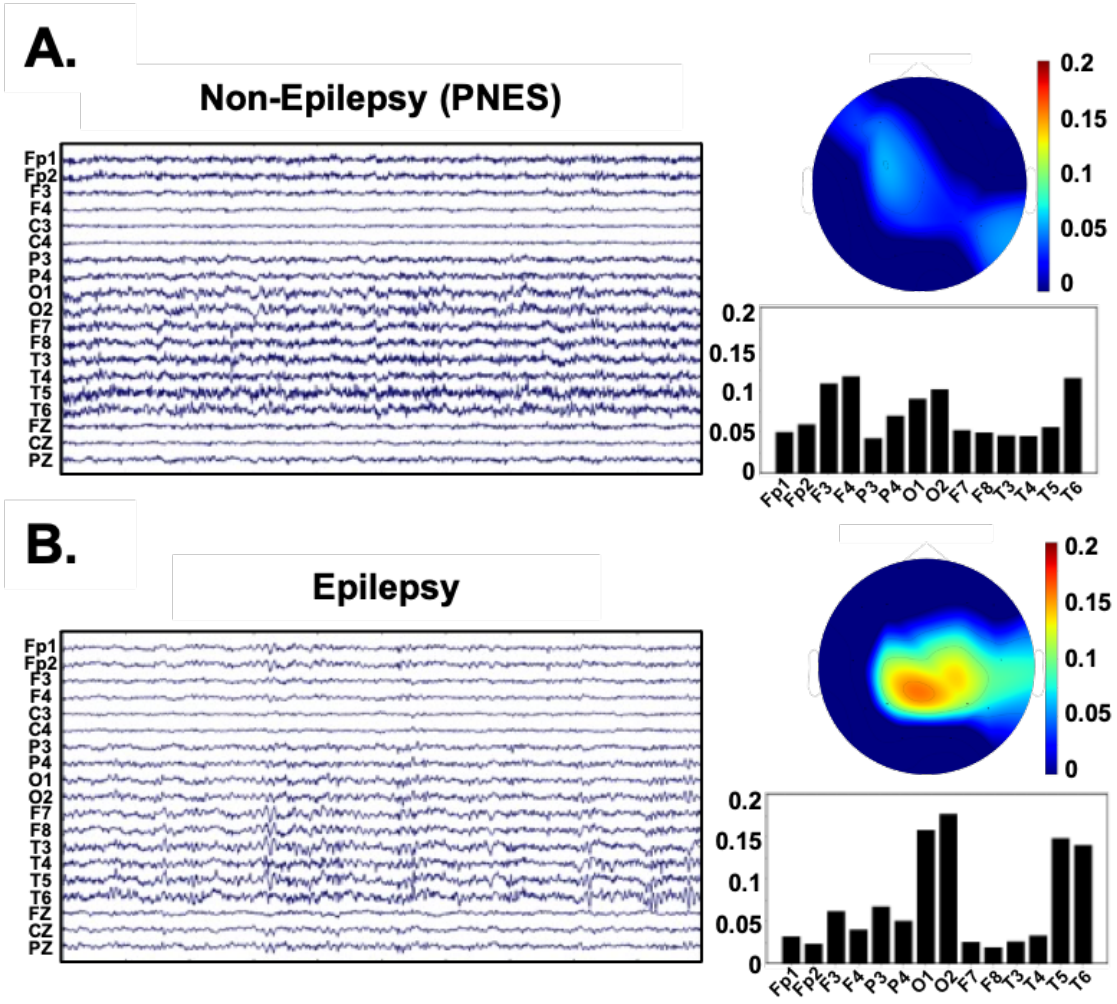


**Figure 4-4.** Two patient examples. A. A scalp EEG snapshot and the corresponding SSI-map and SSI activation distribution for a non-epilepsy (PNES) patient. All indices have a fairly similar SSI resulting in a blue map. B. A scalp EEG snapshot and the corresponding SSI-map and distribution for an epilepsy patient. Note that no abnormalities were present in the EEG snapshot. In this epilepsy patient, four channels have higher SSI values than the rest, as reflected by the warmer colors in the SSI-map.

patients (right), with a generally lower $p_e$ for non-epilepsy patients. The optimal threshold ($\alpha = 0.64$), when applied to $p_e$ rendered an overall accuracy of 84.2%. Further, the model achieved a sensitivity of 81.5% and a 83.3% specificity.

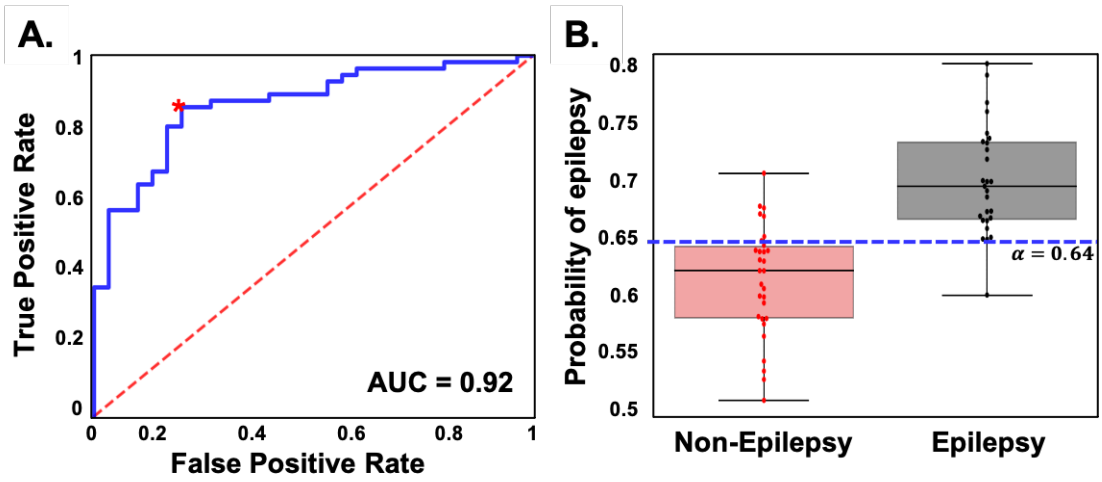


**Figure 4-5.** A. Training set ROC curve. The model was trained using 40 patients. The optimal threshold (red star) yielded an overall accuracy of 84.2%. B. Predicted probability of epilepsy ($p_e$) groupped by actual diagnosis. Each dot represents one patient. The blue line represents the optimal threshold applied to $p_e$ to predict diagnostic outcome.

## 4.4 Discussion

In this preliminary study, we tested the SSI as an interictal EEG marker to assist in the diagnosis of epilepsy. The index was developed based on the hypothesis that when an epilepsy patient is not having a seizure, it is because the epileptogenic regions (sinks) are being strongly inhibited by other regions (sources) to prevent the generation and spread of seizure activity. Subject to the source-sink hypothesis, our conjecture was that the source-sink phenomena (i.e., top sinks strongly influenced by top sources) occurring in an epilepsy patient's brain would manifest as a strong source-sink activation (high SSI in one or a few regions) on scalp EEG, whereas no source-sink activation would appear in non-epilepsy patients. We evaluated the diagnostic power of the SSI by building a logistic regression to model the probability of having epilepsy as a function of the SSI. The analysis was performed on 57 patients and the SSI model achieved an overall accuracy of 84%, as well as 82% sensitivity and 83% specificity. Although preliminary, these results are promising as this is a significant improvement over the reported sensitivity of 22-55% in diagnosing epilepsy,

and specificity estimated at 70% [9]. It is also important to note that these normal EEG recordings are not actionable by clinicians as there are no epileptic abnormalities present in the signals.

### 4.4.1 Limitations of current computational approaches for diagnosing epilepsy

Several computational algorithms have been developed to assist in EEG-based diagnosis of epilepsy. In fact, a google scholar search revealed 4000 computational algorithms focused on detecting IEDs and other abnormalities from EEG recordings ([146–150], to name a few). As the data streams that require analysis may be vast, these tools quickly identify the relevant regions of data, i.e., where events of interest occur, for subsequent visual analysis. They reduce the time clinicians require to search through large amounts of EEG data which often arises during 24-72 hour scalp EEG monitoring or intracranial EEG monitoring, the latter which is done only for surgical candidates [141, 154]. These algorithms, however, still rely on the presence of abnormalities in the short-term EEG.

Others have set out to develop algorithms that do not depend on the presence of epileptic signatures. The GeoSource software (Electrical Geodesic Inc) is a commercialized tool that has the potential to assist in diagnosing epilepsy without abnormalities as it uses source localization technology to identify "pathological sources" of EEG activity inside the brain from scalp EEG recordings. The source localization problem, also called the "EEG inverse problem", is as follows: given a set of electric potentials (EEG signals) from discrete sites on the surface of the head (EEG electrodes), as well as the associated positions of those measurements, and the geometry and conductivity of regions within head, identify the location and magnitude of the current sources that generated those signals within the brain [43]. Since there exists no unique solution to the inverse problem, great care has to be taken to ensure appropriate choice of

analysis parameters and moreover, the results are highly sensitive to both spatial resolution and signal artifacts [155]. Further, GeoSource requires an extra hour of work by a technician, and 20-30 minutes of physician time to review the technician's work and the data produced by the tool. Moreover, digital EEG analysis by source localization is an advanced procedure that is mainly used at epilepsy surgery centers, where staff are familiar with how to perform it. However, even at these centers, it is rarely used as its sensitivity has failed to improve much over visual inspection of the EEG. In contrast, using our tool it takes only minutes to compute a SSI-map, and our preliminary study suggests that it may significantly improve both sensitivity and specificity of diagnosis, even when the EEG has no abnormal epileptiform signatures.

### 4.4.2 Limitations of current clinical gold standard for diagnosing epilepsy

The current gold standard relies on identifying epileptogenic abnormalities in the scalp EEG recordings. As such the utilization of scalp EEG recordings for diagnosing epilepsy becomes a signal processing or pattern recognition problem, concentrating on finding events of interest on individual channels (e.g., IEDs or focal slowing). Consequently, if no abnormalities are captured during the short-term EEG (which commonly occurs [6, 145]), the EEG is of little value. Additionally, both physiological and non-physiological sources of artifacts may occur to fool the interpreter into believing an abnormality exists in the signals. To complicate matters even further, it is important to consider that a normal EEG does not exclude epilepsy, as around 10% of patients with epilepsy never show epileptiform abnormalities on EEG. Further, IEDs are present in a small percentage of individuals who never develop epilepsy, and IEDs may also be found in patients with other neurological disorders than epilepsy [156]. Thus, an abnormal EEG with IED findings does not in itself confirm that an individual has epilepsy.

### 4.4.3 Advantages of the SSI as an EEG marker of epilepsy

Instead of relying on the presence of visually observable abnormalities, we seek to understand how the EEG observations are generated in the first place and how internal network properties can trigger seizures or prevent seizures. Conceptually, our algorithm finds EEG patterns which are below the threshold of traditional visual interpretation. Dynamical network models (DNMs) derived from EEG data characterize the internal properties of the brain, and are necessary to reveal the epileptic network connections and the underlying dynamics of seizure generation. The main advantage of the SSI over the current gold standard is that it exists throughout the entire interictal recording and is as such always present in short-term monitoring.

# Conclusions and future work

### 4.4.4 Conclusions

We introduced the source-sink hypothesis, which states that seizures are suppressed when the epileptogenic regions (sinks) are effectively being inhibited by neighboring brain regions (sources). The source-sink hypothesis is supported by biological evidence based on the levels of excitatory and inhibitory neurotransmitters, and particularly glutamate and glutamate receptors in the brain [46–49] and iEEG studies that have demonstrated strong inward (inhibitory) connectivity to the EZ regions during rest [51, 52, 55, 57]. Subject to the source-sink hypothesis, we then proposed a novel source-sink index (SSI) as a dynamical-network-based interictal EEG marker that detects abnormal pathological connections in the epileptic brain network. More specifically, the SSI is a marker that detects a fundamental property of an epileptic brain, which, unlike epileptiform activity, is not based on pattern recognition and thus always detectable via computation. We proposed a twofold application of the SSI; i) as an iEEG marker to assist in the localization of the EZ and ii) as a scalp EEG marker to assist in the diagnosis of epilepsy.

To evaluate the SSI as an interictal iEEG marker of the EZ, we conducted a retrospective study using iEEG data from 65 patients treated across 6 epilepsy centers. The SSI agreed with clinicians in 93% of success patients but only 54% of failure patients, suggesting that our tool was also highlighting other potentially epileptogenic regions in failure patients. Further, in terms of predicting surgical outcomes, the

source-sink metrics outperformed HFO rate, the most studied interictal iEEG marker of the EZ, achieving a test set accuracy of 79% and average precision of 88%. Overall, our results suggest that the SSI captures the characteristics of the regions responsible for seizure initiation. The SSI is a promising iEEG marker of the EZ and could significantly improve surgical outcomes by increasing the precision of EZ localization. Furthermore, by removing the need to capture seizures, the tool has the potential to substantially reduce invasive monitoring times, avoiding further risks to patients and reducing costs to hospitals.

To test the value of the SSI as an interictal scalp EEG marker of epilepsy, we modeled the probability of having epilepsy as a function of SSI. We applied our model to 57 patients and achieved an overall test set accuracy of 84%, which is a considerable improvement over the current gold standard. Although preliminary, our results suggest that the SSI has the means to reliably detect a fundamental property of an epileptic brain (e.g., abnormal network connectivity) and may be a promising interictal EEG marker of epilepsy. Importantly, by not requiring the presence of IEDs or other abnormalities to diagnose epilepsy, the tool has the potential to make the first EEG consistently actionable and thus significantly improve the speed and accuracy of epilepsy diagnosis, enabling patients to receive effective treatment immediately and reducing the costs of misdiagnosis.

### 4.4.5 Future work

#### 4.4.5.1 Intracranial EEG study

Due to the spatial resolution of the iEEG contacts, the DNMs cannot distinguish between excitatory and inhibitory connections and thus the only information we can glean from the models is the amount of influence between any two nodes in the network. The high predictive performance of the SSI does however suggest that the sources are

likely dominated by inhibitory influence, consistent with the source-sink hypothesis. To better understand the excitatory or inhibitory nature of the connections, future work may entail complementing the iEEG data with resting-state fMRI (rs-fMRI), which has a poorer temporal resolution, but generally a higher spatial resolution compared to iEEG [157]. Thus combining iEEG and rs-fMRI could provide a better understanding of the directionality of the network connections [158].

In patients with electrodes targeting the hippocampal region, the hippocampal contacts were frequently identified as top sinks in the iEEG network. The hippocampus is a highly connected structure, with many bidirectional connections to surrounding regions [159] both intra- and inter-hemispherically [160]. Further, studies of mesial temporal lobe epilepsy (MTLE) have demonstrated the existence of strong connections within the hippocampal network bilaterally, in both epileptogenic as well as non-epileptogenic hippocampi [159, 161, 162]. As such, the hippocampus is a structure that is highly influenced by other regions and by its nature acts as a sink in the brain network, regardless of its epileptogenicity. Moreover, we found that in MTLE patients, contacts recording from the contralateral hippocampus commonly exhibited a stronger sink-like behavior than the epileptogenic hippocampus. This connectivity asymmetry across hemispheres is in line with findings of other studies, which have demonstrated a decreased functional connectivity within the epileptogenic hippocampal networks with a concurrent increased connectivity in contralateral hippocampal functional pathways, possibly reflecting compensatory mechanisms with strengthening of alternative pathways in these patients [159, 163–165].

To that end, the connectivity patterns and natural sink-like behavior of the hippocampus need to be taken into consideration as results of the source-sink analysis are reviewed and interpreted. Although the tool performs well with the hippocampal electrodes included in the datasets, as reflected by our results, there might be cases where these electrodes could simply be removed before the analysis is performed. This

would for example include cases where the hippocampi were sampled but were not suspected to be involved in seizure onset and thus clinical experts would ignore these electrodes in their standard of care analyses regardless. Our preliminary testing has showed that inclusion or removal of hippocampal electrodes does not alter the source-sink behavior of other contacts in the iEEG network and thus, a future augmentation of the tool could include an option to remove the hippocampal electrodes before the visual interpretation of the source-sink results is performed by clinicians.

We showed that the tool is agnostic to different clinical covariates describing case complexity, such as epilepsy type, the presence of lesions and location of seizures. We also showed that the tool is generalizable across centers and treatment methods. However, the algorithm was developed and validated on adult patients only. Although we expect the results to generalize to the pediatric population, an important next step would be a robust evaluation of the SSI on interictal iEEG data from a large population of children with DRE. Lastly, the results of our retrospective study suggest that the SSI has a high value as an iEEG marker and could aid in the localization of the EZ if integrated into the clinical workflow. In future work, we plan to set up clinical trials to clinically validate the SSI in a large prospective study on new patient data.

#### 4.4.5.2 Scalp EEG study

Scalp EEG recordings are prone to artifacts from various sources that may affect the results. Thus, great care has to be taken to properly remove artifacts from the signals before performing the analysis. Our preliminary study required a semi-automated removal of artifacts using EEGLab's ICA tool [152]. For a deployable portable tool that can provide results in minutes, it will be necessary to automate this procedure. An extensive review that compared state-of-the-art automated algorithms for artifact removal [166] noted that the best performing approach is highly dependent

on the artifacts and the signal to noise ratio and may require combining more than one algorithm to achieve best results [166, 167]. In our clinical setting, the most common artifacts are due to eye movements, eye blinks and muscle artifacts (myogenic activity) [166–168]. Future work will entail further exploration of existing automated algorithms to determine whether they may be used for this purpose or if developing a fully automated artifact removal algorithm to integrate into our processing pipeline will be necessary.

Lastly, for any new biomarker to be clinically valuable, a detailed validation is required to ensure its performance remains consistent across applications and is generalizable. Although our preliminary results look promising, all patients in our dataset were treated at a Johns Hopkins center. Further, all non-epilepsy patients had PNES, whereas multiple other conditions may result in a seizure-like event. Thus, we plan to extend the study to a larger patient population, seen at multiple centers (including specialized epilepsy centers, emergency rooms and ICUs). In addition, cross-validation of the SSI model for predicting epilepsy will be necessary to ensure the reliability and robustness of SSI as a marker of epilepsy.

Finally, in future work, we plan to perform a meta analysis to analyze the relationship between SSI performance and the following: a) age of patients to ensure generalizability across all age groups, b) duration of EEG recording, c) EEG arousal state (sleep versus awake), d) diagnostic category (e.g., epilepsy, PNES, syncope, or cardiac-related), e) medication status (on AEDs versus not on AEDs), and f) epilepsy type (generalized versus focal) and epilepsy subtype based on coarse location (brain lobe) of seizures. Although our source-sink hypothesis is solely based on the characteristics of an epileptic brain network, we will explore and compare SSI distributions between non-epileptic patients diagnosed with PNES, syncope or cardiac-related conditions to test if any properties of these distributions suggest that these disorders may be distinguishable by the SSI. Further, within the epilepsy group, we will also

compare the SSI distributions and location of scalp EEG electrodes with highest SSI to the epilepsy subtype of patients (e.g. temporal lobe, frontal lobe) to test whether the SSI may be useful in classifying epilepsy subtypes from scalp EEG.

# References


1. Fiest, K. M. *et al.* Prevalence and incidence of epilepsy. *Neurology* **88,** 296 (Jan. 17, 2017).
2. Stafstrom, C. E. & Carmant, L. Seizures and Epilepsy: An Overview for Neuroscientists. *Cold Spring Harb Perspect Med.* **5,** a022426 (2015).
3. Fisher, R. S. *et al.* Operational classification of seizure types by the International League Against Epilepsy: Position Paper of the ILAE Commission for Classification and Terminology. *Epilepsia* **58,** 522–530 (2017).
4. Falco-Walter, J. J., Scheffer, I. E. & Fisher, R. S. The new definition and classification of seizures and epilepsy. *Epilepsy Research* **139,** 73–79 (2018).
5. Gavvala, J. R. & Schuele, S. U. New-Onset Seizure in Adults and Adolescents: A Review. *JAMA* **316,** 2657–2668 (Dec. 2016).
6. Benbadis, S., Beniczky, S., Bertram, E., MacIver, S. & SL, M. The role of EEG in patients with suspected epilepsy. *Epileptic Discord* **22,** 143–155 (2020).
7. Bernheimer, R., O'Neal, S. & Kellogg, M. Analysis of EEG Use Utilizing the National Inpatient Sample (P3.263). *Neurology* **90.** eprint: https://n.neurology.org/content (2018).
8. Fountain, N. *et al.* Quality improvement in neurology: AAN epilepsy quality measures. *Neurology* **76,** 94–99 (2011).
9. Pillai, J. & Sperling, M. R. Interictal EEG and the Diagnosis of Epilepsy. *Epilepsia* **47,** 14–22 (2006).
10. Kaplan, P. & Fisher, R. *Imitators of epilepsy.* (Jan. 2005).
11. Fisher, R. S. *et al.* ILAE Official Report: A practical clinical definition of epilepsy. *Epilepsia* **55,** 475–482 (2014).
12. Mathias, S. V. & Bensalem-Owen, M. Artifacts That Can Be Misinterpreted as Interictal Discharges. *Journal of Clinical Neurophysiology* **36.** doi:10.1097 (2019).
13. Kural, M. A. *et al.* Criteria for defining interictal epileptiform discharges in EEG. *Neurology* **94,** e2139–e2147 (2020).
14. *Practices in children's nursing e-book* 3rd (eds Ford, L., Trigg, E., Mohammed, T., Montgomery, H. & Vidler Vickyand, E.) (Churchill Livingstone Elsevier, 2010).
15. Blume, W. T. Diagnosis and management of epilepsy. *CMAJ* **168,** 441–448 (2003).
16. Chadwick, D. & Smith, D. The misdiagnosis of epilepsy. *BMJ (Clinical research ed.)* **324,** 495–496 (2002).

17. Xu, Y. *et al.* Frequency of a false positive diagnosis of epilepsy: A systematic review of observational studies. *Seizure* **41,** 167–174 (2016).

18. Smith, D., Defalla, B. & Chadwick, D. The misdiagnosis of epilepsy and the management of refractory epilepsy in a specialist clinic. *QJM: An International Journal of Medicine* **92,** 15–23 (1999).

19. Chowdhury, F. A., Nashef, L. & Elwes, R. D. Misdiagnosis in epilepsy: a review and recognition of diagnostic uncertainty. *Eur J Neurol* **15,** 1034–1042 (2008).

20. Picot, M.-C., Baldy-Moulinier, M., Daures, J.-P., Dujols, P. & Crespel, A. The prevalence of epilepsy and pharmacoresistant epilepsy in adults: a population-based study in a Western European country. *Epilepsia* **49,** 1230–1238 (2008).

21. Kwan, P. & Brodie, M. J. Definition of refractory epilepsy: defining the indefinable? *The Lancet Neurology* **9,** 27–29 (2010).

22. Berg, A. & Kelly, M. M. Defining intractability: comparisons among published definitions. *Epilepsia* **47,** 431–436 (2006).

23. Kwan, P. & Sander, J. The natural history of epilepsy: an epidemiological view. *J Neurol Neurosurg Psychiatry* **75,** 1376–1381 (2004).

24. Laxer, K. D. *et al.* The consequences of refractory epilepsy and its treatment. *Epilepsy & Behavior* **37,** 59–70 (2014).

25. Cost of refractory epilepsy in adults in the USA. *Epilepsy Research* **23,** 139–148 (1996).

26. Begley, C. E. *et al.* The cost of epilepsy in the United States: an estimate from population-based clinical and survey data. *Epilepsy Research* **23,** 139–148 (1996).

27. Begley, C. E. & Durgin, T. L. The direct cost of epilepsy in the United States: A systematic review of estimates. *Epilepsia* **56,** 1376–1387 (2015).

28. Ferro, M. & Speechley, K. Stability of latent classes in group-based trajectory modeling of depressive symptoms in mothers of children with epilepsy: an internal validation study using a bootstrapping procedure. *Soc Psychiatry Psychiatr Epidemiol* **48,** 1077–1086 (2013).

29. Strzelczyk, A., Griebel, C., Lux, W., Rosenow, F. & Reese, J.-P. The Burden of Severely Drug-Refractory Epilepsy: A Comparative Longitudinal Evaluation of Mortality, Morbidity, Resource Use, and Cost Using German Health Insurance Data. *Frontiers in Neurology* **8,** 712 (2017).

30. Beghi, E. Addressing the burden of epilepsy: Many unmet needs. *Pharmacological Research* **107,** 79–84 (2016).

31. Granata, T. *et al.* Management of the patient with medically refractory epilepsy. *Expert Review of Neurotherapeutics* **9,** 1791–1802 (2009).

32. Lüders, H. O., Najm, I., Nair, D., Widdess-Walsh, P. & Bingman, W. The epileptogenic zone: general principles. *Epileptic Disord* **8,** S1–9 (2006).

33. Jeha, L. E. *et al.* Surgical outcome and prognostic factors of frontal lobe epilepsy surgery. *Brain* **130,** 574–584 (2007).

34. Ramey, W. L. *et al.* Current management and surgical outcomes of medically intractable epilepsy. *Clinical Neurology and Neurosurgery* **115,** 2411–2418 (2013).

35. Rosenow, F. & Lüders, H. Presurgical evaluation of epilepsy. *Brain* **124,** 1683–1700 (Sept. 2001).

36. Nair, D. R., Burgess, R., McIntyre, C. C. & Lüders, H. Chronic subdural electrodes in the management of epilepsy. *Clinical Neurophysiology* **119,** 11–28 (2008).

37. Bancaud, J. *et al.* Functional stereotaxic exploration (SEEG) of epilepsy. *Electroencephalogr Clin Neurophysiol* **28,** 85–86 (1970).

38. Dubeau, F. & McLachlan, R. Invasive electrographic recording techniques in temporal lobe epilepsy. *Can J Neurol Sci* **27,** S29–34 (2000).

39. Jung, W. Y., Pacia, S. V. & Devinsky, O. Neocortical Temporal Lobe Epilepsy: Intracranial EEG Features and Surgical Outcome. *Journal of Clinical Neurophysiology* **16,** 419 (1999).

40. Bulacio, J. C., Chauvel, P. & McGonigal, A. Stereoelectroencephalography: Interpretation. *Journal of Clinical Neurophysiology* **33,** 503–510 (2016).

41. P, P., F, D. & J., G. Intracranial electroencephalographic seizure-onset patterns: effect of underlying pathology. *Brain* **137,** 183–196 (2014).

42. Gumnit, R. J., Labiner, D. M., Fountain, N. B. & Herman, S. T. *Prepared by the National Association of Epilepsy Centers. Data on Specialized Epilepsy Centers: Report to the Institute of Medicine's Committee on the Public Health Dimensions of the Epilepsies. In: Institute of Medicine (US) Committee on the Public Health Dimensions of the Epilepsies* (eds England, M., Liverman, C. T., Schultz, A. M. & et al) doi:https://www.ncbi.nlm.nih.gov/books/NBK100603/ (Epilepsy Across the Spectrum: Promoting Health and Understanding. Washington (DC): National Academies Press (US), 2012).

43. Zhukov, L., Weinstein, D. & Johnson, C. Independent component analysis for EEG source localization. *IEEE Engineering in Medicine and Biology Magazine* **19,** 87–96 (2000).

44. Akyuz, E. *et al.* Revisiting the role of neurotransmitters in epilepsy: An updated review. *Life Sciences* **265,** 118826 (2021).

45. Zhou, Y. & Danbolt, N. C. Glutamate as a neurotransmitter in the healthy brain. *Journal of neural transmission* **12,** 799–817 (2014).

46. Greenamyre, J. T. The Role of Glutamate in Neurotransmission and in Neurologic Disease. *Archives of Neurology* **43,** 1058–1063 (1986).

47. Zhang, W. Q., Hudson, P. M., Sobotka, T. J., Hong, J. S. & Tilson, H. A. Extracellular concentrations of amino acid transmitters in ventral hippocampus during and after the development of kindling. *Brain Research* **540,** 315–318 (1991).

48. Sutherland, M., Delaney, T. & Noebels, J. Subtype specific down-regulation of glutamate transporter gene expression in three models of temporal lobe epilepsy. *Epilepsia* **38** (1997).

49. Crino, P. B. *et al.* Increased expression of the neuronal glutamate transporter (EAAT3/EAAC1) in hippocampal and neocortical epilepsy. *Epilepsia* **43,** 211–218 (2002).

50. Badimon, A., Strasburger, H., Ayata, P. & et al. Negative feedback control of neuronal activity by microglia. *Nature* **586,** 417–423 (2020).

51. Narasimhan, S. *et al.* Seizure-onset regions demonstrate high inward directed connectivity during resting-state: An SEEG study in focal epilepsy. *Epilepsia* **61,** 2534–2544 (2020).

52. Gupta, K., Grover, P. & Abel, T. J. Current Conceptual Understanding of the Epileptogenic Network From Stereoelectroencephalography-Based Connectivity Inferences. *Frontiers in Neurology* **11,** 1441 (2020).

53. Korzeniewska, A. *et al.* Ictal propagation of high frequency activity is recapitulated in interictal recordings: Effective connectivity of epileptogenic networks recorded with intracranial EEG. *NeuroImage* **101,** 96–113 (2014).

54. Bandt, S. K. *et al.* The role of resting state networks in focal neocortical seizures. *PloS one* **9,** e107401 (2014).

55. Kini, L. G. *et al.* Virtual resection predicts surgical outcome for drug-resistant epilepsy. *Brain* **142,** 3892–3905 (2019).

56. Schevon, C. A. *et al.* Evidence of an inhibitory restraint of seizure activity in humans. Nature communications. **3,** 1060 (2012).

57. Jerome Engel, J. *Seizures and Epilepsy* doi:10.1093/med/9780195328547.001.0001 (Oxford University Press, Oxford, UK, Aug. 2013).

58. Li, A. *et al. Linear time-varying model characterizes invasive EEG signals generated from complex epileptic networks* in *2017 39th Annual International Conference of the IEEE Engineering in Medicine and Biology Society (EMBC)* (2017), 2802–2805. doi:10.1109/EMBC.2017.8037439.

59. Hermes, D. & Miller, K. J. *Chapter 19, iEEG: Dura-lining electrodes* (eds Ramsey, N. F. & del R. Millán, J.) 3rd series, 264–277. doi:doi:10.1016/B978-0-444-63934-9.00019-6 (Elsevier B.V., 2020).

60. Bernhardt, B. C., Bonilha, L. & Gross, D. W. Network analysis for a network disorder: The emerging role of graph theory in the study of epilepsy. *Epilepsy & Behavior* **50,** 162–170 (2015).

61. Li, A. *et al.* Using network analysis to localize the epileptogenic zone from invasive EEG recordings in intractable focal epilepsy. *Netw Neurosci.* **2,** 281–240 (2015).

62. Bassett, D. & Sporns, O. Network neuroscience. *Nat Neurosci* **20,** 353–364 (2017).

63. Stacey, W. *et al.* Emerging roles of network analysis for epilepsy. *Epilepsy Research* **159.** doi:https://doi.org/10.1016/j.eplepsyres.2019.106255 (2020).

64. Li, A. *et al.* Neural fragility as an EEG marker of the seizure onset zone. *Nat Neurosci.* doi:ttps://doi.org/10.1038/s41593-021-00901-w (2021).

65. Bartolomei, F., Chauvel, P. & Wendling, F. Epileptogenicity of brain structures in human temporal lobe epilepsy: a quantified study from intracerebral EEG. *Brain* **131,** 1818–1830 (June 2008).

66. Gnatkovsky, V. *et al.* Identification of reproducible ictal patterns based on quantified frequency analysis of intracranial EEG signals. *Epilepsia* **52,** 477–488 (2011).

67. Van Mierlo, P. *et al.* Ictal-onset localization through connectivity analysis of intracranial EEG signals in patients with refractory epilepsy. *Epilepsia* **54,** 1409–1418 (2013).

68. David, O. *et al.* Imaging the seizure onset zone with stereo-electroencephalography. *Brain* **134,** 2898–2911 (2011).

69. Schindler, K. *et al.* Ictal time-irreversible intracranial EEG signals as markers of the epileptogenic zone. *Clinical Neurophysiology* **127,** 3051–3058 (2016).

70. Bou Assi, E., Rihana, S., Nguyen, D. K. & Sawan, M. Effective connectivity analysis of iEEG and accurate localization of the epileptogenic focus at the onset of operculo-insular seizures. *Epilepsy Research* **152,** 42–51 (2019).

71. Quitadamo, L. R. *et al.* EPINETLAB: A Software for Seizure-Onset Zone Identification From Intracranial EEG Signal in Epilepsy. *Frontiers in Neuroinformatics* **12,** 45 (2018).

72. Shah, P. *et al.* Local structural connectivity directs seizure spread in focal epilepsy. *bioRxiv.* doi:10.1101/406793. eprint: https://www.biorxiv.org/content/early/2018/09/04/406793.full.pdf (2018).

73. Li, Y.-H. *et al.* Localization of epileptogenic zone based on graph analysis of stereo-EEG. *Epilepsy Research* **128,** 149–157 (2016).

74. Cimbalnik, J. *et al.* Multi-feature localization of epileptic foci from interictal, intracranial EEG. *Clinical Neurophysiology* **130,** 1945–1953 (2019).

75. Dauwels, J., Eskandar, E. & Cash, S. *Localization of seizure onset area from intracranial non-seizure EEG by exploiting locally enhanced synchrony* in *Annu Int Conf IEEE Eng Med Biol Soc. 2009* (2009), 2180–2183. doi:doi:10.1109/IEMBS.2009.5332447.

76. Ortega, G. J., Menendez de la Prida, L., Sola, R. G. & Pastor, J. Synchronization Clusters of Interictal Activity in the Lateral Temporal Cortex of Epileptic Patients: Intraoperative Electrocorticographic Analysis. *Epilepsia* **49,** 269–280 (2008).

77. Monto, S., Vanhatalo, S., Holmes, M. D. & Palva, J. M. Epileptogenic Neocortical Networks Are Revealed by Abnormal Temporal Dynamics in Seizure-Free Subdural EEG. *Cerebral Cortex* **17,** 1386–1393 (2006).

78. Gliske, S. V. *et al.* Universal automated high frequency oscillation detector for real-time, long term EEG. *Clin Neurophysiol* **127,** 105–1066 (2015).

79. Nariai, H. *et al.* Prospective observational study: Fast ripple localization delineates the epileptogenic zone. *Clinical Neurophysiology* **130,** 2144–2152 (2019).

80. Varatharajah, Y. *et al.* Integrating artificial intelligence with real-time intracranial EEG monitoring to automate interictal identification of seizure onset zones in focal epilepsy. *Journal of neural engineering* **15,** 2144–2152 (2018).

81. Murphy, P. M., von Paternos, A. J. & Santaniello, S. *A novel HFO-based method for unsupervised localization of the seizure onset zone in drug-resistant epilepsy.* in *Annu Int Conf IEEE Eng Med Biol Soc. 2017* (2017), 1054–1057. doi:10.1109/EMBC.2017.8037008.

82. Akiyama, T. *et al.* Focal resection of fast ripples on extraoperative intracranial EEG improves seizure outcome in pediatric epilepsy. *Epilepsia* **52,** 1802–1811 (2011).

83. Conrad, E. C. *et al.* Spatial distribution of interictal spikes fluctuates over time and localizes seizure onset. *Brain* **143,** 554–569 (2019).

84. Gaspard, N., Alkawadri, R., Farooque, P., Goncharova, I. & Zaveri, H. Automatic detection of prominent interictal spikes in intracranial EEG: validation of an algorithm and relationsip to the seizure onset zone. *Clin Neurophysiol.* **125,** 1095–1103 (2014).

85. Wang, S. *et al.* Ripple classification helps to localize the seizure-onset zone in neocortical epilepsy. *Epilepsia* **54,** 370–376 (2013).

86. Gliske, S. V. *et al.* Variability in the location of high frequency oscillations during prolonged intracranial EEG recordings. *Nat Commun* **9,** 2155 (2018).

87. Jr, J. E., Ness, P. C. V., Rasmussen, T. B. & Ojemann, L. M. in *Surgical Treatment of the Epilepsies* (ed Jr, J. E.) 609–621 (Raven Press, 1993).

88. On Neurosurgery of the International League Against Epilepsy (ILAE) 1997?2001: C. *et al.* Proposal for a New Classification of Outcome with Respect to Epileptic Seizures Following Epilepsy?Surgery. *Epilepsia* **42,** 282–286 (2001).

89. Li, L. M. *et al.* Surgical outcome in patients with epilepsy and dual pathology. *Brain* **122,** 799–805 (1999).

90. Sheikh, S. *et al.* (Re)Defining success in epilepsy surgery: The importance of relative seizure reduction in patient-reported quality of life. *Epilepsia* **60,** 2078–2085 (2019).

91. Immonen, A. *et al.* Long-term epilepsy surgery outcomes in patients with MRI-negative temporal lobe epilepsy. *Epilepsia* **51,** 2260–2269 (2010).

92. Elsharkawy, A. E. *et al.* Long-term outcome of extratemporal epilepsy surgery among 154 adult patients. *Journal of Neurosurgery JNS* **108,** 676–686 (2008).

93. Breiman, L. Random forest versus logistic regression: a large-scale benchmark experiment. *Machine Learning* **45,** 5–32 (2001).

94. Couronné, R., Probst, P. & Boulesteix, A. Random forest versus logistic regression: a large-scale benchmark experiment. *BMC Bioinformatics* **19.** doi:https://doi.org/10.1186/s12859-018-2264-5 (2018).

95. Tomita, T. M. *et al. Sparse Projection Oblique Randomer Forests* 2019. arXiv: 1506.03410 [stat.ML].

96. Perry, R. *et al. Manifold Oblique Random Forests: Towards Closing the Gap on Convolutional Deep Networks* 2021. arXiv: 1909.11799 [cs.LG].

97. Bragin, A., Engel, J. & Staba, R. J. High-frequency oscillations in epileptic brain. *Current Opinion in Neurology* **23,** 151–156 (2010).

98. Frauscher, B. *et al.* High-frequency oscillations: The state of clinical research. *Epilepsia* **58,** 1316–1329 (Aug. 2017).

99. Jacobs, J. *et al.* Interictal high-frequency oscillations (80?500 Hz) are an indicator of seizure onset areas independent of spikes in the human epileptic brain. *Epilepsia* **49,** 1893–1907 (2008).

100. Fedele, T. *et al.* Automatic detection of high frequency oscillations during epilepsy surgery predicts seizure outcome. *Clinical Neurophysiology* **127,** 3066–3074 (2016).

101. Jacobs, J. *et al.* High-frequency electroencephalographic oscillations correlate with outcome of epilepsy surgery. *Annals of Neurology* **67,** 209–220 (2010).

102. Staba, R. J., Wilson, C. L., Bragin, A., Fried, I. & Engel, J. Quantitative Analysis of High-Frequency Oscillations (80?500 Hz) Recorded in Human Epileptic Hippocampus and Entorhinal Cortex. *Journal of Neurophysiology* **88,** 1743–1752 (2002).

103. Smith, R. J. *et al.* Computational characteristics of interictal EEG as objective markers of epileptic spasms. *Epilepsy Research* **176,** 106704 (2021).

104. Smith, R. J. *et al.* Infant functional networks are modulated by state of consciousness and circadian rhythm. *Network Neuroscience (Cambridge Mass)* **5,** 614–630 (2021).

105. Charupanit, K. & Lopour, B. A Simple Statistical Method for the Automatic Detection of Ripples in Human Intracranial EEG. *Brain Topogr* **30,** 724–738 (2017).

106. Remakanthakurup Sindhu, K., Staba, R. & Lopour, B. A. Trends in the use of automated algorithms for the detection of high-frequency oscillations associated with human epilepsy. *Epilepsia* **61,** 1553–1569 (2020).

107. Papadelis, C. *et al.* Interictal High Frequency Oscillations Detected with Simultaneous Magnetoencephalography and Electroencephalography as Biomarker of Pediatric Epilepsy. *J. Vis. Exp.* **118,** e54883 (2016).

108. Bergey, G. K. *et al.* Long-term treatment with responsive brain stimulation in adults with refractory partial seizures. *Neurology* **84,** 810–817 (2015).

109. Skarpaas, T. L., Jarosiewicz, B. & Morrell, M. J. Brain-responsive neurostimulation for epilepsy (RNS System®). *Epilepsy Research* **153,** 68–70 (2019).

110. Hartshorn, A. & Jobst, B. Responsive brain stimulation in epilepsy. *Therapeutic advances in chronic disease* **9,** 135–142 (2018).

111. Medvedev, A. V., Murro, A. M. & Meador, K. J. Abnormal interictal gamma activity may manifest a seizure onset zone in temporal lobe epilepsy. *International Journal of Neural Systems* **21.** PMID: 21442774, 103–114 (2011).

112. Guggisberg, A. G., Kirsch, H. E., Mantle, M. M., Barbaro, N. M. & Nagarajan, S. S. Fast oscillations associated with interictal spikes localize the epileptogenic zone in patients with partial epilepsy. *NeuroImage* **39,** 661–668 (2008).

113. Chen, D., Wan, S. & Bao, F. S. Epileptic Focus Localization Using Discrete Wavelet Transform Based on Interictal Intracranial EEG. *IEEE Transactions on Neural Systems and Rehabilitation Engineering* **25.** Conference Name: IEEE Transactions on Neural Systems and Rehabilitation Engineering, 413–425 (May 2017).

114. Samuel P. Burns *et al.* Network dynamics of the brain and influence of the epileptic seizure onset zone. *Proceedings of the National Academy of Sciences* **111,** E5321–E5330 (2014).

115. Yaffe, R. B. *et al.* Physiology of functional and effective networks in epilepsy. *Clinical Neurophysiology: Official Journal of the International Federation of Clinical Neurophysiology* **126,** 227–236 (Feb. 2015).

116. Khambhati, A. N., Davis, K. A., Lucas, T. H., Litt, B. & Bassett, D. S. Virtual Cortical Resection Reveals Push-Pull Network Control Preceding Seizure Evolution. *Neuron* **91,** 1170–1182 (Sept. 7, 2016).

117. Zijlmans, M. *et al.* High-Frequency Oscillations as a New Biomarker in Epilepsy. *Annals of neurology* **71,** 169–178 (2012).

118. Jacobs, J. *et al.* Removing high-frequency oscillations: A prospective multicenter study on seizure outcome. *Neurology* **91,** e1040–e1052 (2018).

119. Höller, Y. *et al.* High-frequency oscillations in epilepsy and surgical outcome. A meta-analysis. *Frontiers in Human Neuroscience* **9,** 574 (2015).

120. Wang, S. *et al.* Interictal ripples nested in epileptiform discharge help to identify the epileptogenic zone in neocortical epilepsy. *Clinical Neurophysiology* **128,** 945–951 (2017).

121. Sindhu, K. R., Staba, R. & Lopour, B. A. Trends in the use of automated algorithms for the detection of high-frequency oscillations associated with human epilepsy. *Epilepsia* **61,** 1553–1569 (2020).

122. Van 't Klooster, M. A. *et al.* Tailoring epilepsy surgery with fast ripples in the intraoperative electrocorticogram. *Annals of Neurology* **81,** 664–676 (2017).

123. Worrell, G. & Gotman, J. High-frequency oscillations and other electrophysiological biomarkers of epilepsy: clinical studies. *Biomarkers in Medicine* **5,** 557–566 (2011).

124. Thomschewski, A., Hincapié, A.-S. & Frauscher, B. Localization of the Epileptogenic Zone Using High Frequency Oscillations. *Frontiers in Neurology* **10,** 94 (2019).

125. Fisher, R. S., Webber, W. R., Lesser, R. P., Arroyo, S. & Uematsu, S. High-frequency EEG activity at the start of seizures. *Journal of Clinical Neurophysiology: Official Publication of the American Electroencephalographic Society* **9,** 441–448 (1992).

126. Haegelen, C. *et al.* High-frequency oscillations, extent of surgical resection, and surgical outcome in drug-resistant focal epilepsy. *Epilepsia* **54,** 848–857 (2013).

127. Cho, J. R. *et al.* Resection of individually identified high-rate high-frequency oscillations region is associated with favorable outcome in neocortical epilepsy. *Epilepsia* **55,** 1872–1883 (2014).

128. Liu, C. *et al.* High frequency oscillations for lateralizing suspected bitemporal epilepsy. *Epilepsy Research* **127,** 233–240 (2016).

129. Grinenko, O. *et al.* A fingerprint of the epileptogenic zone in human epilepsies. *Brain: A Journal of Neurology* **141,** 117–131 (2018).

130. Gloss, D., Nevitt, S. J. & Staba, R. The role of high-frequency oscillations in epilepsy surgery planning. *The Cochrane Database of Systematic Reviews* **2017,** CD010235 (2017).

131. Gardner, A. B., Worrell, G. A., Marsh, E., Dlugos, D. & Litt, B. Human and Automated Detection of High-Frequency Oscillations in Clinical Intracranial EEG Recordings. *Clinical neurophysiology : official journal of the International Federation of Clinical Neurophysiology* **118,** 1134–1143 (2007).

132. Tommaso Fedele *et al.* Prediction of seizure outcome improved by fast ripples detected in low-noise intraoperative corticogram. *Clinical Neurophysiology* **128,** 1220–1226 (2017).

133. Halász, P. & Szucs, A. in *Sleep, Epilepsies, and Cognitive Impairment* (eds Halász, P. & Szucs, A.) 1–27 (Academic Press, 2018). doi:10.1016/B978-0-12-812579-3.00001-7.

134. Andrew Matsumoto *et al.* Pathological and physiological high-frequency oscillations in focal human epilepsy. *J Neurophysiol.* **110,** 1958–1964 (2013).

135. Alkawadri, R. *et al.* The spatial and signal characteristics of physiologic high frequency oscillations. *Epilepsia* **55,** 1986–1995 (2014).

136. Engel, J. & da Silva, F. L. High-frequency oscillations - where we are and where we need to go. *Progress in Neurobiology* **98,** 316–318 (Sept. 2012).

137. Staba, R. J. in *Jasper's Basic Mechanisms of the Epilepsies* (eds Noebels, J. L., Avoli, M., Rogawski, M. A., Olsen, R. W. & Delgado-Escueta, A. V.) 4th (National Center for Biotechnology Information (US), Bethesda (MD), 2012).

138. Kobayashi, K. *et al.* Significance of High-frequency Electrical Brain Activity. *Acta Medica Okayama* **71,** 191–200 (2017).

139. Van 't Klooster, M. A. *et al.* Evoked versus spontaneous high frequency oscillations in the chronic electrocorticogram in focal epilepsy. *Clinical Neurophysiology: Official Journal of the International Federation of Clinical Neurophysiology* **128,** 858–866 (2017).

140. Beniczky, S. *et al.* Standardized Computer-based Organized Reporting of EEG: SCORE. *Epilepsia* **54,** 1112–1124 (2013).

141. Kang, J. Y. & Krauss, G. L. Normal Variants Are Commonly Overread as Interictal Epileptiform Abnormalities. *Journal of Clinical Neurophysiology* **36,** 257–263 (2019).

142. Nowack, W. J. Epilepsy: A Costly Misdiagnosis. *Clinical Electroencephalography* **28,** 225–228 (1997).

143. Daly, D. D. in *Current Practice of Clinical Electroencephalography* (eds Daly, D. D. & Pedley, T. A.) 269–334 (Raven Press Publishers, New York, NY, 1990).

144. McKay, J. H. & Tatum, W. O. Artifact Mimicking Ictal Epileptiform Activity in EEG. *Journal of Clinical Neurophysiology* **36,** 275–288 (2019).

145. Maganti, R. & Rutecki, P. EEG and epilepsy monitoring. *Continuum (Minneap Minn)* **19,** 598–622 (2013).

146. Thomas, J. *et al.* Automated Detection of Interictal Epileptiform Discharges from Scalp Electroencephalograms by Convolutional Neural Networks. *International Journal of Neural Systems* **30,** 2050030 (2020).

147. Tjepkema-Cloostermans, M. C., de Carvalho, R. C. & van Putten, M. J. Deep learning for detection of focal epileptiform discharges from scalp EEG recordings. *Clinical Neurophysiology* **129,** 2191–2196 (2018).

148. Gotman, J., Flanagan, D., Rosenblatt, B., Bye, A. & Mizrahi, E. Evaluation of an automatic seizure detection method for the newborn EEG. *Electroencephalography and Clinical Neurophysiology* **103,** 363–369 (1997).

149. Halford, J. J. Computerized epileptiform transient detection in the scalp electroencephalogram: Obstacles to progress and the example of computerized ECG interpretation. *Clinical Neurophysiology* **120,** 1909–1915 (2009).

150. van Putten, M. J. The revised brain symmetry index. *Clinical Neurophysiology* **118,** 2362–2367 (2007).

151. Delorme, A. & Makeig, S. EEGLab: and open source toolbox for analysis of single-trial EEG dynamics. *J Neurosci Methods* **134,** 9–21 (2004).

152. Makeig, S., Bell, A. J., Jung, T.-P. & Sejnowski, T. J. in *Advances in Neural Information Processing Systems 8* (eds Touretzky, D., Mozer, M. & Hasselmo, M.) 145–151 (MIT Press, Cambridge, MA, 1996).

153. Kullback, S. & Leibler, R. A. On Information and Sufficiency. *The Annals of Mathematical Statistics* **22,** 79–86 (1951).

154. Kahane, P. & Spencer, S. Chapter 51. Invasive evaluation. *Handbook of clinical neurology / edited by P.J. Vinken and G.W. Bruyn* **108,** 867–79 (Dec. 2012).

155. Holmes, M. D. in *Management of Epilepsy – Research Results and Treatment (Chapter 8)* 153–168 (2011). doi:10.5772/17244.

156. Smith, S. J. M. EEG in the diagnosis, classification, and management of patients with epilepsy. *Journal of Neurology, Neurosurgery & Psychiatry* **76,** ii2–ii7 (2005).

157. Lachaux, J. P., Rudrauf, D. & Kahane, P. Intracranial EEG and human brain mapping. *Journal of Physiology-Paris. Neuroscience and Computation* **97,** 613–628 (2003).

158. Logothetis, N. K., Pauls, J., Augath, M., Trinath, T. & Oeltermann, A. Neurophysiological investigation of the basis of the fMRI signal. *Nature* **412,** 150–157 (2001).

159. Hays, M. A., Coogan, C., Crone, N. E. & Kang, J. Y. Graph theoretical analysis of evoked potentials shows network influence of epileptogenic mesial temporal region. *Human Brain Mapping* **42,** 4173–4186 (2021).

160. J J Maller *et al.* Revealing the Hippocampal Connectome through Super-Resolution 1150-Direction Diffusion MRI. *Sci Rep* **9,** 2418 (2019).

161. Isokawa-Akesson, M., Wilson, C. L. & Babb, T. L. Inhibition in synchronously firing human hippocampal neurons. *Epilepsy Research* **3,** 236–247 (1989).

162. Haneef, Z. *et al.* Functional Connectivity of Hippocampal Networks in Temporal Lobe Epilepsy. *Epilepsia* **55,** 137–145 (2014).

163. Gaelle Bettus *et al.* Decreased basal fMRI functional connectivity in epileptogenic networks and contralateral compensatory mechanisms. *Human Brain Mapping* **30,** 1580–1591 (2009).

164. Holmes, M. *et al.* Resting state functional connectivity of the hippocampus associated with neurocognitive function in left temporal lobe epilepsy. *Human Brain Mapping* **35,** 735–744 (2014).

165. Pereira, F. R. *et al.* Asymmetrical hippocampal connectivity in mesial temporal lobe epilepsy: evidence from resting state fMRI. *BMC Neuroscience* **11,** 66 (2010).

166. Urigöen, J. A. & Garcia-Zapirain, B. EEG artifact removal—state-of-the-art and guidelines. *Journal of Neural Engineering* **12,** 031001 (Apr. 2015).

167. Romero, S., Mañanas, M. A. & Barbanoj, M. J. A comparative study of automatic techniques for ocular artifact reduction in spontaneous EEG signals based on clinical target variables: A simulation case. *Computers in Biology and Medicine* **38,** 348–360 (2008).

168. *Copyright* (eds Sörnmo, L. & Laguna, P.) doi:https://doi.org/10.1016/B978-0-12-437552-9.50013-1 (Academic Press, Burlington, 2005).

# Appendix I

# Additional results for predicting surgical outcomes using the random forest classifier

## A Statistical analysis of SSI distributions

**Table I-I.** Comparison of SSI distributions in EZ versus non-EZ channels.

| | **P-value** | |
|---|---|---|
| | **Success patients** | **Failure patients** |
| **Sink index** | $1.1997 \times 10^{-6}$ | 0.0076 |
| **Source influence** | $1.6217 \times 10^{-7}$ | 0.3331 |
| **Sink connectivity** | $1.3070 \times 10^{-7}$ | 0.0771 |

# B Test set ROC curves

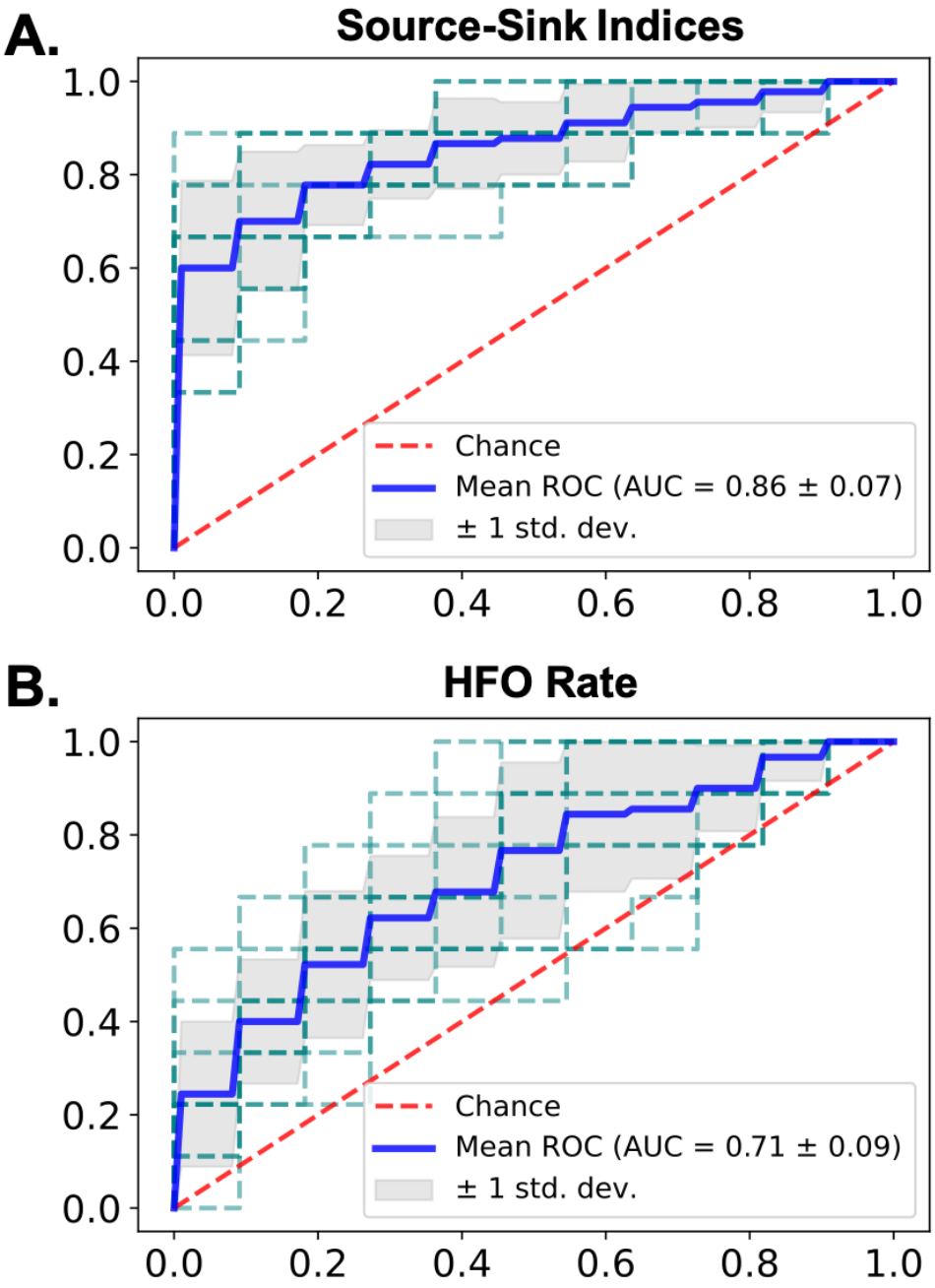


**Figure I-1.** A. ROC curves for the source-sink model. Blue line shows the mean ROC across the ten CV folds and the shaded gray area represents one standard deviation. The resulting ROC of each CV fold is shown with a dashed green line. B. ROC for the HFO model. The mean AUC of the HFO model is significantly lower than the mean AUC of the source-sink model.

# C Probability of success stratified by clinical covariates

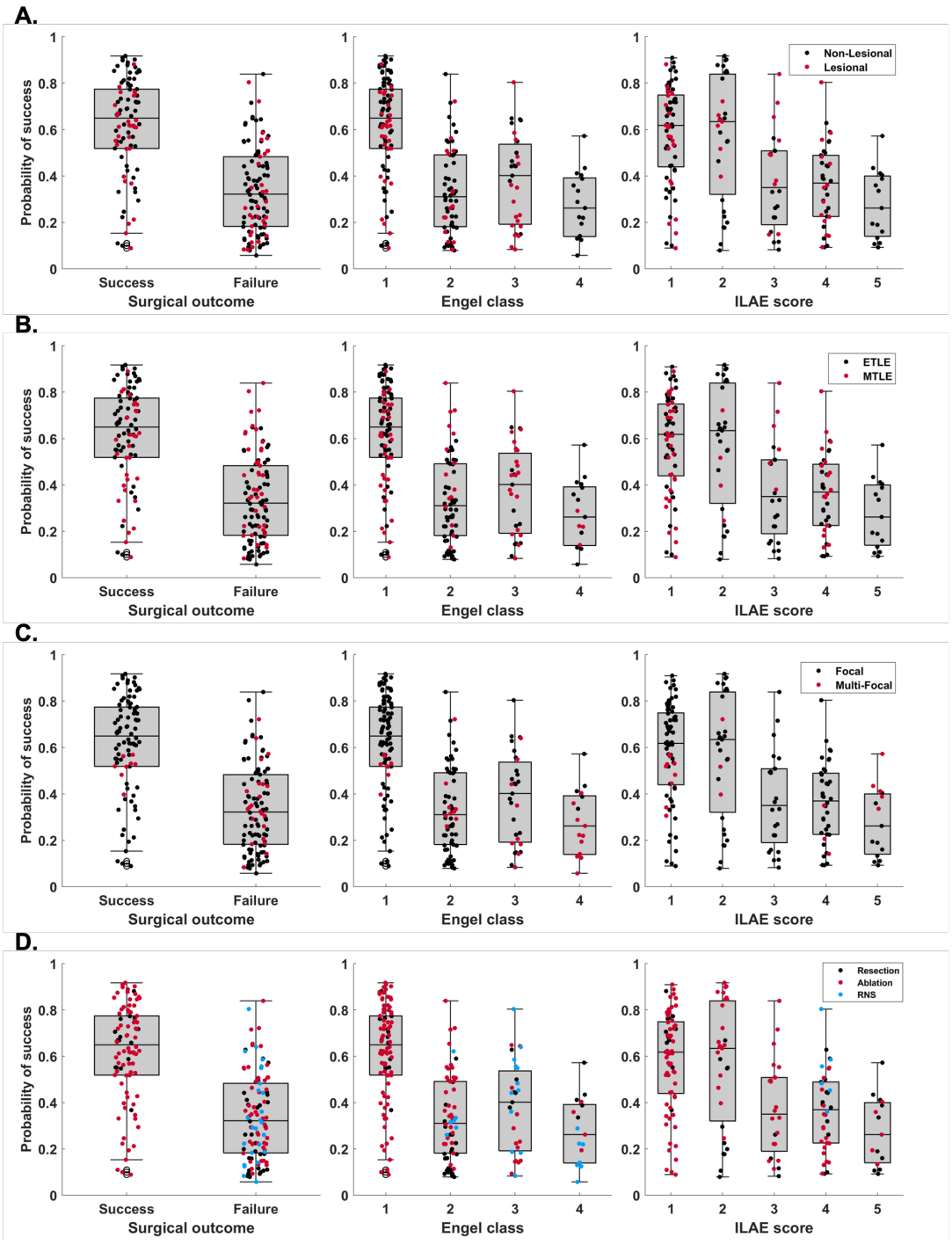


**Figure I-2**

**Figure I-2.** Distributions of $p_s$ across all CV folds as predicted by the source-sink model. The dots represent patients and are color-coded by different clinical covariates. A. Although lesional patients generally have a higher chance of a successful outcome, there is no correlation between $p_s$ and whether patients have a lesion or not. B. Similarly, mesial-temporal epilepsy (MTLE) have higher success rates compared to extra-temporal epilepsy (ETLE) patients, but we see no correlation with $p_s$ values. C. The tool is also agnostic to whether seizures start in one (focal) or a few (multi-focal) regions. D. Patients who receive RNS treatment are generally not expected to achieve complete seizure freedom. This was reflected in our dataset, with only one RNS patient that had a successful surgical outcome. Consequently, the predicted probability of success by the source-sink model was overall lower for RNS patients compared to patients that received surgical treatment.

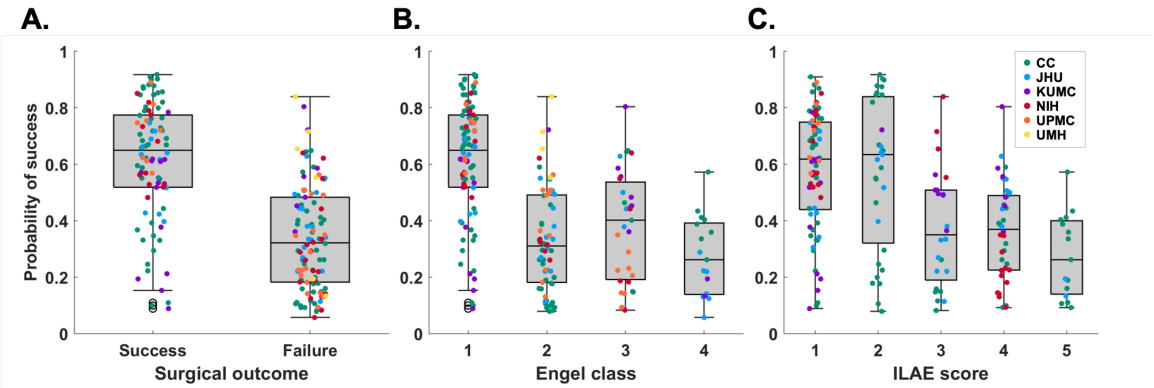


**Figure I-3.** Distributions of $p_s$ across all CV folds as predicted by the source-sink model. The dots represent patients and are color-coded by different clinical centers. The tool generalizes well across data from different clinical centers indicated by the even distribution of $p_s$ values across all centers.

# Appendix II

# Predicting surgical outcomes using logistic regression

## A Methods

### A.1 Modeling the probability of a successful outcome as a function of source-sink indices

To further evaluate the source-sink metrics as interictal iEEG markers of the EZ, we tested their efficacy in predicting surgical outcomes using a simple logistic regression model. Specifically, we modeled the probability of a successful surgical outcome, $p_s$, as a function of the three source-sink index metrics (2.2-2.5) using logistic regression as follows:

$$log\left(\frac{p_s}{1-p_s}\right) = \beta_0 + \beta_1(sink_{EZ} - sink_{NEZ}) + \beta_2(infl_{EZ} - infl_{NEZ}) + \beta_3(conn_{EZ} - conn_{NEZ}) \tag{II.1}$$

where $sink_{EZ}$ is the average sink index over all CA-EZ channels and $sink_{NEZ}$ is the

average sink index over the rest of the implanted channels. Similarly, $infl_{EZ}$ is the average source influence index over all CA-EZ channels and $infl_{NEZ}$ is the average source influence index over the rest of the channels. Finally, $conn_{EZ}$ is the average sink connectivity index over all CA-EZ channels and $conn_{NEZ}$ is the average sink connectivity index over the rest of the channels in the network.

The model performance was evaluated on a held-out test data set (30%) using a 10-fold cross-validation, and the same training and test set partitions as for the RF model, as described in section A.2 below.

## A.2 Statistical Analysis

### A.2.1 Predictive Power of SSIs

The LR model was validated using a 10-fold cross-validation (CV) by creating ten random splits of the dataset into training and test sets. We used the same training and test set splits as were used for the RF model for a fair comparison. In each such split, 70% of the patients (n=45) were assigned to the training set while also ensuring a balanced number of success and failure patients, and the remaining 30% (n=20) were used for testing. The model was fit to the training data and validated on the test set by applying a varying threshold to the model's output and computing a receiver operating characteristic (ROC) curve which plots true positive rates against false positive rates for various threshold values. As we explained in section 3.2.9, the area under the curve (AUC) is a measure of separability, i.e., it tells us how well the model can distinguish between success versus failed outcomes. The larger the AUC, the more predictive the model is. Next, we selected the threshold that maximized prediction accuracy in each split and evaluated performance by comparing each patient's predicted outcome to the actual surgical outcome.

In addition to the AUC, we used four metrics to measure model performance:

a) prediction accuracy, which is the fraction of patients whose outcome the model predicted correctly, b) precision, which is the proportion of predicted successful results that are actual successful surgeries, c) sensitivity, which measures the proportion of actual successful surgeries that were identified correctly and d) specificity, which refers to the proportion of failed surgeries that the models predicted correctly We report results of the ten CV iterations (mean ± standard deviation) below.

# B Results

## B.1 Source-sink metrics perform well in predicting surgical outcomes

As stated above, the SSI, and consequently the three metrics (sink index, source influence and sink connectivity) used to compute the SSI, are significantly higher in CA-EZ channels compared to the rest of the iEEG network in patients with successful surgical outcomes but not necessarily in failure patients ($p_{SSI}^{success} = 1.16 \times 10^{-4}$ and $p_{SSI}^{failure} = 0.0359$, see other p-values in Supplementary Table I-I). Taking advantage of this assumption, we built the logistic regression model in eq. II.1 to predict the probability of a successful surgical outcome for each patient. The resulting ROC curve (mean ± standard error) obtained from training the models is shown in Fig. II-1A and Fig. II-1B shows the test set ROC for comparison. The AUC of the test set was $0.85 \pm 0.02$ which was equal to the AUC of the training set, suggesting that the model generalizes well across different datasets. Fig. II-1C shows distributions of model coefficient estimates and associated p-values across the ten CV iterations. Using the source-sink indices, the optimal threshold ($\alpha = 0.57 \pm 0.16$, see Fig. II-2), when applied to the estimated probability of a successful outcome for each subject ($p_s$) rendered a test set accuracy of $73.5 \pm 4.7\%$ and an accuracy of $80.0 \pm 1.8\%$ on the

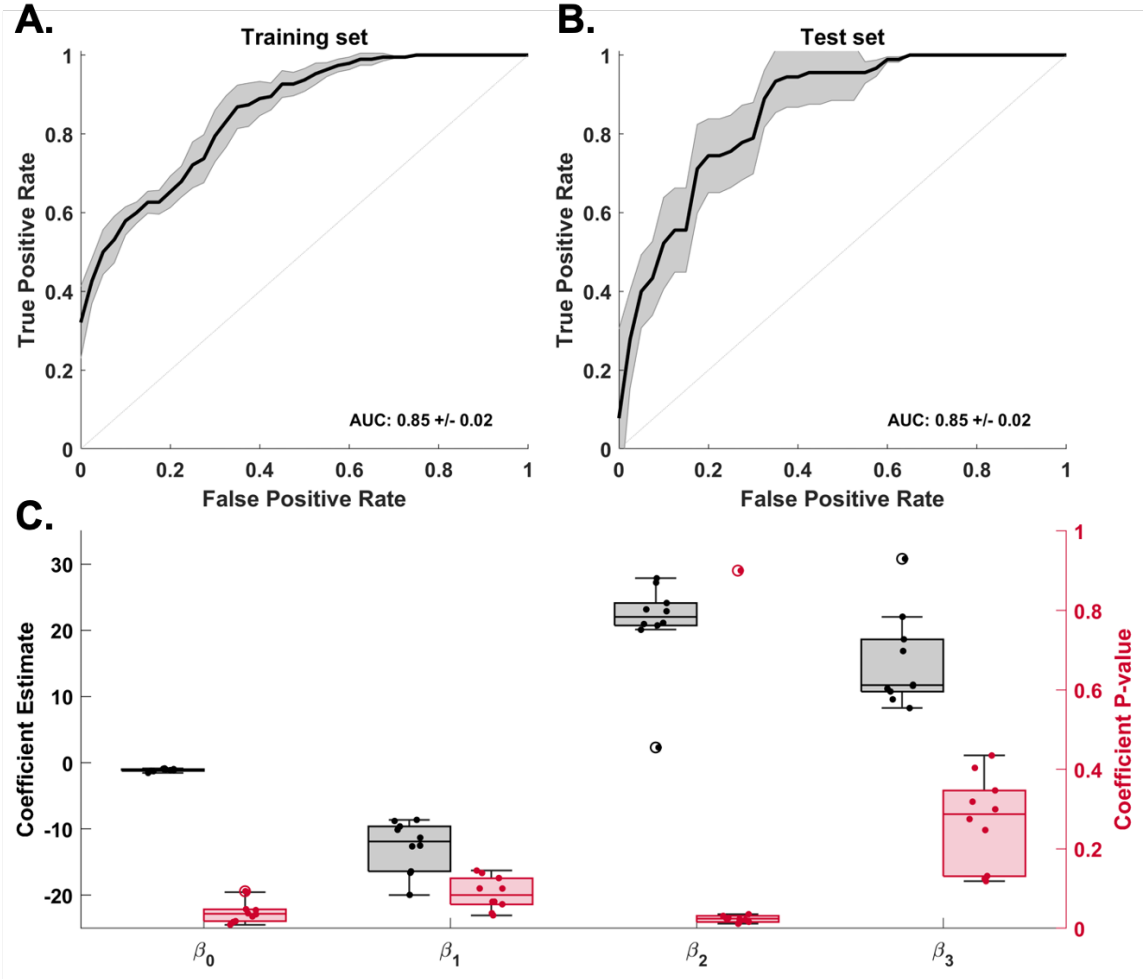


**Figure II-1.** A. Training set ROC curve across the ten CV folds. The black line represents the mean ROC curve and the shaded gray area represents standard error across the folds. B. Test set ROC curve (mean ± standard error). Note that the AUC of the test set is equal to that of the training set, indicating generalizability of the model across different datasets. C. Model coefficient distributions across the ten CV folds (gray) and their associated p-values (red).

training set. Further, the model yielded a test set precision of $0.81 \pm 0.15$, a sensitivity of $0.62 \pm 0.22$ and a specificity of $0.83 \pm 0.16$. These results are highly comparable to the results obtained using the RF model (see section 3.3.4). Additionally, as Fig. II-2 shows, the performance of the LR model on the test set was highly comparable to that of the training set, suggesting robustness of performance on different data sets.

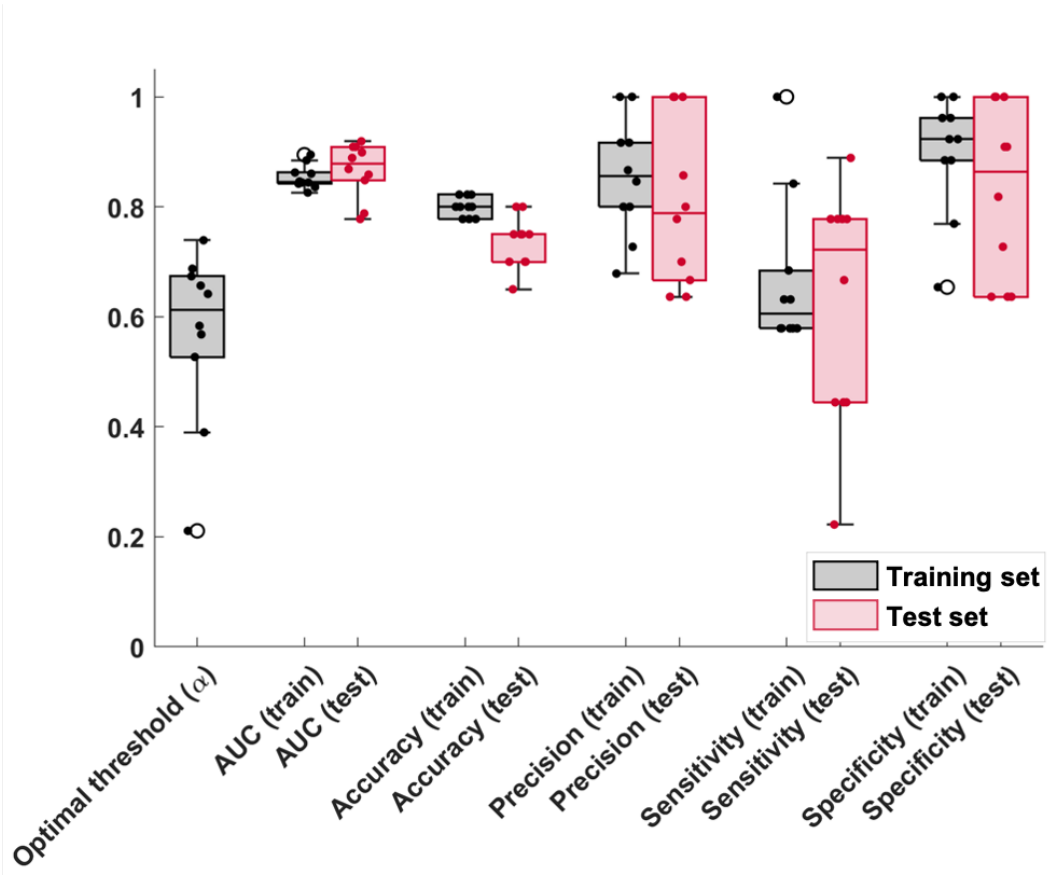


**Figure II-2.** Model performance on the training set (gray) and test set (red). Boxes show distributions of each metric across the ten CV folds. Although there is more variability across the CV folds for the test set, the test set performance is comparable to that of the training set which suggests robustness of performance on different data sets.

## B.2 The source-sink metrics are highly correlated with treatment outcomes

Fig. II-3A compares the predicted probability of success ($p_s$) in success versus failure patients using the mean model (averaged across all ten CV iterations) of the source-sink metrics. The model performs well in discriminating between the two outcome possibilities as reflected in the separation between the $p_s$ distributions of success versus failure patients ($p = 5.89 \times 10^{-8}$). Similar to the RF model, we observed a general pattern of decreasing $p_s$ as outcome scores (and thus also the severity of post-operative seizure outcome) increased as shown in Figs. II-3B and II-3C.

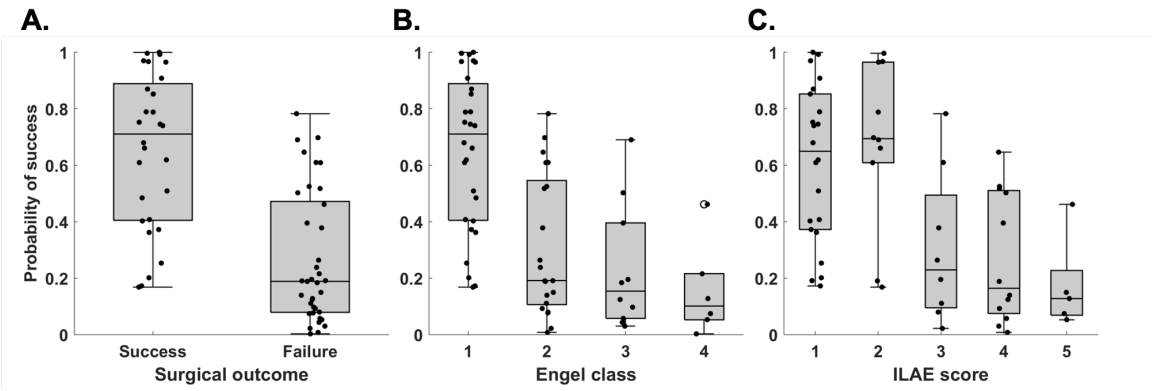


**Figure II-3.** Distributions of $p_s$ as predicted by the source-sink model. Each dot represents one patient. A. There is a good separation of the distributions for successful cases versus failed cases. B. Distributions of $p_s$ stratified by Engel Class (Success = Engel 1, Failure = Engel 2-4). There is a general trend of decreasing $p_s$ values as the Engel class (and thus also severity of surgical outcome) increases. C. Distributions of $p_s$ stratified by ILAE scores follow a similar trend to those observed for the Engel class in B. For ILAE scores, ILAE 1-2 are considered a successful outcome whereas ILAE 3-5 correspond to failed outcomes.

## B.3 Generalizability of source-sink indices

We compared $p_s$ for three categories that describe the clinical complexity of each patient. Although lesional patients frequently have better localizable EZ and thus tend to have higher chances of successful outcomes, we saw no correlation to the predicted probability of success in our models (Fig. II-4A). Similarly, patients with extra-temporal epilepsy (ETLE) generally have lower success rates compared to mesial-temporal epilepsy (MTLE) patients, but our tool was also agnostic to whether patients had ETLE or MTLE (Fig. II-4B). Patients with multi-focal epilepsy are often more difficult to treat because the seizures can originate from more than one brain area. This was reflected in our data where only one multi-focal patient had a successful surgical outcome and in turn, the predicted success probability of the source-sink model (Fig. II-4C) was commonly lower for these patients.

Next, we analyzed the success probability with respect to treatment method (Fig. II-4D). Patients who are surgical candidates (i.e., the seizure focus can be localized and treated) generally undergo either resective surgery or laser ablation. In patients

with poorly localizable or multiple seizure foci, or when the EZ is located in eloquent cortex, surgical resection may not be an option. In these cases, many patients opt for RNS treatment instead. Because of the higher clinical case complexity, patients who receive RNS treatment are not expected to achieve complete seizure freedom, but rather a reduction in seizure frequency [108–110]. This was reflected in the predicted probability of success by the source-sink model, which was overall lower for RNS patients compared to patients that received surgical treatment. In contrast, there was no observable correlation between $p_s$ and surgical resection or laser ablation.

Finally, we compared $p_s$ across clinical centers. As Fig. II-5 shows, the range of $p_s$ values is similar across centers and outlier values of $p_s$ in each surgical-outcome distribution are from various centers. As such, the distributions are not skewed by $p_s$ values from any particular center, indicating generalizability of the model across different datasets.

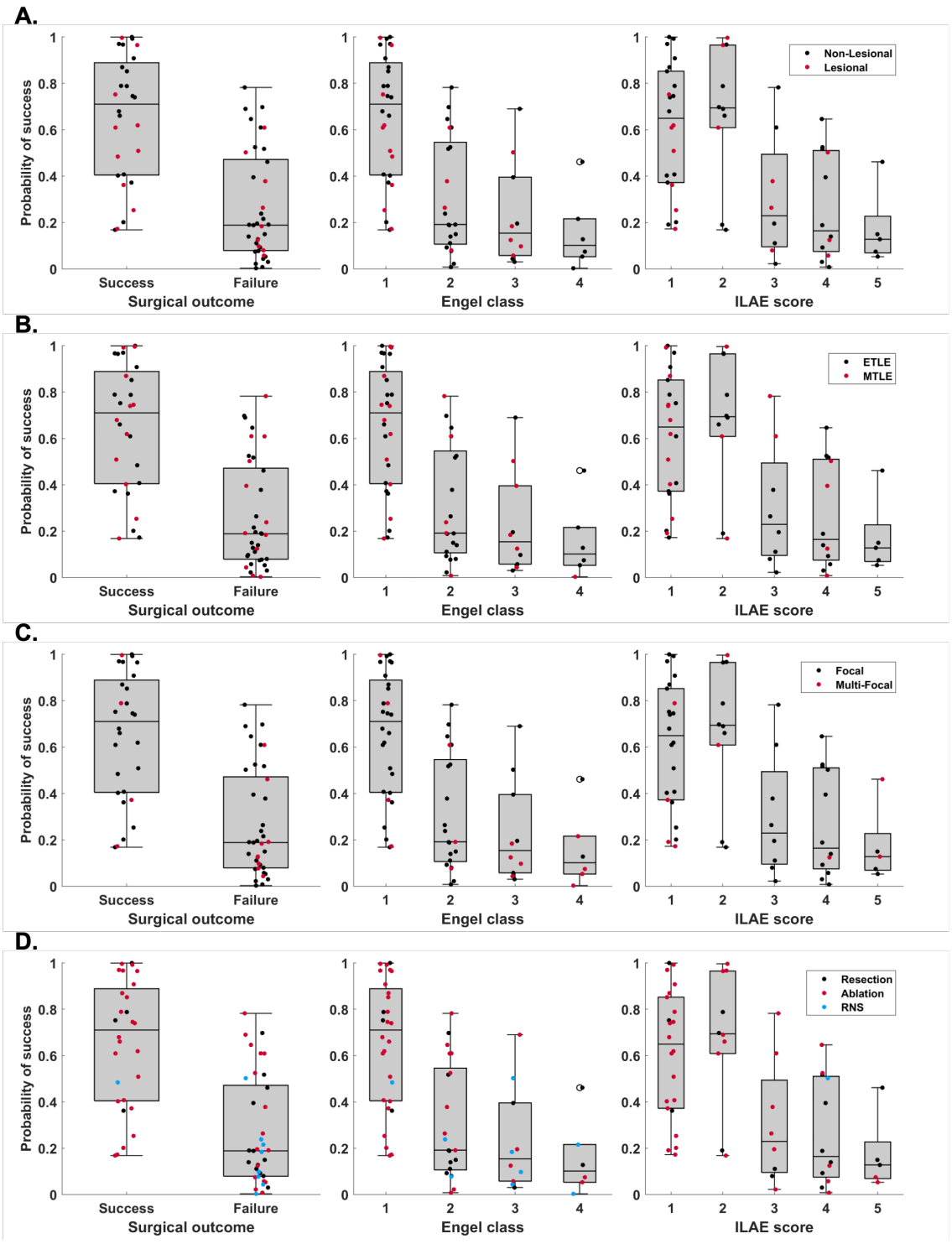
A.
Probability of success
Success
Failure
Surgical outcome
Engel class
ILAE score
Non-Lesional
Lesional
B.
ETLE
MTLE
C.
Focal
Multi-Focal
D.
Resection
Ablation
RNS

**Figure II-4**

**Figure II-4.** Distributions of $p_s$ as predicted by the source-sink model, color-coded by different clinical covariates. Each dot represents one patient. A. Although lesional patients generally have a higher chance of a successful outcome, there is no correlation between $p_s$ and whether patients have a lesion or not. B. Although patients with mesial-temporal epilepsy (MTLE) have higher success rates compared to extra-temporal epilepsy (ETLE) patients, we see no correlation with $p_s$ values. C. The tool is also agnostic to whether seizures start in one (focal) or a few (multi-focal) regions. D. Patients who receive RNS treatment are generally not expected to achieve complete seizure freedom. This was reflected in the predicted probability of success by the source-sink model, which was overall lower for RNS patients compared to patients that received surgical treatment.

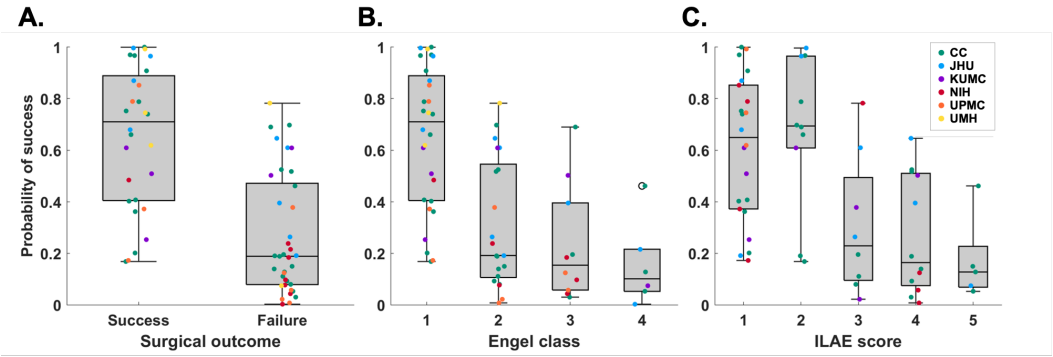


**Figure II-5.** Distributions of $p_s$ as predicted by the source-sink model, color-coded by different clinical centers. Each dot represents one patient. The tool generalizes well across data from different clinical centers.

# Appendix III

# Clinical correspondence stratified by clinical covariates

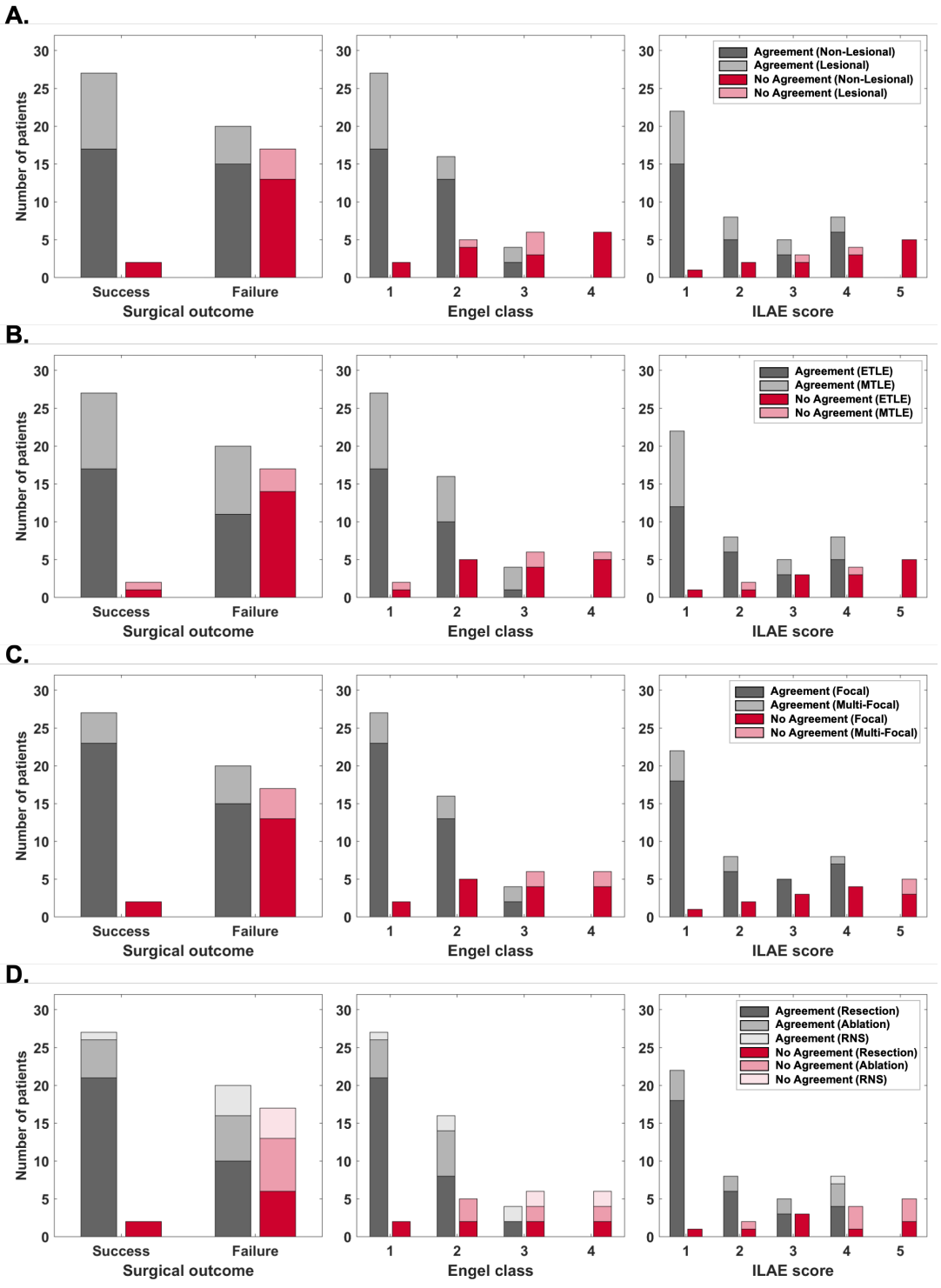
A.
Number of patients
Success
Failure
Surgical outcome
Engel class
ILAE score
Agreement (Non-Lesional)
Agreement (Lesional)
No Agreement (Non-Lesional)
No Agreement (Lesional)
B.
Agreement (ETLE)
Agreement (MTLE)
No Agreement (ETLE)
No Agreement (MTLE)
C.
Agreement (Focal)
Agreement (Multi-Focal)
No Agreement (Focal)
No Agreement (Multi-Focal)
D.
Agreement (Resection)
Agreement (Ablation)
Agreement (RNS)
No Agreement (Resection)
No Agreement (Ablation)
No Agreement (RNS)

**Figure III-1**

**Figure III-1.** Clinical correspondence stratified by clinical covariates. A. Lesional versus non-lesional patients. The proportion of each group is similar across all scores, indicating that the tool is not sensitive to whether patients have a visible lesion on MRI (which often leads to a higher chance of surgical success). B. Mesial-temporal lobe epilepsy (MTLE) versus extra-temporal lobe epilepsy (ETLE). The proportion of each group is similar across all correspondence scores. C. Epilepsy type defined as either focal or multi-focal. The tool is not sensitive to epilepsy type. D. The tool is agnostic to treatment methods. Note however, that in this dataset all but one RNS patients are classified as failed outcomes. RNS treatment is often used if the EZ is in eloquent cortex and as such, patients are not expected to achieve complete seizure freedom.

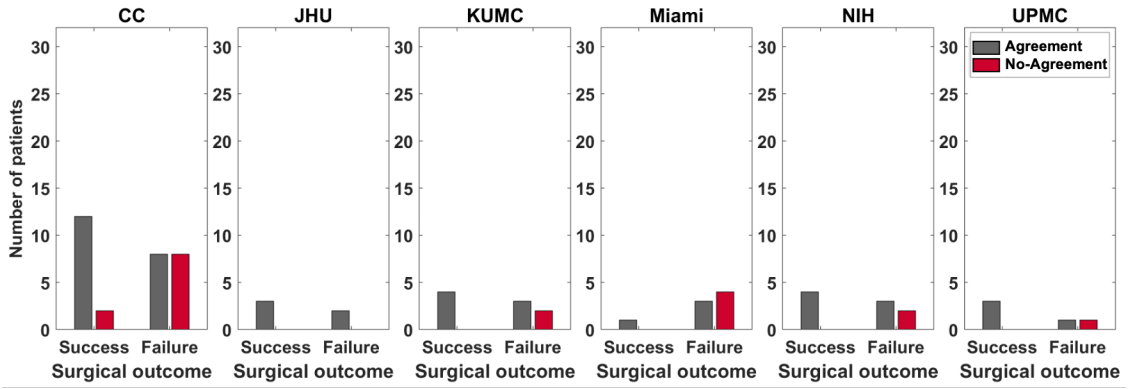


**Figure III-2.** Clinical correspondence stratified by clinical centers. The distribution of agreement scores is similar across centers.

# KRISTIN MARIA GUNNARSDOTTIR

116 West University Parkway, Baltimore, MD 21210 | 443-315-7676 | krimgun@gmail.com

## EDUCATION

| | |
|---|---|
| 2016 – 2021 | **Ph.D. in Biomedical Engineering**<br>Johns Hopkins University, Baltimore, Maryland, USA |
| 2014 – 2016 | **M.Sc. in Biomedical Engineering**<br>Johns Hopkins University, Baltimore, Maryland, USA |
| 2010 – 2013 | **B.Sc. in Biomedical Engineering**<br>Reykjavik University, Iceland |

## HONORS AND AWARDS

| | |
|---|---|
| 2018 | **AES Predoctoral Research Fellowship**<br>American Epilepsy Society |
| 2018 | **Scholarship for graduate studies at university level**<br>Landsbankinn hf., Bank |
| 2017 | **Scholarship for graduate studies abroad**<br>Iceland Chamber of Commerce |
| 2013 | **Graduated with highest GPA over the School of Science and Engineering**<br>Reykjavik University, Iceland |
| 2013 | **Certificate of appreciation for valuable contributions to Reykjavik University**<br>Reykjavik University, Iceland |
| 2010-2013 | **Dean's list, all semesters**<br>Reykjavik University, Iceland |
| 2011 | **Award for achieving the best results in physics in Iceland**<br>The Physics Association of Iceland, Iceland |
| 2010 | **Freshman's grant**<br>Reykjavik University, Iceland |

## WORK AND RESEARCH EXPERIENCE

| | |
|---|---|
| August 2014 – October 2021 | **Graduate Research Assistant (Supervisor: Dr. Sridevi V. Sarma)**<br>*Neuromedical Control Systems Lab, Johns Hopkins University, USA* |
| July 2016 – August 2016 | **Mentor**<br>*Diversity and Academic Advancement Summer Institute (DAASI), USA* |
| May 2013 – May 2014 | **Research Technician (Supervisor: Dr. Þorgeir Pálsson)**<br>Estimated cabin air quality in commercial aircrafts<br>*Reykjavik University, Iceland* |
| January 2013 –<br>April 2013 | **Engineering Intern**<br>Estimated signal quality of RIP breathing belts<br>*Research and Development, Nox Medical, Iceland* |
| May 2012 -<br>August 2012 | **Summer Employee**<br>Projects related to mechanical prosthetic knees<br>*Research & Development, Ossur hf., Iceland* |
| May 2011 | **Office Assistant**<br>Worked on the school's database of graduate students<br>*School of Science and Engineering, Reykjavik University, Iceland* |
| May – August 2007, 2008,<br>2010, 2011 & 2014 | **Nursing Aid**<br>Took care of elderly residents<br>*Sunnuhlíð nursing home, Iceland* |

**TEACHING EXPERIENCE**

| | |
|---|---|
| August 2014 – December 2017 | **Teaching Assistant**, Introduction to Computational Medicine; Systems Bioengineering III; Systems and Controls; BME Modeling and Design<br>*Johns Hopkins University, Baltimore* |
| January 2012 - December 2013 | **Teaching Assistant,** Calculus II; Feedback Control Systems<br>**Instructor,** Homework and other academic support for 1st year students<br>*Reykjavik University, Iceland* |

**CERTIFICATES**

| | |
|---|---|
| 2013 | **Dale Carnegie Training**<br>Dale Carnegie Generation.Next, Reykjavik, Iceland |

**OTHER EXPERIENCE**

| | |
|---|---|
| 2019 – 2021 | **Co-President**<br>Women of Whiting |
| 2018 – 2019 | **Executive Board Member (Professional Development Co-Chair)**<br>Women of Whiting |
| 2017 – 2018 | **Executive Board Member**<br>Women of Whiting (a graduate student organization at JHU dedicated to supporting women in STEM) |
| 2018, 2019, 2020 | **Project Coordinator**<br>JHU-Girl Scout Roller Coaster Competition (An outreach program designed to promote STEM to young girls) |

**PUBLICATIONS**

**Gunnarsdottir, K.M.**, Li, A., Smith, R., et al. (2021). Source-sink connectivity: a novel resting-state EEG marker for seizure localization. bioRxiv 2021.10.15.464594; doi: https://doi.org/10.1101/2021.10.15.464594. (Under review in Brain)

**Gunnarsdottir, K.M.**, Wing S., Gonzalez-Martinez, J., Sarma, S.V. (2021). Sources and Sinks in Interictal iEEG Networks: An iEEG Marker of the Epileptogenic Zone. In *2021 43rd Annual International Conference of the IEEE Engineering in Medicine and Biology Society (EMBC)*

Wing S., **Gunnarsdottir, K.M.**, Gonzalez-Martinez, J., Sarma, S.V. (2021). Transfer Entropy between Intracranial EEG Nodes Highlights Network Dynamics That Cause and Stop Epileptic Seizures. In *2021 43rd Annual International Conference of the IEEE Engineering in Medicine and Biology Society (EMBC)*

Azimi, H., **Gunnarsdottir, K.M**., Sarma, S.V., Gamaldo, A., Salas, R.M.E., Gamaldo, C. (2020). Identifying Sleep Biomarkers to Evaluate Cognition in HIV. In *2020 42nd Annual International Conference of the IEEE Engineering in Medicine and Biology Society (EMBC)* (pp. 2332-2336)

**Gunnarsdottir, K.M.**, Gamaldo, C, Salas, R.M., Ewen, J.B., Allen, R.P., Hu, K., Sarma, S.V. (2020). A novel sleep stage scoring system: Combining expert-based features with the generalized linear model. *J Sleep Res.* 29:e12991. https://doi.org/10.1111/jsr.12991

Stacey, W., Kramer, M., **Gunnarsdottir, K.M.,** Gonzalez-Martinez, J., Zaghloul, K., Inati, S., Sarma, S.V., et al. (2020). Emerging roles of network analysis for epilepsy. *Epilepsy Research.* 159:106255. https://doi.org/10.1016/j.eplepsyres.2019.106255

**Gunnarsdottir, K.M.**, Bulacio, J., Gonzalez-Martinez, J., Sarma, S.V. (2019). Estimating Intracranial EEG Signals at Missing Electrodes in Epileptic Networks. In *2019 41st Annual International Conference of the IEEE Engineering in Medicine and Biology Society (EMBC)* (pp. 3858-3861)

**Gunnarsdottir, K.M.**, Gamaldo, C., Salas, R.M.E., Ewen, J., Allen, R., Sarma, S.V. (2018). A Novel Sleep Stage Scoring System Combining Expert-Based Rules with a Decision Tree Classifier. In *2018 40th Annual International Conference of the IEEE Engineering in Medicine and Biology Society (EMBC)* (pp. 3240-3243).

**Gunnarsdottir, K.M.**, Li, A., Bulacio, J., Gonzalez-Martinez, J., Sarma, S.V. (2017). Estimating Unmeasured Invasive EEG Signals Using a Reduced-Order Observer. In *2017 39th Annual International Conference of the IEEE Engineering in Medicine and Biology Society (EMBC)* (pp. 3216-3219).

Li, A., **Gunnarsdottir, K.M.**, Inati, S., Zaghloul, K., Gale, J., Bulacio, J., Gonzalez-Martinez, J., Sarma, S.V. (2017). Linear Time-Varying Model Characterizes Invasive EEG Signals Generated from Complex Epileptic Networks. In *2017 39th Annual International Conference of the IEEE Engineering in Medicine and Biology Society (EMBC)* (pp. 2802-2805).

**Gunnarsdottir, K.M.**, Sadashivaiah V., Kerr M., Santaniello S., Sarma, S.V. (2016). Using demographic and time series physiological features to classify sepsis in the intensive care unit. In *2016 38th Annual International Conference of the IEEE Engineering in Medicine and Biology Society (EMBC)* (pp. 778-782).

**Gunnarsdottir, K.M**., Kang, Y.M., Kerr, M.S.D., Sarma, S.V., Ewen, J., Allen, R., Gamaldo, C., Salas, R.M.E. (2015). A look at the strength of micro and macro EEG analysis for distinguishing insomnia within an HIV cohort. In *2015 37th Annual International Conference of the IEEE Engineering in Medicine and Biology Society (EMBC)* (pp. 6622–6625).

Kang, Y.M., **Gunnarsdottir, K.M.**, Kerr, M.S.D., Salas, R.M.E., Ewen, J., Allen, R., Gamaldo, C., Sarma, S.V. (2015). To Score or Not to Score? A look at the distinguishing power of micro EEG analysis on an annotated sample of PSG studies conducted in an HIV cohort. In *2015 37th Annual International Conference of the IEEE Engineering in Medicine and Biology Society (EMBC)* (pp. 6626–6629).

## PRESENTATIONS

### ORAL PRESENTATIONS

**Gunnarsdottir, K.M.**, Wing S., Gonzalez-Martinez, J., Sarma, S.V. (November 1st-5th, 2021). *Sources and Sinks in Interictal iEEG Networks: An iEEG Marker of the Epileptogenic Zone*. Presented at the 43rd Annual International Conference of the IEEE Engineering in Medicine and Biology Society (EMBC), Online.

**Gunnarsdottir, K.M.**, Bulacio, J., Gonzalez-Martinez, J., Sarma, S.V. (July 26th, 2019). *Estimating Intracranial EEG Signals at Missing Electrodes in Epileptic Networks*. Presented at the 41st Annual International Conference of the IEEE Engineering in Medicine and Biology Society (EMBC), Berlin, Germany.

**Gunnarsdottir, K.M.**, Gonzalez-Martinez, J., Sarma, S.V. (December 1st, 2018). *Using Network Models of Invasive EEG to solve the Missing Electrode Problem.* Presented at the 2018 AES Annual Meeting, New Orleans, Louisiana.

**Gunnarsdottir, K.M.,** Gamaldo, C., Salas, R.M.E., Ewen, J., Allen, R., Sarma, S.V. (July 20th, 2018). *A Novel Sleep Stage Scoring System Combining Expert-Based Rules with a Decision Tree Classifier*. Presented at the 40th Annual International Conference of the IEEE Engineering in Medicine and Biology Society (EMBC), Honolulu, Hawaii.

**Gunnarsdottir, K.M.,** Li, A., Bulacio, J., Gonzalez-Martinez, J., Sarma, S.V. (October 20th, 2017). *Estimating Unmeasured Invasive EEG Signals Using a Reduced-Order Observer.* Presented at the 2017 Annual Retreat of the Institute for Computational Medicine (ICM), Johns Hopkins University, Baltimore, Maryland.

**Gunnarsdottir, K.M.,** Li, A., Bulacio, J., Gonzalez-Martinez, J., Sarma, S.V. (July 14th, 2017). *Estimating Unmeasured Invasive EEG Signals Using a Reduced-Order Observer*. Presented at the 39th Annual International Conference of the IEEE Engineering in Medicine and Biology Society (EMBC), Jeju Island, Korea.

**Gunnarsdottir, K.M.,** Kang, Y.M., Salas, R.M.E, Gamaldo, C.E., Sarma, S.V. (June 12th, 2015). *Spatio-Temporal Dynamics of Sleep EEG in a Seropositive HIV Cohort.* Presented at CFAR Annual Meeting. Center for AIDS Research, Johns Hopkins University, Baltimore, Maryland.

### POSTER PRESENTATIONS

**Gunnarsdottir, K.M.**, Gonzalez-Martinez, J., Sarma, S.V. (December 4th, 2021). *Source-Sink Analysis for Localization of the Epileptogenic Zone on Interictal Intracranial EEG Data.* Poster presented at the 2021 Annual Meeting of the American Epilepsy Society, Chicago, Illinois.

**Gunnarsdottir, K.M.,** Sadashivaiah, V., Kerr, M.S.D., Santaniello, S., Sarma, S.V. (August 17th, 2016). *Using Demographic and Time Series Physiological Features to Classify Sepsis in the Intensive Care Unit*. Poster presented at the 38th Annual International Conference of the IEEE Engineering in Medicine and Biology Society (EMBC), Orlando, Florida.

**Gunnarsdottir, K. M**., Kang, Y.M., Kerr, M.S.D., Sarma, S.V., Ewen, J., Allen, R., Gamaldo, C., Salas, R.M.E. (August 28th, 2015). *A look at the strength of micro and macro EEG analysis for distinguishing insomnia within an HIV cohort*. Poster presented at the 37th Annual International Conference of the IEEE Engineering in Medicine and Biology Society (EMBC), Milan, Italy.

Kang, Y. M., **Gunnarsdottir, K.M.,** Kerr, M.S.D., Salas, R.M.E., Ewen, J., Allen, R., Gamaldo, C., Sarma, S.V. (August 28th, 2015). *To Score or Not to Score? A look at the distinguishing power of micro EEG analysis on an annotated sample of PSG studies conducted in an HIV cohort.* Poster presented at the 37th Annual International Conference of the IEEE Engineering in Medicine and Biology Society (EMBC), Milan, Italy.

**Gunnarsdottir, K.M**., Kang, Y.M., Kerr, M.S.D., Sarma, S.V., Ewen, J., Allen, R., Gamaldo, C., Salas, R.M.E. (June 22nd, 2015). *A look at the strength of micro and macro EEG analysis for distinguishing insomnia within an HIV cohort*. Poster presented at Johns Hopkins University 1st Annual Sleep and Circadian Research Day, Baltimore, Maryland.

Kang, Y. M., **Gunnarsdottir, K.M.,** Kerr, M.S. D., Salas, R. M. E., Ewen, J., Allen, R., Gamaldo, C., Sarma, S. V. (June 22nd, 2015). *To Score or Not to Score? A look at the distinguishing power of micro EEG analysis on an annotated sample of PSG studies conducted in an HIV cohort.* Poster presented at Johns Hopkins University 1st Annual Sleep and Circadian Research Day, Baltimore, Maryland.

**Gunnarsdottir, K. M**., Kang, Y. M., Kerr, M. S. D., Sarma, S. V., Ewen, J., Allen, R., Gamaldo, C., Salas, R. M. E. (May 28th, 2015). *A look at the strength of micro and macro EEG analysis for distinguishing insomnia within an HIV cohort*. Poster presented at the Seventh International Workshop Statistical Analysis of Neuronal Data (SAND7), Pittsburgh, Pennsylvania.

**PATENTS**

**Gunnarsdottir, K.M.**, Sarma, S.V., Gonzalez-Martinez, J. *Locating an epileptogenic zone for surgical planning*. The Johns Hopkins University and The Cleveland Clinic Foundation, assignees. Patent Application No. 63/123417. December 9th, 2020.